

**FLOCCULATION AND SETTLING PROPERTIES OF
DISCHARGED DRILLING WASTE**

CENTRE FOR NEWFOUNDLAND STUDIES

**TOTAL OF 10 PAGES ONLY
MAY BE XEROXED**

(Without Author's Permission)

HAIBO NIU





National Library
of Canada

Bibliothèque nationale
du Canada

Acquisitions and
Bibliographic Services

Acquisitions et
services bibliographiques

395 Wellington Street
Ottawa ON K1A 0N4
Canada

395, rue Wellington
Ottawa ON K1A 0N4
Canada

Your file *Votre référence*

ISBN: 0-612-89657-9

Our file *Notre référence*

ISBN: 0-612-89657-9

The author has granted a non-exclusive licence allowing the National Library of Canada to reproduce, loan, distribute or sell copies of this thesis in microform, paper or electronic formats.

L'auteur a accordé une licence non exclusive permettant à la Bibliothèque nationale du Canada de reproduire, prêter, distribuer ou vendre des copies de cette thèse sous la forme de microfiche/film, de reproduction sur papier ou sur format électronique.

The author retains ownership of the copyright in this thesis. Neither the thesis nor substantial extracts from it may be printed or otherwise reproduced without the author's permission.

L'auteur conserve la propriété du droit d'auteur qui protège cette thèse. Ni la thèse ni des extraits substantiels de celle-ci ne doivent être imprimés ou autrement reproduits sans son autorisation.

In compliance with the Canadian Privacy Act some supporting forms may have been removed from this dissertation.

Conformément à la loi canadienne sur la protection de la vie privée, quelques formulaires secondaires ont été enlevés de ce manuscrit.

While these forms may be included in the document page count, their removal does not represent any loss of content from the dissertation.

Bien que ces formulaires aient inclus dans la pagination, il n'y aura aucun contenu manquant.

Canada

**FLOCCULATION AND SETTLING PROPERTIES OF
DISCHARGED DRILLING WASTE**

by

© **Haibo Niu**

A Thesis Submitted to the School of Graduate Studies
in Partial Fulfillment of the Requirements for the
Degree of Master of Engineering

**Faculty of Engineering and Applied Science
Memorial University of Newfoundland**

February 2003

St. John's

Newfoundland

Canada

ABSTRACT

In order to determine the potential environmental effects of offshore discharges of synthetic based drilling fluids (SBFs) and associated drilling cuttings, it is necessary to understand the physical transport mechanisms of SBFs associated with drilling discharges in the marine environment. The purpose of this work was to study the flocculation and settling properties of SBFs associated with drilling cuttings in both freshwater and seawater and provide more appropriate equations for existing transport models.

A digital imaging system was employed in this research to study the flocculation and settling processes. The effects of particle shape and size on the settling mechanism and the effects of salinity, fluid shear, discharge concentration and oily components on the rate of flocculation and the settling speeds of flocs were studied.

The cutting sample for this study was collected from an exploration oil well in the east coast of Canada. The settling velocities of coarse particles from both untreated and thermally treated cuttings were measured in a 2.5m high and 14cm inner diameter Plexiglas settling column using both freshwater and seawater. The flocculation of fine grain particles was performed using a laboratory paddle stirrer in both freshwater and seawater. The applied shears ranged from 25 to 200 s⁻¹, and the concentrations ranged from 25 to 200mg/L. In order to study the effects of oily components on flocculation, a thermally treated sample was also used. From the experimental results it was shown that the untreated cuttings tend to clump together and settle fast while the treated cuttings

settle as individual particles with relatively low speeds. The settling velocities of treated and untreated coarse particles were found to be functions of both particle sphericity and diameter following a power law. It was demonstrated by the flocculation tests that the steady state median floc size decreases as the shear stress and concentration increase, and the particles flocculate faster in seawater than in freshwater. For the same diameter and salinity, the flocs formed at high fluid shears have a higher settling velocity than do flocs formed at low shears. It was also shown that the flocs formed by untreated cuttings settle faster than flocs formed by thermally treated cuttings in the same conditions (shear rate and concentration) under which the flocs were produced.

ACKNOWLEDGEMENT

First and foremost, I am highly indebted to Dr. Tahir Husain, Dr. Brian Veitch, and Dr. Neil Bose for their excellent supervision and guidance during the course of my research. Without their support this thesis would not have been possible. I am very grateful to Dr. Kelly Hawboldt and Dr. Rehan Sadiq for their continuous guidance and help.

I also gratefully acknowledge the Faculty of Engineering and Applied Science, Memorial University of Newfoundland (MUN), and the NSERC Strategic Project (Offshore Environmental Engineering using Autonomous Underwater Vehicles) for financial support.

Personal thanks are extended to Carolyn J. Emerson, Roy Ficken, Tom Pike, and Richard Newman for their help during the research. An expression of thanks is also extended to The National Institutes of Health (USA) and Gary Chinga for their supply of image processing software.

Last but by no means least, I would like to offer my deepest appreciation to my wife Liping Wang, my mother Jinzhi Xue, my father Zhijun Niu and my elder sister Hongxia Niu for their love and encouragement.

Table of Contents

Abstract	ii
Acknowledgements	iv
Table of Contents	v
List of Tables	viii
List of Figures	ix
List of Symbols	xiv
List of Acronyms	xvii
Chapter 1 Introduction	1
1.1 Background of Research	2
1.1.1 Drilling Wastes.....	2
1.1.2 Transport Modeling.....	5
1.1.3 Summary	9
1.2 Objective and Scope of the Study	10
1.3 Outline of the Thesis	11
Chapter 2 Flocculation and Settling Mechanisms	13
2.1 Flocculation Mechanisms.....	13
2.1.1 Aggregation.....	15
2.1.2 Dissagregation Due to Shear	17
2.1.3 Dissagregation Due to Collision	18
2.2 Previous Work on Flocculation.....	19
2.3 Settling Mechanisms	22
2.3.1 Terminal Settling Velocity of Spherical Particles.....	22
2.3.2 Drag Coefficient and Reynolds Number.....	23
2.3.3 Time and Distance to Reach Terminal Settling Velocity.....	26

2.3.4	Size and Shape Characterization of Non-Spherical Particles.....	28
2.3.5	Settling velocity of Non-Spherical Particles	32
2.4	Previous Work on Settling	33
2.5	Summary	38
Chapter 3	Experimental Methods and Apparatuses	39
3.1	Sample Preparation	39
3.1.1	Sample Preparation of Drying Treated Cuttings	40
3.1.2	Sample Preparation of Untreated Cuttings.....	43
3.2	Flocculator.....	44
3.3	Settling Column.....	49
3.4	Digital Imaging System.....	50
3.4.1	Camera and Lens.....	53
3.4.2	Image Processing.....	54
3.5	Experimental Methods	57
3.5.1	Procedure for Flocculation Test	57
3.5.2	Procedure for Floc Settling Test.....	58
3.5.3	Test Procedure for Column Settling Test	59
3.6	Summary	60
Chapter 4	Results and Discussions	61
4.1	Flocculation Experiments.....	62
4.1.1	Untreated Cuttings in Seawater.....	62
4.1.2	Treated Cuttings in Seawater	69
4.1.3	Untreated Cuttings in Freshwater.....	75
4.2	Coarse Particle Settling Velocity Results.....	82
4.2.1	Settling Velocity Results for Untreated Cuttings	82
4.2.2	Settling Velocity Results for Treated Cuttings	90
4.3	Floc Settling Velocity Results.....	99
4.3.1	Seawater Settling Velocity for Flocs formed from Untreated Cuttings	99
4.3.2	Seawater Settling Velocity for Flocs formed from Treated Cuttings.....	107

4.3.3 Freshwater Settling Velocity of Floccs.....	115
4.4 Summary	119
Chapter 5 Conclusions and Recommendations.....	121
5.1 Conclusions	121
5.2 Research Contributions	124
5.3 Recommendation.....	125
References	128
Appendix	137

List of Tables

Table 1-1 Major ingredients of a typical Poly Alpha Olefins based drilling fluid (SBF) compared to a typical mineral oil based fluid (OBF), (U.S. MMS 2000).....	3
Table 2-1 Relationship between Reynolds number and drag coefficient for spherical particles	26
Table 2-2 Difference between the ϕ and ψ for five geometric forms	31
Table 3-1 Shapes description of irregular particles of Rawle (1994)	56
Table 4-1 Time (minutes) to reach steady state of flocculation for untreated drilling cuttings in seawater	66
Table 4-2 Steady state floc median diameter (μm) for untreated drilling cuttings in seawater	66
Table 4-3 Time (minutes) to reach steady state of flocculation for treated drilling cuttings in seawater.....	72
Table 4-4 Steady state floc median diameter (μm) for treated drilling cuttings in seawater	72
Table 4-5 Time (minutes) to reach steady state of flocculation for untreated drilling cuttings in freshwater	78
Table 4-6 Steady state floc median diameters (μm) for untreated drilling cuttings in freshwater	78
Table 4-7 Values of a , b for various shaped particles.....	95
Table 4-8 A and m values for seawater tests of untreated cuttings	104
Table 4-9 Values for the regression of A , m for seawater tests of untreated cuttings	104
Table 4-10 A and m values for seawater tests of treated cuttings	112
Table 4-11 Values for the Regression of A , m for seawater tests of treated cuttings.....	112
Table 4-12 A and m values for the freshwater settling velocity of flocs formed at concentration of 100mg/L and shear rate of 100G.....	115
Table 4-13 Summary of developed equations.....	120

List of Figures

Figure 1-1 Generalized drilling fluid circulation system (Ayers 1981).....	4
Figure 1-2 Transport processes of discharged drilling wastes	6
Figure 2-1 The drag coefficient (C_D) vs Reynolds number (Re) for spherical particles ...	25
Figure 3-1 The stack of sieves on the analytical shaker.....	41
Figure 3-2 Particle size distribution of dried drill cuttings (the horizontal axis is the particle diameters, in mm).....	41
Figure 3-3 Untreated cuttings and dried cuttings	42
Figure 3-4 Phipps & Bird six paddle stirrer	48
Figure 3-5 Velocity gradient vs RPM for a 2-Liter square beaker using a Phipps & Bird stirrer, source: Wagner (1993)	49
Figure 3-6 Settling column.....	50
Figure 3-7 System configuration for settling column test and jar test	52
Figure 3-8 Lenses and extension tubes	53
Figure 4-1 Suspension of untreated SBM drilling cuttings.....	63
Figure 4-2 Particle size distribution of unflocculated untreated SBF drilling cuttings.....	63
Figure 4-3 Time variation of median floc diameter for untreated cuttings at 25mg/L in seawater.....	64
Figure 4-4 Time variation of median floc diameter for untreated cuttings at 50mg/L in seawater.....	65
Figure 4-5 Time variation of median floc diameter for untreated cuttings at 100mg/L in seawater.....	65
Figure 4-6 Time variation of median floc diameter for untreated cuttings at 200mg/L in seawater.....	66
Figure 4-7 Time variation of median floc diameter for untreated cuttings at 25G in seawater.....	68
Figure 4-8 Time variation of median floc diameter for untreated cuttings at 200G in seawater.....	68
Figure 4-9 Particle size distribution of unflocculated treated SBF drilling cuttings.....	70
Figure 4-10 Time variation of median floc diameter for treated cuttings at 25mg/L in seawater.....	70

Figure 4-11 Time variation of median floc diameter for treated cuttings at 50mg/L in seawater.....	71
Figure 4-12 Time variation of median floc diameter for treated cuttings at 100mg/L in seawater.....	71
Figure 4-13 Time variation of median floc diameter for treated cuttings at 200mg/L in seawater.....	72
Figure 4-14 Time variation of median floc diameter for treated cuttings at 25G in seawater.....	74
Figure 4-15 Time variation of median floc diameter for treated cuttings at 200G in seawater.....	74
Figure 4-16 Time variation of median floc diameter for untreated cuttings at 25mg/L in freshwater.....	76
Figure 4-17 Time variation of median floc diameter for untreated cuttings at 50mg/L in freshwater.....	77
Figure 4-18 Time variation of median floc diameter for untreated cuttings at 100mg/L in freshwater.....	77
Figure 4-19 Time variation of median floc diameter for untreated cuttings at 200mg/L in freshwater.....	78
Figure 4-20 Time variation of median floc diameter for untreated cuttings at 25G in freshwater.....	80
Figure 4-21 Time variation of median floc diameter for untreated cuttings at 200G in freshwater.....	80
Figure 4-22 Seawater settling velocity data of untreated cuttings (F3070-3090) of various shapes.....	83
Figure 4-23 Power law fit of the seawater settling velocity data of untreated cuttings (F3070-3090) of various shapes.....	83
Figure 4-24 Seawater settling velocity data of untreated cuttings (F3050-3069) of various shapes.....	84
Figure 4-25 Power law fit of the seawater settling velocity data of untreated cuttings (F3050-3069) of various shapes.....	84
Figure 4-26 Freshwater settling velocity data of untreated cuttings (F3070-3090) of various shapes.....	85
Figure 4-27 Power law fit of the freshwater settling velocity data of untreated cuttings (F3070-3090) of various shapes.....	85

Figure 4-28 Drag coefficient vs Reynolds number for untreated drill cuttings (experimental data).....	87
Figure 4-29 Drag coefficient vs Reynolds number for untreated drill cuttings (regression results)	88
Figure 4-30 Settling velocity of untreated drill cuttings	89
Figure 4-31 Seawater settling velocity data of treated cuttings (F3070-3090) of various shapes	91
Figure 4-32 Power law fit of the seawater settling velocity data of treated cuttings (F3070-3090) of various shapes.....	91
Figure 4-33 Seawater settling velocity data of treated cuttings (F3050-3069) of various shapes	92
Figure 4-34 Power law fit of the seawater settling velocity data of treated cuttings (F3050-3069) of various shapes.....	92
Figure 4-35 Freshwater settling velocity data of treated cuttings (F3070-3090) of various shapes	93
Figure 4-36 Power law fit of the freshwater settling velocity data of treated cuttings (F3070-3090) of various shapes.....	93
Figure 4-37 Drag coefficient vs Reynolds number for treated drill cuttings (experimental data).....	94
Figure 4-38 Drag coefficient vs Reynolds number for treated drill cuttings (regression results)	95
Figure 4-39 Relationship between parameter a and sphericity	96
Figure 4-40 Relationship between parameter b and sphericity	96
Figure 4-41 Settling velocity of various shaped treated SBM drilling cuttings particles .	98
Figure 4-42 Seawater settling velocity data of flocs formed from untreated cuttings at 25G	99
Figure 4-43 Power law fit of seawater settling velocity of flocs formed from untreated cuttings at 25G	100
Figure 4-44 Seawater settling velocity data of flocs formed from untreated cuttings at 50G	100
Figure 4-45 Power law fit of seawater settling velocity of flocs formed from untreated cuttings at 50G	101
Figure 4-46 Seawater settling velocity data of flocs formed from untreated cuttings at 100G	101

Figure 4-47 Power law fit of seawater settling velocity of flocs formed from untreated cuttings at 100G	102
Figure 4-48 Seawater settling velocity data of flocs formed from untreated cuttings at 200G	102
Figure 4-49 Power law fit of seawater settling velocity of flocs formed from untreated cuttings at 200G	103
Figure 4-50 Parameter A and m for untreated cuttings as a function of shear rate G	105
Figure 4-51 Relationship between seawater settling velocity and floc diameter of untreated SBF cuttings. The data for WBFs by Huang (1992) are presented for reference	106
Figure 4-52 Relationship between seawater settling velocity and floc diameter of untreated SBF cuttings. The data for clay minerals by Gibbs (1985) are presented for reference	106
Figure 4-53 Seawater settling velocity data of flocs formed from treated cuttings at 25G	108
Figure 4-54 Power law fit of seawater settling velocity of flocs formed from treated cuttings at 25G	108
Figure 4-55 Seawater settling velocity data of flocs formed from treated cuttings at 50G	109
Figure 4-56 Power law fit of seawater settling velocity of flocs formed from treated cuttings at 50G	109
Figure 4-57 Seawater settling velocity data of flocs formed from treated cuttings at 100G	110
Figure 4-58 Power law fit of seawater settling velocity of flocs formed from treated cuttings at 100G	110
Figure 4-59 Seawater settling velocity data of flocs formed from treated cuttings at 200G	111
Figure 4-60 Power law fit of seawater settling velocity of flocs formed from treated cuttings at 200G	111
Figure 4-61 Parameter A and m for treated cuttings as a function of Shear rate G	113
Figure 4-62 Relationship between seawater settling velocity and floc diameter of treated SBF cuttings. The data for WBFs by Huang (1992) are presented for reference ...	114
Figure 4-63 Relationship between seawater settling velocity and floc diameter of treated SBF cuttings. The data for clay minerals by Gibbs (1985) are presented for reference	114

Figure 4-64 Freshwater settling velocity data of flocs formed in seawater at the concentration of 100mg/L and shear rate of 100G..... 116

Figure 4-65 Freshwater settling velocity data of flocs formed in freshwater at the concentration of 100mg/L and shear rate of 100G..... 116

Figure 4-66 Settling velocity of flocs formed from SBF cuttings, the data of Gibbs (1985) and Burban et al. (1990) are plotted for reference. 118

Figure 4-67 Settling velocity of natural Sediment flocs produced at 100mg/L (Data of Burban et al 1990)..... 118

List of Symbols

A	Projected area of a particle
A_p	Projected area of paddle
B_k	Break-up coefficient
C	Concentration
C_D	Drag coefficient
C_{ij}	Probability of disaggregation of a particle of size k after collision with a particle of size i
D	Diameter of particle
D_a	Paddle diameter
D_C	Diameter of the smallest circle circumscribing the particle
D_p	Diameter of primary particle
d_{cn}	Diameter of a circle equal in size to the cross-section area of particle
d_i, d_j	Diameter of the i 'th and j 'th floc
F	Gravitational force
G	Velocity gradient
g	Gravitational acceleration
g_c	Newton's-law conversion factor
h	Distance settled
K	Boltzman Constant

K_T, K_L	Empirical constant
n	Rotation speed
nf	Fraction dimension
n_i, n_j	Particles per unit volume in size range i and j
n_k	Particles per unit volume in size range k
P	Power dissipation
R	Resisting force
R_1	Outer radius of the inner cylinder
R_2	Inner radius of the outer cylinder
R_e	Reynolds number
r_a	Sphere radius
r	Correlation coefficient
S.F.	Shape factor
T	Absolute temperature
T_q	Torque
t	Time
u	Settling velocity of particle
u_t	Terminal Settling Velocity
W	Dissipation function or power input per unit volume
W_s	Floc settling velocity
$W_{s,aggr}$	Floc settling velocity

$W_{s,part}$	Stokes' settling velocity
W_{so}	Reference settling velocity, defined as kC^m
V	Volume
v_p	Paddle velocity
v	Suspension velocity
α, β	Empirical constant
α_{ij}	Probability of cohesion of particle i and j after collision
β_{ij}	Collision frequency function for collisions between particle i and j
γ_{ij}	Probability that particle of size k will be formed after disaggregation of a particle of size j
μ	Dynamic viscosity
ρ_s, ρ_f	Density of particle and fluid
$\Delta\rho_i$	Difference in the effective density of i 'th floc and the density of fluid
ε	Energy dissipation
ν	Kinetic Viscosity
ψ	Sphericity
ϕ	Approximated sphericity
ω	Velocity of outer cylinder

List of Acronyms

IJ	Image Java
JPEG	Joint Photographic Experts Group
NEB	National Energy Board
NRC	National Research Council
OBFs	Oil Based Drilling Fluids
OOC	Offshore Operators Committee
PIV	Particle Image Velocimetry
RPM	Revolutions Per Minute
SBFs	Synthetic Based Drilling Fluids
TSS	Total Suspended Solids
US EPA	United States Environmental Protection Agency
US MMS	United States Mineral Management Service
WBFs	Water Based Drilling Fluids

Chapter 1

Introduction

Synthetic based drilling fluids (SBFs) are a relatively new class of drilling muds that were developed to have the same performance as oil based drilling fluids (OBFs), but with a lower environmental impact. The technical and economic benefits of using SBFs are clear, and a number of fate models have been developed to evaluate the environmental impacts of discharged drilling cuttings produced during use of SBFs. However, due to the fact that the transport mechanisms of discharged SBFs and their associated drilling cuttings in the marine environment are still only partially understood, most of the existing models were developed by employing the transport mechanisms of other types of drilling fluids and cuttings rather than SBFs and the cuttings associated with them. As the physical and chemical characteristics (such as density, particle shape, size distribution, flocculation ability, settling behavior and so on) of SBFs produced drilling cuttings are different from that produced by other types of drilling fluids, the transport processes are different. In order to better approximate the transport processes of SBFs and associated drilling cuttings and improve the accuracy of existing prediction models, it is necessary to conduct experimental studies on the transport properties of SBFs produced drilling cuttings.

In the following sections, the characteristics of drilling waste will be described followed by a brief review of existing drilling waste transport models. The objective of this research and the outline of the thesis will also be included in this Chapter.

1.1 Background of Research

1.1.1 Drilling Wastes

The exploration and extraction of offshore oil and gas from beneath the ocean floor requires the disposal of drilling wastes such as used (spent) drilling fluids and rock cuttings. The drilling fluids, also called drilling muds, are an essential component of the rotary drilling processes used to drill for oil and gas on land and in offshore environments. The most important functions of drilling fluid are to transport cuttings to the surface, balance subsurface and formation pressure to prevent a blowout, cool and lubricate, and support part of the weight of the drill bit and drill pipe (Neff 1987; Darley & Gray 1988).

Drilling fluids or muds are a suspension of solids and dissolved materials in a base of water, oil or other synthetic material. According to the base materials used, different varieties of drilling fluids can be broadly categorized into water based, oil based or synthetic based fluids. Normally, water based drilling fluids (WBFs) are used in less difficult wells and the shallow portion of difficult, deeper wells. The use of WBFs in certain formations may cause the hole to be instable due to the swelling of water-absorbing rock. This problem can be greatly alleviated by the use of OBFs and SBFs. OBFs and SBFs are used in deeper well

intervals and complex drilling situations because of their superior performance. The compositions of drilling fluids vary with both the depth and the location of the well. A typical composition of an SBF and OBF is listed in Table (1-1).

Table 1-1 Major ingredients of a typical Poly-Alpha -Olefins based drilling fluid (SBF) compared to a typical mineral oil based fluid (OBF), (U.S. MMS 2000)

Component	Concentration in Drilling Mud	
	Poly-Alpha - Olefin Mud	Mineral Oil Mud
Base Liquid/Water Ratio	70/30	80/20
Density (lb/gal & kg/L)	11.0 (1.32)	7.43 (0.89)
Base Liquid	163.4 (470)	217.0 (620)
Water	83.5 (238)	64.3 (183)
CaCl ₂	36.6 (104)	8.58 (24)
Emulsifier	5.0 (14)	1.9 (5)
Wetting Agent	2.0 (6)	1.0 (3)
Lime (CaCO ₃)	6.0 (17)	---
Hot Lime (CaO)	---	2.0 (6)
Organophilic Clay	2.0 (6)	10.0 (28)
Rheology Modifier	---	4.0 (11)
Barite	164.5 (469)	---

*Concentrations (except for density) are pounds per barrel and kilograms per cubic meter (in parentheses)

Drilling cuttings are particles of crushed rock produced by the grinding action of the drill bit as it penetrates into the formation. Drilling cuttings range in size from clay-sized particles to coarse gravel and have an angular configuration. The particle size distribution of drilling cuttings varies with well site and well depth.

To drill a well offshore, the drilling fluid is first pumped from the mud tanks down the hollow drillstring to lubricate the drill bit. After passing through the nozzles of the drill bit, the flowing drilling fluids sweep the crushed rock cuttings from beneath the bit and carries

them up the annular space between the drillstring and the hole to the surface. As the mixture of drilling fluid and cuttings returns to the surface, it passes through a solids control system to remove the drilling cuttings. The cuttings waste stream normally consists of larger cuttings from the primary shale shakers and fines from a fine mesh shaker or centrifuge, and may also consist of smaller cuttings from a secondary shale shaker (US EPA 1999). A schematic diagram of a drilling fluid circulation system is shown in Figure (1-1).

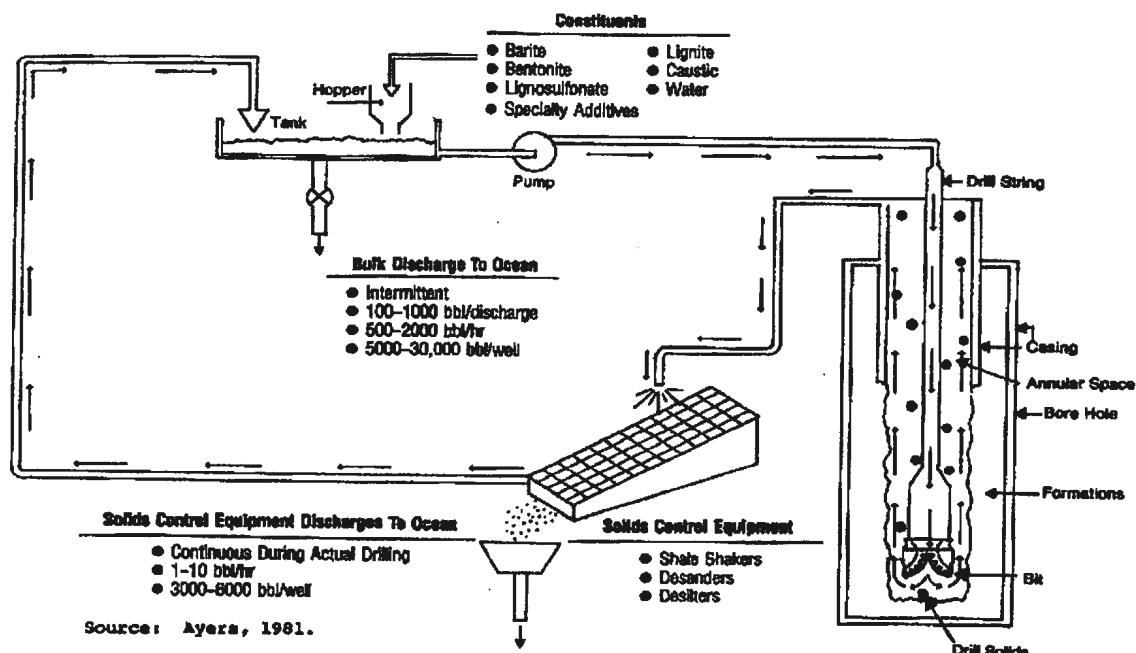


Figure 1-1 Generalized drilling fluid circulation system (Ayers 1981)

After passing through the solid control system, the drill cuttings can be discharged directly or sent to undergo further treatment. Finally, they will be discharged offshore, re-injected on-site, or transported to shore. Offshore discharge is in most cases the least expensive and operationally least complicated, of the three options. Under the current Canadian

regulations, WBFs can be discharged without treatment; whole SBFs and OBFs cannot be discharged; for drilling cuttings associated with SBFs and OBFs, where re-injection is not technically or economically feasible, the on-site discharge of these cuttings is permitted provided the attached drilling fluid concentration of 6.9g/100g or less on wet solids is achieved; the cuttings associated with diesel or other high aromatic OBFs cannot be discharged (NEB et al. 2002).

Drilling cuttings produced using SBFs are typically discharged continuously as they are separated from the solids separation equipment. These cuttings contain rock fragments contaminated with a small amount of liquid, solid drilling fluid components. Although the cuttings themselves are considered toxicologically inert, the high quantity of TSS (Total Suspended Solids) that makes up the bulk discharges can cause benthic smothering (US MMS 2000). The alteration of sediment grain size may bring potential damage to invertebrate populations and potential alterations in spawning grounds and feeding habits (US EPA 1999). Thus the quantitative assessment of both the long-term and short-term fates of these discharges become important.

1.1.2 Transport Modeling

Once discharged, the fate of drilling wastes is controlled by various transport mechanisms, which include flocculation, settling, re-entrainment, and re-suspension. These transport processes are illustrated in Figure (1-2).

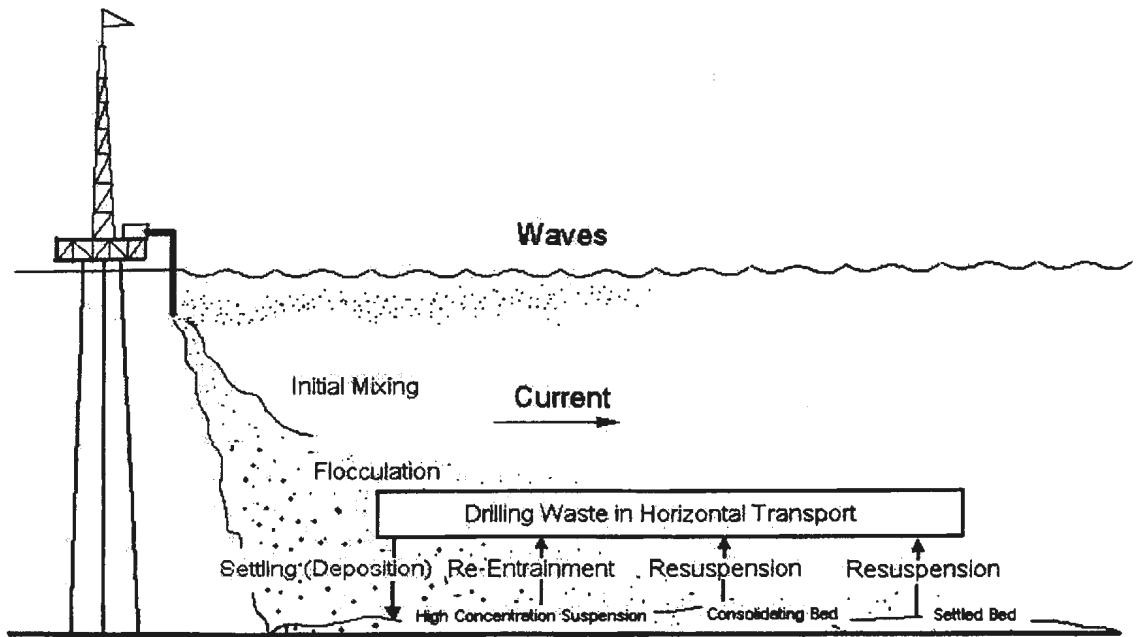


Figure 1-2 Transport processes of discharged drilling wastes

In the case of cuttings discharge, fractionation of the drilling wastes may occur during any stages of transport, depending on whether the materials are soluble or solids heavier or lighter than seawater. Most of the materials (barite, flocculated clays, and formation solids) sink down quickly to the bottom near the well site. These materials usually accumulate in an area about 40 to 50m in diameter immediately down current of the well site; the diameter is strongly dependent on the water depth and current speeds of the site (NRC 1983). In many areas, because of the strong tidal currents, dispersion of the settled materials is rapid, and no visible accumulation of cuttings in the sea floor is shown. During the settling process of drilling cuttings, soluble and particulate fluid additives adhering to the cuttings are to some extent washed off into water column. The suspending

time of cuttings in the water column and deposition distance from the discharge site depend on the conditions of discharge (e.g. depth of water, net currents) and the cuttings characteristics (e.g. relative density, particle size and shape, drilling fluid type). The flocculation process, which changes the particle size distribution, has significant effects on the transport distance and transport time. The deposited wastes may later be re-suspended due to the effects of wave and currents. The re-suspended materials will be transported away by ocean currents and re-deposited depending on environmental factors (such as water depth, bottom configuration, and energy regime).

When whole fluid is discharged, most of the materials form a plume. The plume descends rapidly until it encounters the sea bed or reaches neutral buoyancy due to water entrainment and solids loss during settling. In addition, a visible upper plume is formed due to turbulent mixing of the low plume with seawater (Brandsma & Saucer 1983). Under most conditions, this portion is of primary concern in considering the fates of materials in the water column. In deep water (water depth $\geq 80\text{m}$), the lower plume will reach neutral buoyancy before encountering the bottom (NEB et al. 2002).

The transfer processes of pollutants from discharged wastes in the seawater depend on a great number of properties of these substances. When dissolved, the substances are diluted in sea water, but when in particulate form and having a specific gravity higher than sea water, they will be precipitated to the sea floor. Equally, substances adsorbed to sedimenting materials will ultimately arrive at the seawater/seafloor interface. Sorption of

dissolved compounds directly from the supernatant water to the bottom interfacial layer is another process which exists.

In order to give operators and regulatory agencies the capability of predicting the fate of drilling discharges under a variety of ocean conditions, mathematical modeling of the drilling waste transport processes become important. These models can be explored from two aspects: (a) The physical transport of drilling cuttings and fluids, and (b) the chemical transfer processes. The physical transport models are fundamental to all the other models.

The most widely used model is known as the OOC (Offshore Operators Committee) model. It was developed by Brandsma & Saucer (1983) to model the short term transport. The OOC model is the only model that has been calibrated to field data of real drilling discharges (O'Reilly, et al. 1988) and is based on observations of the behavior of drilling mud plumes in the field. Other studies (deMargerie 1988; Ozretich & Baumgartner 1990) have also emphasized the near field settling of effluents or have been designed to evaluate the dilution effects over large distances (Walker et al. 1990). Coats (1991) has adopted a diagnostic approach, with the intent of deriving the conditions which produce a given distribution of drilling waste products. A systematic review of some available models was done by Khondaker (2000).

Although simulation models have been developed by many investigators, no single, fully validated and universal drilling waste transport model exists (Khondaker 2000). The ultimate accuracy of transport models relies on our knowledge of complex processes

related to the transport, which involve: (i) advection, (ii) dispersion, (iii) flocculation, (iv) settling, (v) deposition, (vi) consolidation, (vii) erosion, (viii) re-suspension, (ix) re-entrainment, and (x) change in bed elevation. These processes are still only partially understood and not well incorporated into hydrodynamic models. For example, the flocculation process (which will change the density and particle size distribution of the drilling discharge and therefore the whole settling process) is not considered by most dispersion models (Brandsma & Saucer 1983, Hannah et al. 1995 & 1996, Bryden & Carles 1998). Most of the existing models assume that cuttings are spherical, limited range of size, and use very simplified equations for settling. As the transport models are very sensitive to the settling velocity equation (Carles & Bryden 1999), these simplified assumptions may cause a lack of precision in prediction. Moreover, the flocculation and settling are also greatly influenced by the type of base fluids used and the characteristics of the cutting discharged, but most previous works on flocculation and settling were based on the study of WBFs produced cuttings. The study on flocculation and settling of SBFs produced cuttings is still a gap in the knowledge base. In order to accurately predict the impact of discharged SBFs and their associated drilling cuttings, it was considered essential to conduct research on this subject.

1.1.3 Summary

The characteristics of drilling wastes have been introduced in section 1.1.1. The offshore drilling fluid circulating system was also described. The transport processes of drilling

wastes in the marine environment have been discussed in section 1.1.2. A review of some existing transport models was also provided in this section.

1.2 Objective and Scope of the Study

As mentioned above in section 1.1 , the transport properties of drilling wastes are very important for the accurate prediction of both the short term and long term transport of drilling wastes disposed in the ocean, and must be determined experimentally. Very limited work on this subject using real drilling wastes have been reported. Only Xu (1988) has done flocculation tests using pure barite and bentonite, the major component of drilling muds; Huang (1992) has studied the re-suspension, flocculation and settling of WBFs, and Gerard (1996) has studied flocculation and settling using cuttings produced by OBFs. No experimental work using synthetic based cuttings can be found.

The objective of this study was to improve the understanding of the transport properties of synthetic based drilling cuttings and provide important parameters for the numerical modeling of the transport of synthetic based drilling wastes in the marine environment. This study focuses on the two controlling transport processes which affect the deposition of drilling wastes: particle aggregation (flocculation) and gravitational settling. The scope of the current study includes:

1. To develop an experimental method and set up an experimental system to investigate the flocculation and gravitation settling of both large and fine-grained drilling waste particles.

2. To study the effects of thermal treatment on the transport properties of synthetic based drilling cuttings.
3. To evaluate the effects of different receiving environments (turbulence, salinity) on the transport of synthetic based drilling cuttings.
4. To investigate the effects of discharge scenario (concentration) on flocculation properties.
5. To study the effects of particle shape on the settling of coarse particulates.

1.3 Outline of the Thesis

This thesis is divided into five chapters. Chapter 1 described the characteristics of drilling wastes and reviewed the existing transport models. Chapter 2 presents an overview of the flocculation and settling mechanisms of particulate materials; previous works in this field are reviewed in this part. In Chapter 3, the experimental apparatus and experiment methods are described. This includes a description of the Jar flocculator, settling column, and the digital imaging system. The experimental methods and data processing technologies are also presented in this chapter. Both the flocculation and settling experiment results of untreated and thermally treated drilling cuttings are presented in Chapter 4. The experimental results under freshwater and synthetic seawater conditions are compared. The effects of concentration, salinity, and shear rate on flocculation are

investigated. The shape effects on particle settling velocity are also studied. Concluding remarks and recommendations for future work are given in Chapter 5.

Chapter 2

Flocculation and Settling Mechanisms

2.1 Flocculation Mechanisms

Flocculation has been observed and studied for a long time due to its significance in many fields, such as water treatment, ocean disposal of particulate materials, and sediment transport.

Flocculation is a dynamic process in which particles with small diameters continuously collide together to form flocs with relatively larger diameters. It also includes the break up of the flocs into smaller particles. The aggregation and disaggregation depend on the relative motion of particles. This relative motion may be caused by Brownian motion, fluid movement giving rise to velocity gradients (also called fluid shear), or by particle motion due to external forces (e.g. gravity force causing differential settling). The rate of flocculation is determined by the collision frequency induced by the relative motion. Where it is caused by Brownian movement it is called perikinetic flocculation; and where it is caused by a velocity gradient it is called orthokinetic flocculation. Flocculation caused by external forces is treated as a special case of orthokinetic flocculation, as the movement of a particle relative to the liquid also creates velocity gradients.

Among these three mechanisms, Brownian motion is only valid for particles less than about $1\mu\text{m}$, which is not generally the situation for typical fine-grained sediment (in the clay and silt size ranges). The importance of differential settling depends on the differences of settling speed of particles. Fluid shear is often large near the sediment/water interface, in shallow, near-shore areas, and in drilling mud plumes (jets) during the initial mixing process. Fluid shear is often the dominant mechanism for typical fine grained sediments (Huang 1992) and is the only motion that will be investigated in this study.

When two particles collide, they may or may not aggregate together to form a large particle depending on the attraction and repulsion forces between the particles. If there is no surface repulsion between the particles, then every collision leads to aggregation and the process is called rapid flocculation. If a significant repulsion force exists, then only a fraction of the collisions result in aggregation. This process is called slow flocculation.

Many flocculation models exist, and these models can be categorized as microscale and macroscale. Microscale models basically describe aggregation at a particle-particle level. To predict time dependent positions of every particle in the dispersion, microscale models solved the equations of motion of individual particles in a suspension by taking consideration of particle interaction forces (Batchelor & Green 1972, Adler 1981, van de Ven & Mason 1977, Han & Lawler 1991). In addition, the interactions of these forces determine the trajectory of particles approaching each other and, eventually, aggregate geometry (Elimelech & Song 1992).

With the use of Eulerian methods, macroscale models describe system properties in terms of particle concentrations in space and time, either for a steady-state condition or to reveal time-dependent behavior. The rate theory, which was developed by Smoluchowski (1917), best represents macroscale models. By considering how often particles collide (collision frequency) and how often they stick together when they collide (collision efficiency), rate theory generally simulates changes in concentrations of different sized particles. Rate theory has been used by many researchers in aggregation related studies (Ives 1978a, Lick et al. 1992, Filella & Buffle 1993, Casson & Lawler 1990, Valioulis & List 1984a, 1984b). Gain and loss of particles in different size classes due to aggregation and disaggregation processes are the common mechanisms that are included in these models. The basic theories of these models are summarized in the following sections.

2.1.1 Aggregation

A general formula for the time rate of change of the particle size distribution due to aggregation was given by Lick & Lick (1988) as follows. Denote the number of particles per unit volume in size range k by n_k . The time rate of change of n_k is then given by

$$\frac{dn_k}{dt} = \frac{1}{2} \sum_{i+j=k} \alpha_{ij} \beta_{ij} n_i n_j - n_k \sum_{i=1}^{\infty} \alpha_{ik} \beta_{ik} n_i \quad \text{Equation (2-1)}$$

where α_{ij} is the probability of cohesion of particle i and j after collision and β_{ij} is the collision frequency function for collisions between particles i and j . The first term on the

right hand side of the equation is the rate of formation of flocs by collisions between particles of size i and j . The second term represents the loss of flocs of size k due to cohesive collisions with all other particles. Although the collisions may happen between two particles or among three particles or more, binary collisions are assumed here to simplify the analysis.

The value of β_{ij} depends on the mechanisms of collision, Brownian motion, fluid shear or differential settling. For Brownian motion

$$\beta_{ij} = \frac{2}{3} \frac{KT}{\mu} \frac{(d_i + d_j)^2}{d_i d_j} \quad \text{Equation (2-2)}$$

where K is the Boltzman constant ($1.38 \times 10^{-23} \text{Nm}^\circ\text{K}$), T is the absolute temperature, μ is the dynamic viscosity of the fluid, and d_i and d_j are the diameters of the colliding particles.

For differential settling

$$\beta_{ij} = \frac{\pi g}{72\mu} (d_i + d_j)^2 |\Delta\rho_i d_i^2 - \Delta\rho_j d_j^2| \quad \text{Equation (2-3)}$$

where g is the acceleration due to gravity and $\Delta\rho_i = \rho_i - \rho$ and is the difference in the effective density of i 'th floc and the density of water.

For fluid shear

$$\beta_{ij} = \frac{G}{6} (d_i + d_j)^2 \quad \text{Equation (2-4)}$$

where G is the mean velocity gradient in the fluid. For a turbulent fluid, G can be approximated by $\left(\frac{\varepsilon}{\nu}\right)^{1/2}$, where ε is the energy dissipation and ν is the kinematic viscosity. The calculation of G within different flocculation systems will be discussed in Chapter 3 in detail.

2.1.2 Disaggregation Due to Shear

A general expression for the time rate of change of the particle size distribution because of disaggregation due to fluid shear can be written as

$$\frac{dn_k}{dt} = -B_k n_k + \sum_{j=k+1}^{\infty} \gamma_{jk} B_j n_j \quad \text{Equation (2-5)}$$

The first term on the right-hand side represents the loss of flocs of size k due to shear. The break-up coefficient B_k is a function of shear stress, diameter, and the floc density. A number of investigators (Argamann & Kaufman 1970, Parker et al. 1972, Matsuo & Unno 1981, Paker 1982, Clark 1982) have attempted to determine this quantity from basic theoretical considerations. Unfortunately, because the resulting theories involve complicated functions of flocs and fluid properties, some of which are vaguely defined or immeasurable (Spielman 1978), none of these attempts succeeded in giving sufficient information to determine the function form of B_k . As a result, the direct effects of shear on disaggregation were ignored so that $B_k=0$.

The second term on the right-hand side represents the rate of increase of n_k due to the disaggregation of flocs of size $j > k$. The quantity γ_{jk} is the probability that a particle of size k will be formed after disaggregation of a particle of size j . With the assumption made by Lick and Lick (1988), for all j greater than k , this quantity becomes

$$\gamma_{jk} = \frac{2}{j-1} \quad \text{Equation (2-6)}$$

2.1.3 Disaggregation Due to Collisions

By assuming binary collision, the time rate of change of n_k because of disaggregation can be written as

$$\frac{dn_k}{dt} = -n_k \sum_{i=1}^{\infty} C_{ij} \beta_{ik} n_i + \sum_{j=k+1}^{\infty} \gamma_{jk} n_j \sum_{i=1}^{\infty} C_{ij} \beta_{ij} n_i \quad \text{Equation (2-7)}$$

The first term on the right represents the loss of flocs of size k due to the collision with all other particles. The quantity C_{ik} is the probability of disaggregation of a particle of size k after collision with a particle with size i . The second term represents the rate of increase of particles of size k after collisions between all particles i and j , where j is greater than k .

The parameters in above equations can be determined by using data on the time variation of particles sizes derived from experiments. With the determined parameters, the flocculation processes can be modeled quantitatively.

2.2 Previous Work on Flocculation

As mentioned before, flocculation is important in such areas as water treatment, sediment transport and contaminant transport. Most of the previous work concerning flocculation has been in these areas.

In the area of water treatment, the strength and density of aluminum-clay flocs where the flocculation is induced by the addition of an aluminum ion solution has been studied by Tambo & Watanabe (1979) and Tambo & Hozumi (1979). Similar works have been conducted by Boadway (1978), Argamann & Kaufman (1970), and Parker et al. (1972). Delichatsios & Probstein (1975) studied the flocculation of colloidal particles in turbulent pipe flows. Their works were motivated by the importance of learning the behavior, handling and treatment of dispersions.

It was demonstrated both through observation of natural samples (Biddle & Miles 1972, Sheldon 1968, Kranck 1975, Eisma 1986) and in laboratory experiments (Gripenberg 1934, Whitehouse et al. 1960) that most of the particulate matter in rivers, lakes, and oceans exists in the form of floc. Considerable work on the flocculation and deflocculation processes of natural particles has also been conducted. Hunt (1982) studied three clay minerals (Kaolinite, illite, and montmorillonite) and a silica mineral in artificial seawater by using a vertical Couette flocculator. The particle size distribution was measured with Coulter Counter (a particle sizer which uses the Coulter Principle to measure particle volume providing both size and volume distributions of particles). Hunt & Pandya (1984) also studied sewage sludge with the same experimental configuration.

Tsai et al. (1987) studied the flocculation of fine-grained lake sediment due to fluid shear with a horizontal Couette flocculator. Similar tests can be found from Lick and Lick (1988), and Burban et al. (1989). Due to the fact that most previous work on flocculation of fine-grained sediments has emphasized the effects of fluid shear, Lick et al. (1993) studied the flocculation due to differential settling by using a disk flocculator.

Like all fine-grained particles, discharged drilling muds do not exist as individual particles, but rather as flocs. Field tests of water based drilling mud discharges performed by Ayers et al. (1981) indicate rapid flocculation. Field studies (Neff et al. 1989, Muschenheim et al. 1995, and Muschenheim & Milligan 1996) have shown that the flocculated drilling wastes can be found at considerable distances from drilling platforms in high energy environments. In laboratory studies, Xu (1988) investigated the flocculation of barite and bentonite, the major components of drilling muds, due to fluid shear using a Couette flocculator. Huang (1992) studied the flocculation due to both fluid shear and differential settling using real water based drilling muds from Santa Barbara oil platforms. The fluid shear effect was investigated using a horizontal Couette flocculator while the differential settling effect was tested using a disc flocculator. Curran et al. (2002) also studied the flocculation properties of water based drilling muds using a recirculating flume channel 6.25m in length and 0.5m in width and depth. All these previous studies were based on water based wastes, the only research using oily based wastes was that by Gerard (1996). The flocculation of oil based drilling wastes was

studied in a grid column, where the particle size was measured by a laser beam particle sizer. The effects of turbulent energy and concentration were examined.

Although those previous works have made contributions to understanding the flocculation processes, there is still no published work on the flocculation of synthetic based drilling wastes. This gap is the reason for the present study. It should also be mentioned that the results of flocculation experiments were affected by the limitations of available apparatus, especially the particle sizer (Xu 1988). Most of the previous works were conducted using Couette type flocculators and the particle sizes were analyzed using a Coulter counter or laser particle sizer. The Coulter counter utilizes an electrical sensing zone to measure the volume equivalent diameter. This method is not accurate for flocs and can only size a fairly narrow range (e.g., 2-40 μm) on a single pass through the aperture (McCave & Syvitski 1991). Most of the laser particle sizer use the laser diffraction principle and generate volume equivalent diameter. This method is only valid for very small particles (usually $d < 1\text{mm}$). Both the Coulter counter and laser particle sizer require the sampling process, this may cause the breakup of flocs and resulted a inaccurate measurement. The present research uses a different approach to investigate the flocculation due to fluid shear. The experiment was conducted using a blade type flocculator, and direct image analysis was employed to obtain particle size data. The results are compared with previous studies. The experiment apparatus and methods will be discussed in Chapter 3.

2.3 Settling Mechanisms

2.3.1 Terminal Settling Velocity of Spherical Particles

When a spherical particle falls from rest in a stationary fluid under the action of gravity, it is acted upon by two forces: a gravitational force F acting downwards and a resisting force R acting upwards. As a result, the particle will at first accelerate as it does in a vacuum, but unlike in a vacuum, its acceleration will be retarded due to friction with the surrounding fluid. As the resisting forces increase with the velocity, this force will eventually reach a value equal to that of the gravitational force. From this point on, the two forces will balance and the particle will continue to fall with constant velocity. Since this velocity is attained at the end of the acceleration period, it is called terminal velocity.

Consider a solid sphere of density ρ_s falling in a stationary fluid of density ρ_f under the action of gravity. Let D be the diameter of the particle, then $\frac{\pi D^3}{6}$ is its volume, and

$\frac{\pi D^3 \rho_s}{6}$ is its mass. The gravitational force is the difference between weight and

buoyancy

$$F = \frac{\pi D^3 \rho_s g}{6} - \frac{\pi D^3 \rho_f g}{6} \quad \text{Equation (2-8)}$$

where g is the gravitational acceleration.

By assuming that the resisting force R is a function of the diameter of the particle, its velocity u , and surrounding fluid density, ρ_f and viscosity, μ and conducting dimensional analysis, the R was obtained as:

$$R = kD^2u^2\rho_f \left[\frac{\mu}{Du\rho_f} \right]^s \quad \text{Equation (2-9)}$$

Where exponent s is the value that need to be determined for different flow conditions. From Equation (2-9), it can be seen that the drag force is determinable provided the exponent s is clearly determinable. This condition only exists for laminar flow (Michell 1970). For a spherical particle settling at its terminal velocity, the two opposing forces are in balance. By substituting s and k in equation (2-9) with 1 and 3π (Michell 1970), the terminal velocity is obtained as

$$u_t = \frac{D^2(\rho_s - \rho_f)g}{18\mu} \quad \text{Equation (2-10)}$$

Equation (2-10) is also called Stokes equation.

2.3.2 Drag Coefficient and Reynolds Number

The projected area of a particle is defined as the area of its profile when the particle is in its most stable position. For a spherical particle, this area A is

$$A = \frac{\pi D^2}{4} \quad \text{Equation (2-11)}$$

By substituting equation (2-11) into equation (2-9), the resistance force is obtained as

$$R = C_D \frac{\pi D^2 u^2 \rho_f}{8} \quad \text{Equation (2-12)}$$

where $C_D = \frac{2kD^2}{A} \left[\frac{\mu}{Du\rho_f} \right]^s$ Equation (2-13)

The C_D in Equation (2-13) is called the drag coefficient

For a particle settling at its terminal velocity u_t , the two opposing forces, F and R , are in a balance, making use of equation (2-8) and (2-13)

$$u_t = \sqrt{\frac{4}{3C_D} \frac{D(\rho_s - \rho_f)g}{\rho_f}} \quad \text{Equation (2-14)}$$

From the equation (2-14), it can be seen that terminal velocity can be calculated provided the drag coefficient is known.

By analogy to flow in pipes, it may be assumed that resistance in laminar flow motion is inversely proportional to the dimensionless group of terms known as the Reynolds number defined as

$$Re = \frac{Du\rho}{\mu} \quad \text{Equation (2-15)}$$

It can be seen from equation (2-13) and (2-15) that the drag factor is some function of the Reynolds number. For spherical particles in the laminar range ($Re < 0.2$), the relationship between C_D and Re may be obtained

$$C_D = \frac{24}{Re} \quad \text{Equation (2-16)}$$

Figure (2-1) is a logarithmic plot of C_D versus Re for spherical particles. For the laminar range, by substituting equation (2-16) into equation (2-14) for Re from equation (2-15), the equation (2-14) becomes the Stokes Equation as equation (2-10).

It can be seen from the above analysis that the settling velocity can be obtained provided the C_D vs Re relationship is known.

No regular relationship exists between C_D and Re for the transitional range and turbulent ranges ($Re > 0.2$). The curve within this range is described by a number of investigators for spherical particles and these equations are shown in Table (2-1).

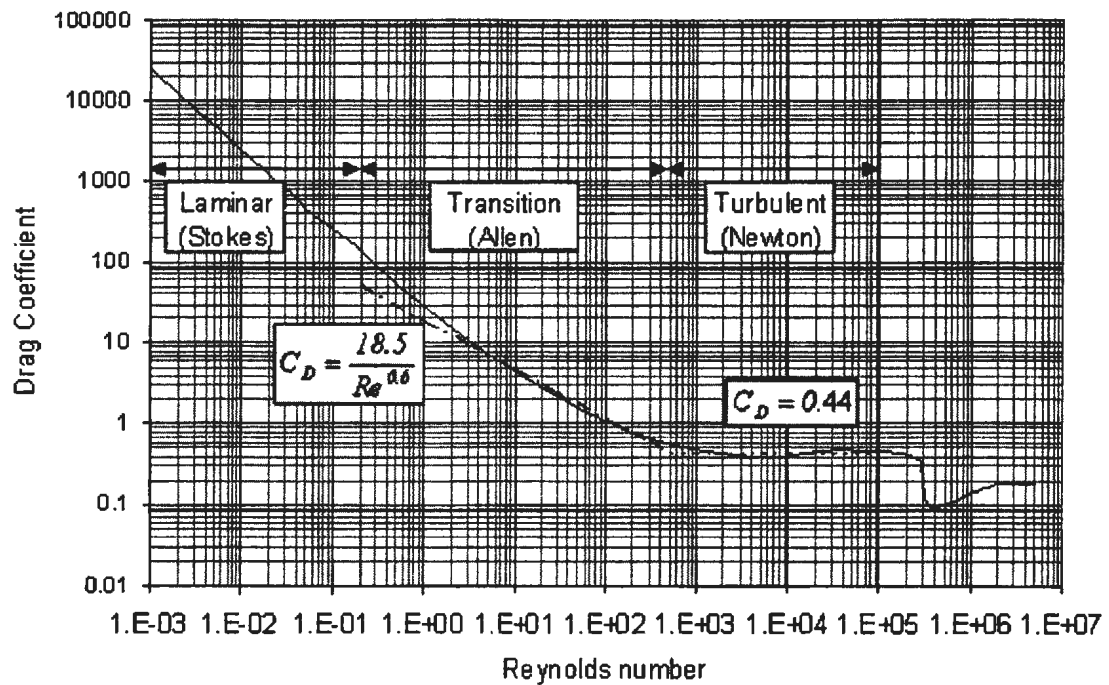


Figure 2-1 The drag coefficient (C_D) vs Reynolds number (Re) for spherical particles

Table 2-1 Relationship between Reynolds number and drag coefficient for spherical particles

Author(s)	Range	Relationship for C_D
Schiller and Naiman	$Re < 800$	$\frac{24}{Re} (1 + 0.15 Re^{0.687})$
Lapple	$Re < 1000$	$\frac{24}{Re} (1 + 0.125 Re^{0.72})$
Langmuir and Blodgett	$1 < Re < 100$	$\frac{24}{Re} (1 + 0.197 Re^{0.63} + 2.6 \times 10^{-4} Re^{1.38})$
Allen	(a) $2 < Re < 500$ (b) $1 < Re < 1000$	$10Re^{-1/2}$ $30Re^{-0.625}$
Gilbert et al.	$0.2 < Re < 2000$	$0.48 + 28Re^{-0.85}$
Kurten et al.	$0.1 < Re < 4000$	$0.28 + \frac{6}{Re^{1/2}} + \frac{21}{Re}$
Abraham	$Re < 6000$	$0.2924(1 + 9.06Re^{-1/2})^2$
Ihme et al.	$Re < 10^4$	$0.36 + \frac{5.48}{Re^{0.573}} + \frac{24}{Re}$
Rumpf	$Re < 10$ $Re < 100$ $Re < 10^5$	$\frac{24}{Re}$ $\frac{24}{Re}$ $\frac{0.5 + 24/Re}{Re}$
Clift and Gauvin	$Re < 3 \times 10^5$	$\frac{24}{Re} (1 + 0.15 Re^{0.687}) + \frac{0.42}{1 + 4.25 \times 10^4 Re^{-1.16}}$
Brauer	$Re < 3 \times 10^5$	$0.40 + \frac{4}{Re^{1/2}} + \frac{24}{Re}$
Tanaka and Inoya	$Re < 7 \times 10^4$	$\log_{10} C_D = a_1 w^2 + a_2 w + a_3$, where $w = \log_{10} Re$, and a_1, a_2, a_3 are given for 7 intervals or Re

*Reproduced from Clift (1978)

2.3.3 Time and Distance to Reach Terminal Settling Velocity

Assuming a spherical particle is falling from rest in a still fluid under the gravity force, the equation of motion for the particle settling may be expressed as

$$F - R = \frac{\pi}{6} \rho_s D^3 \frac{du}{dt} \quad \text{Equation (2-17)}$$

Substituting equation (2-8) and (2-12) into (2-17) and solving the equation, the time t required to reach terminal velocity is obtained as

$$t = \frac{4D^2 \rho_s}{3\mu} \int \frac{d(Re)}{S - C_D Re^2} \quad \text{Equation (2-18)}$$

where the S is the simplification of $\frac{4D^3 \rho_f (\rho_s - \rho_f) g}{3\mu^2}$.

By substituting equation (2-16) into (2-18), the time for laminar range becomes

$$t = \frac{D^2 \rho_s}{18\mu} \ln \frac{u}{u_t - u} \quad \text{Equation (2-19)}$$

At 99% of the terminal velocity, the equation (2-19) becomes

$$t = \frac{4.6D^2 \rho_s}{18\mu} \quad \text{Equation (2-20)}$$

For turbulent range, by substituting C_D in equation (2-18) with 0.44, which is a approximate value for turbulent range shown in Figure (2-1), the time t required to reach terminal velocity is obtained as

$$t = \frac{1.52D\rho_s}{u_t \rho_f} \ln \left[\frac{(u_t + u)(u_t - u_0)}{(u_t - u)(u_t + u_0)} \right] \quad \text{Equation (2-21)}$$

where u_0 is the minimum velocity that makes particle Reynolds number reached turbulent range. By assuming u_0 equals to 0, at 99% of the terminal velocity, the equation (2-21) becomes

$$t = \frac{8.04D\rho_s}{u_t\rho_f} \quad \text{Equation (2-22)}$$

From equation (2-20) and (2-22), it can be seen that the time needed for a particle to reach terminal velocity is very short. For laminar range, it is usually several milliseconds. For turbulent range, for example in this research, all the D/u_t values obtained are less than 0.035 which means the maximum t in this research is 0.56s while the density is around 2kg/m^3 .

2.3.4 Size and Shape Characterization of Non-Spherical Particles

For spherical particles, the problem seems to have been solved through the analysis above. However, for any particle other than a sphere, the problem becomes hard to treat because of the influence of particle orientation and the lack of a single unambiguous dimension upon which to base dimensionless groups. Therefore, the size and shape of these non-spherical particles have to be discussed before going further.

A number of sizes and shapes can be presented when a non-spherical particle is viewed from different orientations and with different definitions even from the same orientation. The assigned size of irregular particles usually depends upon the method of measurement which includes sedimentation, sieve, microscopy and so on. It is impossible to characterize irregular particles only by one parameter due to the complex structure. However, in order to simplify the problem, equivalent diameters can be used. The particle thus can have a free falling diameter, Stokes' diameter, volume diameter, surface

diameter, projected diameter and so on. A complete explanation of these diameters has been given by Allen (1990).

For our purpose here, the settling mechanism of particles with different sizes and shapes in sea water is of interest and needs to be characterized. When dealing with this kind of motion, the parameters, such as the volume, surface area, and cross-sectional area normal to motion become important. Thus, selecting the volume equivalent diameter, which is defined as the diameter of a sphere which has the same volume as the particle, is suitable. If the volume and behavior of each single particle is known, along with the total volume of discharged drilling cuttings, the thickness and wideness of cuttings accumulation on seafloor can be predicted. However, to characterize the irregular particles, a diameter parameter only is not enough; a shape factor is needed as a second parameter. This is due to the fact that even with the same volume, particles with different shapes can have different settling velocities. The shape of solids (in physico-chemical meaning) has been discussed in many different fields of science. According to the purpose of the research and nature of particles, the shape factor is given by many different definitions, for example, sphericity, roundness, and elongation (Hawkins 1993). Through the comparison of these available shape factors, the degree of sphericity, ψ , defined as the ratio of the surface area of the sphere of same volume as the particle and the surface area of the particle, is selected here.

As described above, the sphericity can be calculated by

$$\psi = \frac{\text{Surface of Sphere of Same Volume as Particle}}{\text{Surface Area of Particle}} \quad \text{Equation (2-23)}$$

However, in practice, the volume and surface area of a discharged particle is hard to measure unless it has a unique shape (e.g. sphere, cube, and parallelopiped). The present research attempts to obtain data from the analysis of a number of two dimensional images. The surface area and volume of the particle cannot be measured by the technology used in this research and it is very time consuming to measure even with other technologies. Thus, some practical methods must be employed to estimate the volume, surface area and sphericity, and the method must be such that the obtained value approaches as closely as possible the degree of true sphericity.

Wadell (1932, 1933, and 1935)'s formula for approximating the shape of quartz grain was selected

$$\phi = \frac{d_{cn}}{D_C} \quad \text{Equation (2-24)}$$

where ϕ is the approximated degree of sphericity, d_{cn} is the diameter of a circle equal in size to the cross-section area of the particle. D_C is the diameter of the smallest circle which can circumscribe the grain, generally the longest diameter of the object (Luo 1998).

The difference between computed and actual sphericity for five geometric prototypes is listed in Table (2-2). It is shown from Table (2-2) that for spheres $\phi = \psi$. For other forms, the value of ϕ approaches that of ψ , except for No.5, which is a very flat and

rather square shaped solid. It should be noted that a circular disk obtains a maximum ϕ -value, while its actual ψ -value may be very low. Therefore, this method is not valid for very flat particles. Most of the drilling cutting particles do not in general attain very flat shapes, so this approximation is valid. It should also be noted that according to the drill bits and type of fluid used, a certain amount of cuttings with flat shapes will be produced. The settling velocity of flat shaped particles is quite different from particles with relatively spherical shapes. The settling velocity of flat shaped particle is very sensitive to the settling orientation as a different orientation will give a different settling velocity. The settling orientation of flat shaped particles may change during settling. As a result, the settling velocity will change during settling. This increases the difficulty in studying the settling velocity of flat shaped particles. In this study, the particles with flat shape were discarded.

Table 2-2 Difference between the ϕ and ψ for five geometric forms (Wadell 1935)

No.	Geometric Form	Dimensions (cm)	Volume	ψ	ϕ	Difference $\psi - \phi$
1	Sphere	Diam. 2.48	8	1.00	1.00	0.00
2	Cube	2×2×2	8	0.80	0.79	0.01
3	Parallelopiped	4×2×1	8	0.69	0.71	0.02
4	Parallelopiped With re-entrance	4×2×1	7	0.63	0.66	0.03
5	Parallelopiped	5×3.2×0.5	8	0.48	0.75	0.27
6	Parallelopiped	8×2×0.5	8	0.46	0.54	0.08

2.3.5 Settling Velocity of Non-Spherical Particles

A sphere is unique in that it presents the same surface to the oncoming fluid whatever its orientation is. Non-spherical particles are more difficult to treat because of the influence of shape and orientation. From equation (2-13) and (2-15), it can be seen that the drag coefficient as a function of Reynolds number varies with the position of the particle relative to the fluid motion. If the particle is a sphere, the cross-section areas A are the same for all orientations. If a particle is irregularly shaped, the cross-section area A varies with the particle position, thus the drag coefficient varies (Allen 1990). The drag coefficient as a function of Reynolds number for non-spherical particles can be correlated in the same way as for the spherical particles.

It has been shown by Wadell (1934) that the surface area and the size and degree of circularity of the cross-sectional area influence the numerical value of the drag coefficient as a function of Reynolds number. These factors are the most important factors influencing the fluid motion about the solid. Because the sphere has the greatest relative volume with the smallest surface area, the smallest cross-sectional area taken as an average of a great number of such sections, and a maximum degree of circularity in all cross-sectional planes, the sphere has the greatest settling velocity of any other solid of the same volume and density.

Other features that influence the settling velocity are the roughness of the surface and the roundness of the corners and edges (Wadell 1934). The influence of surface roughness is comparatively small and can be neglected. The roundness of the corners and edges of a

solid is recognized as an important factor that affects the settling. Vortices are more readily formed in the presence of sharp corners and edges than in the case of well rounded ones.

2.4 Previous Work on Settling

Traditionally, experimental results of settling velocity studies have been used to develop a graph of the dependency of C_D on Re . From such a graph, it is possible by iteration to estimate the settling velocity knowing the particle size. Similarly, particle size can be calculated if settling velocity is known.

The C_D versus Re relationship for spherical particles has been studied by a number of investigators and a series of equations developed are summarized in Table (2-1). For non-spherical particles, the drag coefficient as a function of Reynolds number for solids of various shapes has been reported by Wadell (1934). Many other studies on the settling of non-spherical particle were reviewed by Hoerner (1958) and Torbin & Gauvin (1960).

Among those previous works, Gibbs et al.'s (1971) and Sleath's (1984) work will be mentioned here because of their application in some transport models. Gibbs et al. (1971) studied the settling of glass spheres and derived an experimental relationship for spherical particles of density ρ_s falling in a fluid of density ρ_f

$$u_t = \frac{-3\mu + \sqrt{9\mu^2 + gr^2(\rho_s - \rho_f)(0.015476 + 0.019841r_a)}}{(0.011607 + 0.14881r_a)\rho_f} \quad \text{Equation (2-25)}$$

where u_t is the settling velocity in cm/sec, μ is water dynamic viscosity in poises, r_a is the sphere radius in cm, g is the acceleration of gravity in cm/s^2 , ρ_s and ρ_f are in g/cm^3 .

This equation has been employed by Arcilla et al. (1998) in a three dimensional model to simulate the pollutant dispersion for near and far fields in coastal waters. Another application of this equation is deMargrie (1988) in the modeling of drill cuttings discharges. Sleath (1984) reported the settling velocity for quartz particles at the range $90 > D > 3 \text{mm}$ with three different shape factors ($S.F.$)

$$\begin{aligned} S.F. = 1.0 & \quad u_t = 6.5D^{1/2} \\ S.F. = 0.7 & \quad u_t = 4.2D^{1/2} \\ S.F. = 0.3 & \quad u_t = 2.8D^{1/2} \end{aligned} \quad \text{Equation (2-26)}$$

The $S.F.$ is calculated by

$$S.F. = \frac{D_1}{(D_2 D_3)^{0.5}} \quad \text{Equation (2-27)}$$

where the D_1 , D_2 , D_3 are respectively the lengths of the shortest, intermediate, and longest mutually perpendicular axes.

And for $D < 0.1 \text{mm}$.

$$u_t = 92 \times 10^4 D^2 \quad \text{Equation (2-28)}$$

The equation (2-26) with the $S.F.=0.7$ has been used by Hodgins & Hodgins (2000) in the modeling of drilling cutting deposition.

The studies discussed above mainly focused on coarse particles. In a given fluid, the settling velocity of fine grain particles also increases as the particle diameter is increased, although the rate of increase is different for coarse particles. For the settling of cohesive sediments, due to the effects of flocculation, the particles will settle in clusters with fall velocities many times larger than the isolated particles. In these cases, the Stokes' law is not directly applicable, because it is only valid for slow falling ($Re < 0.5$) impermeable spheres. However, many investigators have attempted to extend its application to other shapes and higher Reynolds numbers by using empirically determined correlation factors (Graf 1971, Raudkivi 1976). Migniot (1989) proposed an equation for the settling of aggregates using the flocculation factor

$$W_{s,agg} = Fa \times W_{s,part} \quad \text{Equation (2-29)}$$

where the $W_{s,part}$ is the Stokes' settling velocity, in the form of equation (2-10), and Fa is the flocculation factor given as

$$Fa = 250D^{-1.8} \quad \text{Equation (2-30)}$$

For natural aggregates, their densities cannot be measured directly. The usual procedure has been to assume Stokes' equation is correct and calculate density from measurements of the particle size and velocity. McCave (1975) reviewed previous determinations of this type, developed a formula which predicts the aggregate's density as a function of size, and used his results to calculate aggregate settling velocities using Stokes' equation. After measuring of over 200 oceanic aggregates with diameters between 50 and 100

microns, Kawana and Tanimoto (1976, 1979) fitted their result with an equation of the form

$$u_t = aD^b \quad \text{Equation (2-31)}$$

where a , and b are constants determined empirically. The same form was also given by Kajihara (1971), and Gibbs (1985a, 1985b). The studies by Kawana & Tanimoto (1976, 1979) show that the aggregates settle far more quickly than McCave (1975) predicted, this reason for this is that the fluid flow around a settling flocs is relatively turbulent rather than laminar due to the porous structure and irregular shape of floc, which is not the case for Stokes' law.

For the turbulent effect on the settling of aggregates, Van Leussen (1994) utilized a formula which modifies the settling velocity in still water, by a growth factor due to turbulence divided by a turbulent disruption factor

$$W_s = W_{s0} \frac{1 + aG}{1 + bG^2} \quad \text{Equation (2-32)}$$

where W_s is the settling velocity, G is the root mean square of the gradient in turbulent velocity fluctuations, and a and b are the empirically determined constants. W_{s0} is the reference settling velocity, which is given as

$$W_{s0} = kC^m \quad \text{Equation (2-33)}$$

where k is an empirical constant and m is the exponent.

Based on the assumption that flocculated mud could be represented by a self-similar fractal structure, a more complex equation was proposed by Winterwerp (1998)

$$W_s = \frac{\alpha}{18\beta} \frac{(\rho_s - \rho)}{\mu} D_p^{3-nf} \frac{D_p^{nf-1}}{1 + 0.15 \text{Re}^{0.687}} \quad \text{Equation (2-34)}$$

where α and β are empirical constants, and D_p is the diameter of the primary particle and nf is the fractal dimension which appears to vary between 1.4 and 2.5.

Although settling speeds of flocs in both freshwater and seawater have been observed and studied by many investigators (Kajihara 1971, Silver & Alldredge 1981, Hawley 1982, Gibbs 1985a 1985b, Van Leussen 1994, Winterwerp 1998 etc.), the settling velocities of flocs are not well known, and in particular, the parameters on which these settling velocities depend are not well understood (Burban et al. 1990). In the references cited above, many types of particles have been studied and in most cases the settling velocity was given as a function of diameter, see equation (2-30). The empirical constants a and b probably depend on the type of particles being investigated and the condition under which the flocs were produced. For the synthetic based drilling wastes, no previous research can be found to provide such information, therefore, one of the key purposes of the present work was to measure the settling velocity of flocs produced from the flocculation of synthetic based drilling waste under turbulent shear in both fresh and sea water and in this way, to determine quantitatively the dependence of settling velocity on these parameters as well as on the diameter.

2.5 Summary

The flocculation mechanism was discussed in section 2.1. A flocculation model by Lick & Lick (1988) was described. Previous work on flocculation of both natural sediments and WBFs were reviewed in section 2.2. The settling mechanisms of both spherical and irregular particles in stationary fluids were discussed in section 2.3. It was shown that the drag coefficient correlation is important in obtaining the settling velocity equation. The previous works on the settling of both individual particles and flocs were described in section 2.4. Several settling velocity equations were reviewed.

Chapter 3

Experimental Methods and Apparatus

3.1 Sample Preparation

In this study, rock cuttings from the drilling of a production offshore well on east coast Canada using synthetic based drilling fluids were used. The cuttings produced from section 3050-3069 and section 3070-3090 was collected directly from the shale shaker. As described in Chapter 1, SBF cuttings containing several percent adhering SBF do not disperse effectively in the water column following discharge, rather they settle rapidly as clumps of solids through the water column and accumulate on the bottom near the platform discharge site. Depending on the rate of deposition, potentially harmful concentration may accumulate in the sediments near the discharge site (U.S. MMS 2000). The rate of settling of SBF cuttings through the water column and the areal extent and concentrations of cuttings accumulating on the bottom depend on the density and size distribution of settling particles, water depths, and the three dimensional water current regimes in the water column. Offshore waste treatments remove parts of the oily components from cuttings and change the physical properties of cuttings, such as density and particle size distribution. After the treatment, SBF associated cuttings can have relatively low density and small median diameter, which makes the treated cuttings more

dispersible and lower environmental risk. The treatment methods can be centrifuge, thermal, combustion, solvent extraction and others. Drying is an important method for treating drilling cuttings; it can be used independently or usually together with other methods. In the present work, the drying method was selected to remove the oily and evaporation components from SBF cuttings. An evaluation of treatment methods is being done by Worakanok Thanyamanta, an M.Eng student in the Faculty of Engineering & Applied Science, MUN, under the NSERC supported project.

3.1.1 Sample Preparation of Drying Treated Cuttings

A 2 kg sample was taken from each of the two bulk drilling cutting samples. The sample was placed on an aluminum pan and put in an oven at 110°C for 24 hours. The sample was weighed and then loaded into the top sieve of a sieve stack (75 μ m, 106 μ m, 150 μ m, 250 μ m, 300 μ m, 425 μ m, 595 μ m, 850 μ m, 1.18mm, 2mm, 2.36mm, 2.5mm, and 5.0mm).

The sieve stack was loaded in a sieve shaker, which is located in the soil laboratory at Memorial University of Newfoundland, and shaken for 10 minutes. The cuttings in each sieve were carefully removed to labeled aluminum pans and weighed. The percent retained on each sieve was calculated and the results are shown in Figure (3-2).

The sieve test results show that around 4 percent of particles from formation 3070-3090 and 2 percent of particles from formation 3050-3069 are finer than 100 μ m. This percent would likely increase with the shaker running time due to the fragile property of the dried

cuttings. From Figure (3-2), it is shown that the particles are finer from the 3070-3090 section than from the 3050-3069 section. Figure (3-3) shows the untreated and dried cuttings.



Figure 3-1 The stack of sieves on the analytical shaker

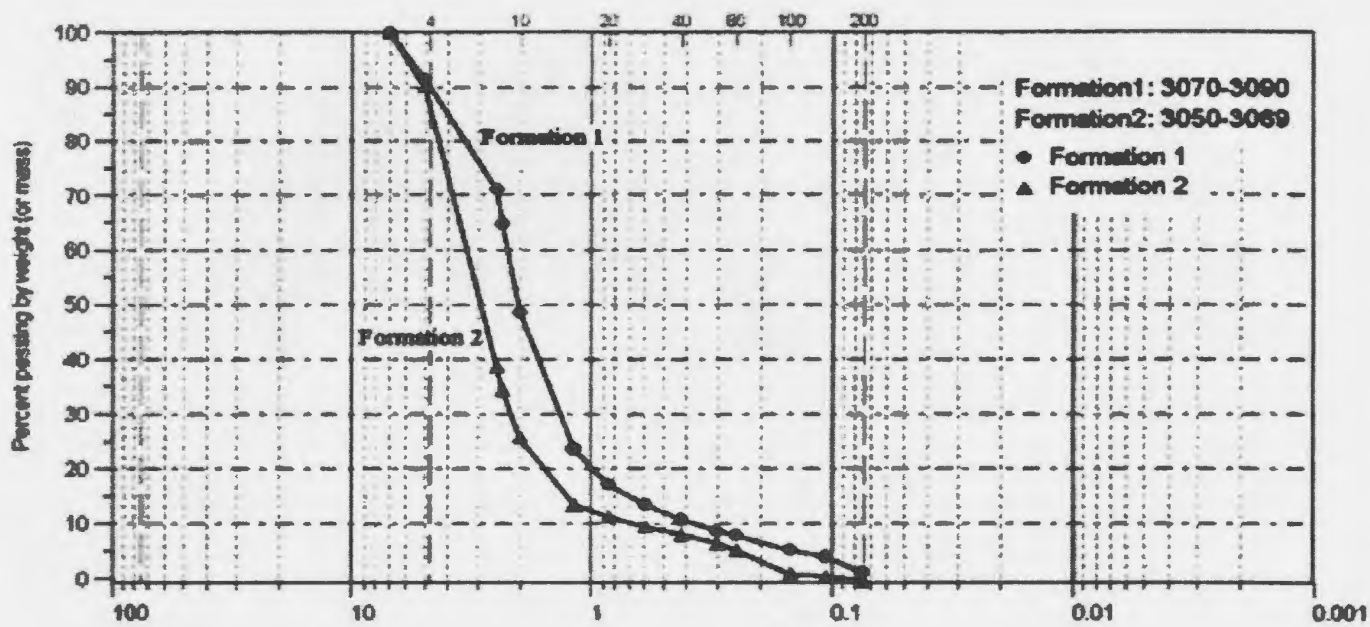


Figure 3-2 Particle size distribution of dried drill cuttings (the horizontal axis is the particle diameters, in mm)

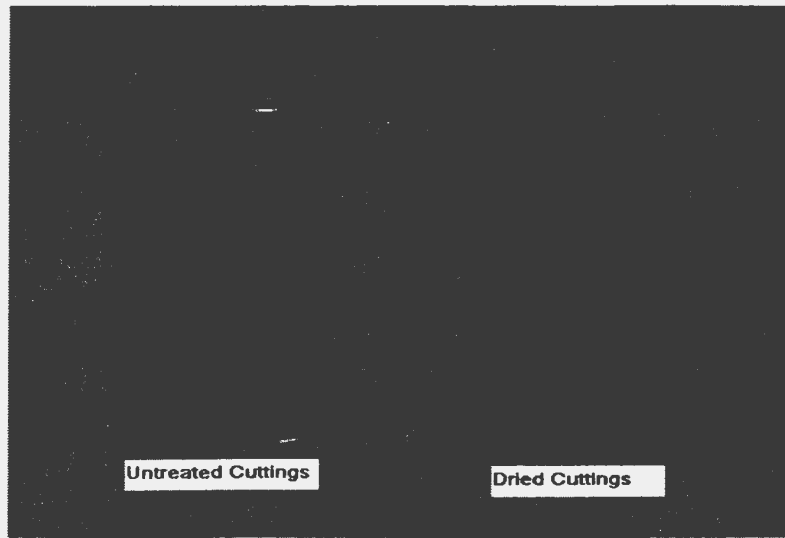


Figure 3-3 Untreated Cuttings and Dried Cuttings

The dried particles were then dumped into containers with freshwater, or synthetic seawater (a solution of synthetic sea salts) depending on the experiment, until fully mixed. The advantages of synthetic seawater are that it has good water quality, high solubility and pureness and can be prepared quickly. The salinity of the synthetic seawater was 34.86, which is the monthly average value at the sampling site. The suspensions with particles larger than $75\ \mu\text{m}$ were then ready for the settling test. For the flocculation tests, the present work investigated fine grained particles in the range of 1 to 40 microns. The suspensions with particle sizes less than $75\ \mu\text{m}$ were filtered using a $40\ \mu\text{m}$ sieve to remove the coarse particles. The sample was then stored in sealed containers. Before the flocculation test started, the concentration of the suspension with particle size less than $40\ \mu\text{m}$ was measured by a filtration method. The suspension was then diluted to the

desired concentration (50mg/L, 100mg/L, 200mg/L, and 400mg/L) in a 2-liter test beaker and was then ready for the flocculation test.

3.1.2 Sample Preparation of Untreated Cuttings

As the untreated wet cuttings exist as wet large clumps, they are not suitable for immediate tests and must be pre-separated. The reason for pre-separating for the flocculation tests is that only the particles smaller than 40 μm were of interest, so the coarser particles had to be removed. For the settling column test, since there was no external force (e.g. turbulence) present, the large clumps were not easy to separate within the relatively short testing time. In order to get enough data points with different diameters, the coarse particles were separated before conducting the column settling test. A simplified wet sieve method was used in the present work to do the pre-separating work.

A sieving tower (5mm, 2.5mm, 2mm, 1.18mm, 595 μm , 250 μm , and 40 μm) was assembled with the coarsest sieve on top and the finest sieve at the bottom, underlain by the fine material pan. The untreated wet cuttings were poured carefully onto the top sieve. The sample was spread evenly with a soft brush and then flushed gently using a squirting plastic bottle with freshwater (or seawater depending on the experiment) until it disintegrated. The process was repeated from the top sieve to bottom sieve until enough samples were obtained on each sieve. The retained materials were collected from each

sieve and dispersed in freshwater (or seawater depending on the experiment) at which time the sample was ready for the settling column test. The particles in the bottom fine material pan were allowed to settle and the top suspension was then removed. The residual suspension was transferred into a sealed container and the concentration was measured. Before the flocculation test started, the concentration of the suspension with particle sizes less than $40\mu\text{m}$ was checked by a filtration method. The suspension was then diluted using freshwater (or seawater depending on the experiment) to the desired concentration (50mg/L, 100mg/L, 200mg/L, and 400mg/L) in a 2-liter test beaker after which it was ready for the flocculation test.

3.2 Flocculator

The flocculation experiment can be conducted by using a Couette viscometer, jar test stirrer, baffled mixer, small-bore tube, granular filter or fluidized bed (Ives 1978b). Among these devices, the Couette viscometer and jar test stirrer are the most commonly used.

The Couette type viscometer basically consists of two concentric cylinders with one rotating relative to the other. In this way, a velocity gradient is generated in the fluid in the annular gap between the cylinders. By rotating only the outer cylinder, the generated velocity gradient across the annular gap is calculated as

$$G = \frac{2\omega R_1 R_2}{R_2^2 - R_1^2} \quad \text{Equation (3-1)}$$

where R_1 is the outer radius of the inner cylinder and R_2 is the inner radius of the outer cylinder, and ω is the velocity of outer cylinder. The advantage of this type of flocculator is that the shear stress generated is well defined, fairly uniform, and easy to adjust to a desired value. A detailed analysis of this type of flocculator can be found in the references by Van Duuren (1968) and Iacobellis (1984). The Coutte type of flocculator has been used recently by Tsai et al. (1987) for a flocculation study of fine-grained lake sediments, by Xu (1988) on bentonite and barite, and by Huang (1992) on water based drilling mud.

The waterworks laboratory test of paddle stirring in beakers, known as the jar test, has been used for more than eighty years and is still widely used in the evaluation of flocculation processes. A stirrer with flat paddles has traditionally been used as the impeller in the jar test. A 2 liter square-beaker is often used. Although most jar test apparatus are similar, they are not identical, and there is no standard design. The comparison of variations in the design and operation of jar test is based on the mean velocity gradient, which is defined by Camp and Stein (1943) as:

$$G = \frac{du}{dz} = \sqrt{\frac{W}{\mu}} \quad \text{Equation (3-2)}$$

Where G is the velocity gradient (s^{-1}), W is the dissipation function or power input per unit volume of fluid, and μ is the absolute viscosity of the fluid. By substituting W in equation (3-2) with power per unit volume, we get:

$$G = \sqrt{\frac{P}{V\mu}} \quad \text{Equation (3-3)}$$

where P is the power dissipated in the water (Watt), μ is the viscosity (N-s/m²), and V is the volume of the suspension (m³).

Normally there are two approaches that can be used to determine the power transmitted from the stirrer blade to the water. The first approach requires a sensitive torque meter (0.01-0.2 Nmm) on the stirrer drive shaft. The power is then calculated by (Bhole 1970, Camp 1968, Lai et al. 1975, Wagner 1993):

$$P = T_q \cdot \omega \quad \text{Equation (3-4)}$$

The second approach is to calculate P from the drag force on the paddle blade multiplied by the velocity of the blade relative to the suspension. The drag force is the Bernoulli dynamic pressure $\rho(v_p - v)^2/2$ multiplied by the area A_p and the drag coefficient C_D . Therefore the power P is given by Ives (1978b) as:

$$P = C_D A_p \rho \frac{(v_p - v)^3}{2} \quad \text{Equation (3-5)}$$

However, the drag coefficient C_D and the velocity of the suspension v in equation (4) are difficult to determine. The value of C_D has been assumed in various publications to be between 0.8 and 2.0 when the value of the relative velocity ratio v/v_p has been reported to be between 0.25 and 0.53.

Although the power dissipated cannot be estimated theoretically, it can be studied by the same type of quantitative experiments, guided by dimensional analysis. Through the dimensional analysis of McCabe & Smith. (1967) and experimental results of Rushton et al. (1950), it was shown that the geometry of the tank has almost no effect on power input; the blade with the same projected area produces the same velocity gradient, and the variation of distance of the blade from the beaker bottom did not change the power input. These conclusions are in agreement with Camp (1969) and Lai et al.'s (1975) experiment results. By assuming the liquid is Newtonian, the power P is given as (McCabe & Smith 1967)

$$P = \frac{K_L n^2 D_a^3 \mu}{g_c} \text{ (Laminar Flow)} \quad \text{Equation (3-6)}$$

$$P = \frac{K_T n^3 D_a^5 \rho}{g_c} \text{ (Turbulent Flow)} \quad \text{Equation (3-7)}$$

where P is the power, n is the rotation speed, D_a is the paddle diameter, μ is the dynamic viscosity, ρ_f is the liquid density, g_c is the Newton's-law conversion factor (32.17 lb-ft/lbf-s²), and K_T , and K_L are empirical constants.

For the present research, a Phipps & Bird Six Paddle Stirrer (Model 7790-400), see Figure (3-4), and a 2 liter square beaker were employed. This instrument located in the environment laboratory at Memorial University of Newfoundland. The paddle of this stirrer is a 2-flat blade paddle with a length of 76mm and width of 25mm. The velocity gradient of this kind of paddle in 2 –liter rounded or square beaker has been measured by a number of investigators (Camp 1968; Cornwell et al. 1983; Lai et al. 1975; Wagner

1993). The data by Wagner (1993), which shows the relationship between velocity gradient and rotation speeds (Figure 3-5), was directly used for this study. For other beakers using the same stirrer, the G versus rotational speed relationship can be calculated by equation (3-6) and (3-7) from the constants K_T and K_L , which can be obtained from the analysis of experimental data presented in Figure (3-5).

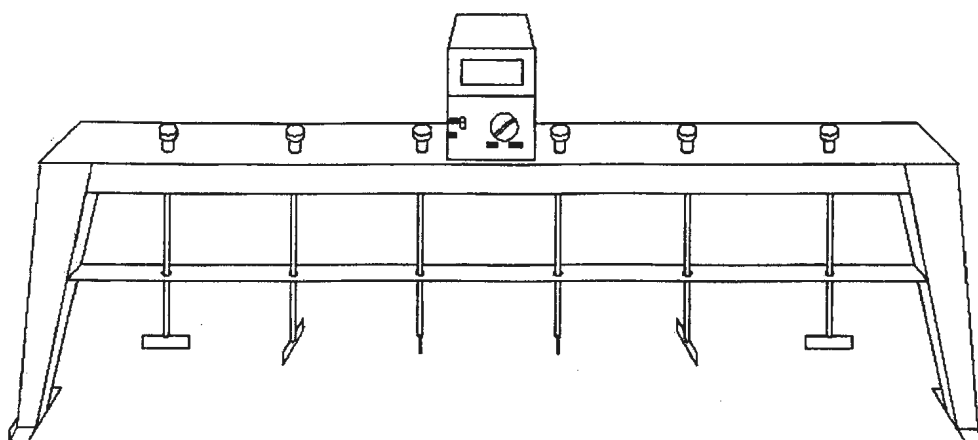


Figure 3-4 Phipps & Bird Six Paddle Stirrer

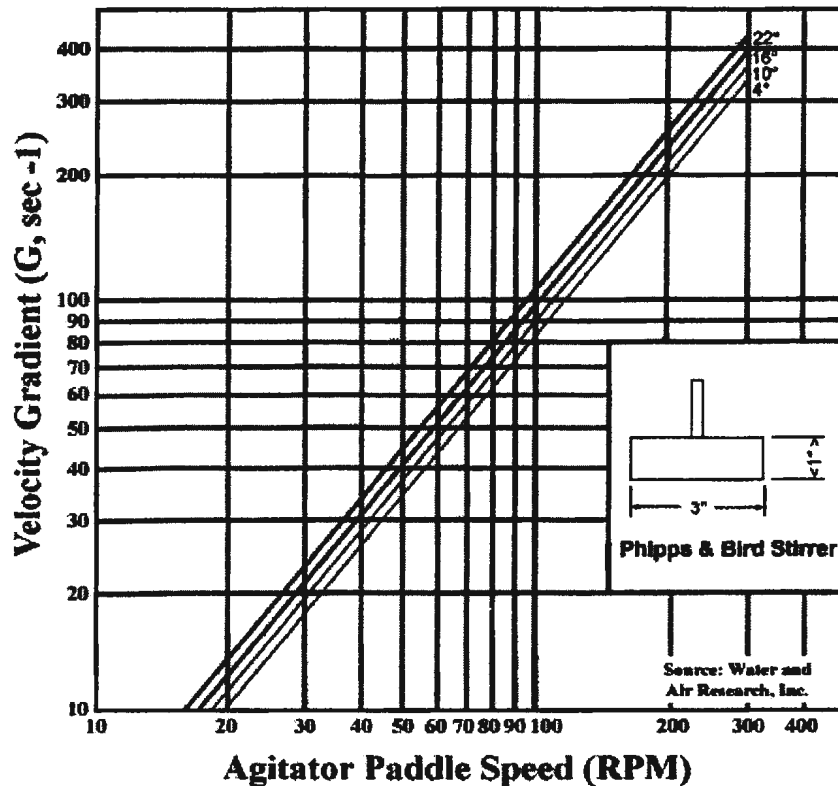


Figure 3-5 Velocity Gradient vs RPM for a 2-liter Square Beaker Using a Phipps & Bird Stirrer, Source: Wagner (1993)

3.3 Settling Column

The column shown in Figure (3-6) was used in this work for drilling wastes settling tests. The column is constructed of 14-cm-inner diameter Plexiglas tubing and could be easily cleaned. The total height of the column is 250cm and 5 ports are provided for extraction of samples at various depths during testing. The distance between the sample ports is 40cm each.

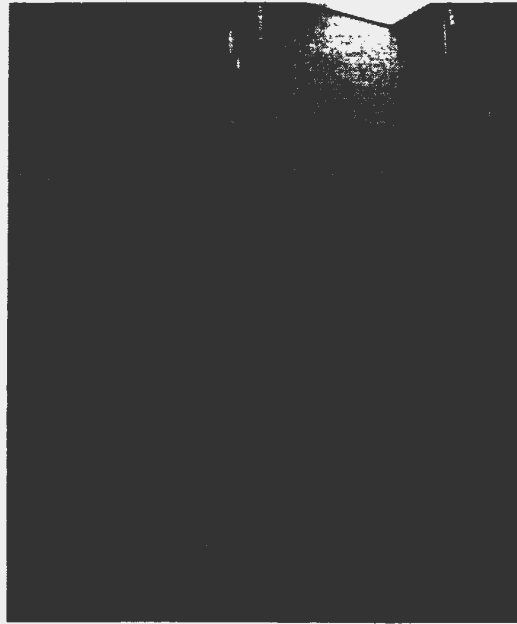


Figure 3-6 Settling Column

3.4 Digital Imaging System

Imaging technology has been used in many fields for several decades. Advantages of digital imaging systems are that they can be non-intrusive (Chen & Fan 1992) and realistic aggregate images can be obtained (Eisma et al. 1990). An imaging system consists of digital data (imaging acquisition), storage, processing, and display. These functions are easily integrated into computer systems using a digital video camera, optical system (lens, extension tubes) and lighting system.

The lighting system is the most important component for the digital imaging system. With different lighting techniques, the resulting image types will be different. A well selected lighting method can provide the best quality images for analysis while a badly

lighted image will be hard to interpret. The light scattering and back lighting methods are two commonly used illuminating methods and both were considered in the present study.

The light scattering image is produced when an illuminated image is viewed from an angle different from the angle of light. The light scattering method is useful, but there are problems with calibration and with obtaining detailed information for irregular shaped particles (Berkelmann & Renz 1988). In a back lighting setup, light is transmitted from the back of the test cell so that particles appear as dark images against a light background. Either a coherent light source, such as a laser, or a diffusive light source, such as a regular light bulb, can be used as the backlight source. If a coherent source is used, a diffraction fringe pattern is formed on the image. Oberdier (1984) used this pattern as a means of focus discrimination in size analysis. However, as pointed out by Zhang & Talley (1990), this diffraction fringe pattern is only good for spherical particles because a non-spherical particle can introduce complications as a result of fringe interference from different parts of the same particle. Since both the flocs and coarse cuttings in the present study are non-spherical particles, problems were anticipated with the use of a coherent light source. Diffraction patterns can be eliminated with the use of a diffusive light source. The advantage of this method is that the shape of an object can be seen. In addition, this type of image is independent of the particle's refractory properties. With sufficient magnification, this technique is similar to inspecting an object with a microscope with light transmitted from the back of the object. However, a balance must be obtained among lighting, camera and optics, and the size of particle studied.

Because the lighting is critical for image quality, several approaches were examined in an effort to obtain the best quality images using diffusive light sources. For the settling column test, a back lighting technique that consisted of two 500W halogen photography lamps reflected off a white wall was used. However, for the jar test, it was hard to get good quality images using the backlighting method due to the depth of the test cell. Therefore, a photography lamp with a convex focus lens was installed at a 90° angle to the camera and to light the front area the test cell. With this technique, images with a number of white particles appearing on the black background were obtained.

The system configurations for both the settling column test and jar test are shown in Figure (3-7).

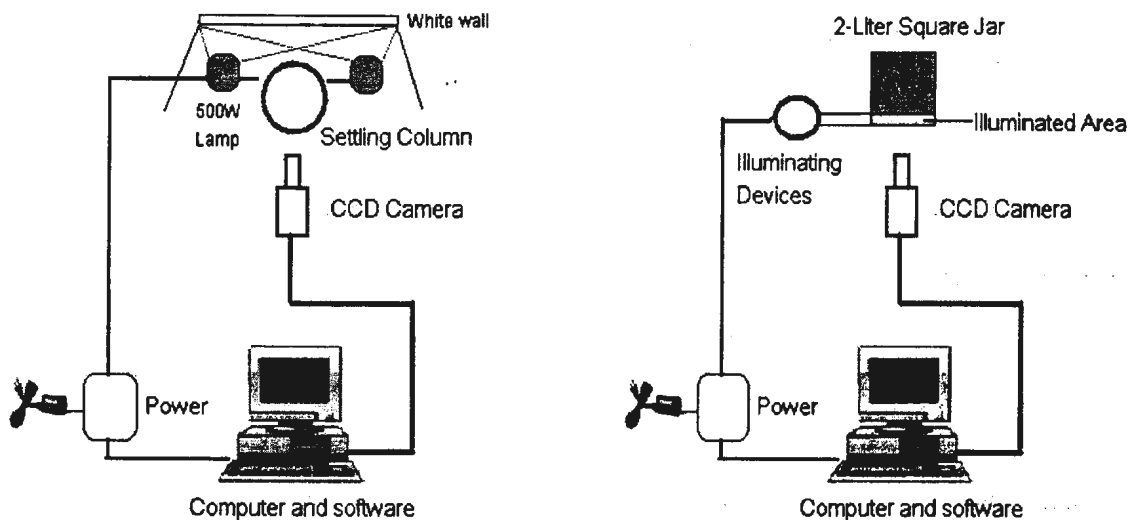


Figure 3-7 System configuration for settling column test and jar test

3.4.1 Camera and Lens

The camera system includes a CCD camera, 3 lenses, and 3 extension tubes. The CCD camera used in the present study is a MotionScope PCI 1000s model. The camera can record a sequence of digital images at a pre-selected frame rate between 60 to 1000 fps (frames per second), and store the frames in an image memory on the controller unit. The CCD sensor of the camera has a resolution of 656×495 pixels with each pixel occupying 7.4 square microns (Hiscock 2000). Although the system is capable of recording images at 1000 fps, a frame rate of 60 fps was selected throughout the present tests. The time between two continuous images was 1/60 seconds.

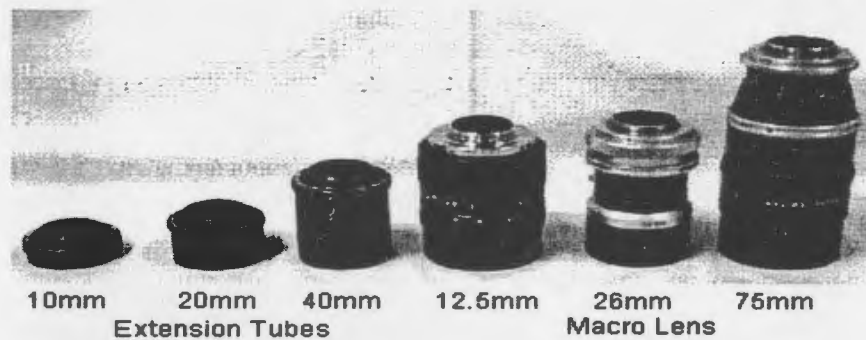


Figure 3-8 Lens and extension tubes

Three macro-lenses, $f=12.5\text{mm}$, 26mm , 75mm , and three extension tubes, 10mm , 20mm , 40mm were selected in the present work, as shown in Figure (3-8), which provide a high magnification and enable the system to capture the particles as small as 1 micron. Guidance on the selection of lenses and calculation of magnification can be found in Howard (2000).

3.4.2 Image Processing

Computer images generally are in raster format. This means that they consist of a number of points containing information of light intensity and color. The simplest image is in binary format. Each pixel of a binary image can be either black or white. Thus, only one bit (taking values of 0 or 1) for each pixel is sufficient to store an image. By contrast, a full color image requires storing many more bits of information than a binary image. A popular image format is an eight-bit gray scale format that contains 256 possible gray levels for each pixel and is used by most of the PIV systems.

The images recorded from the present work were stored as gray scale JPEG (Joint Photographic Experts Group) format. Using the edge detection algorithm, sharp edged particles (in focus) are first separated from those which were out of focus by introducing a user defined threshold level. The pixels that have very low gray level are eliminated by this process. Once threshold is complete, the image is transformed into a binary (black-white) format to count particles. Because the particles appear black in the binary image, the algorithm uses a scanning routine to find a pixel with a black value (normally the value 1). When such a black pixel is found, an image boundary search is then performed to trace the boundary of the particle until the initial pixel is encountered again. The particle is then labeled and the centroid and other values are computed. The scanning and boundary searching routines are then resumed until the whole image is processed. This “trace” procedure is usually done automatically in image processing packages.

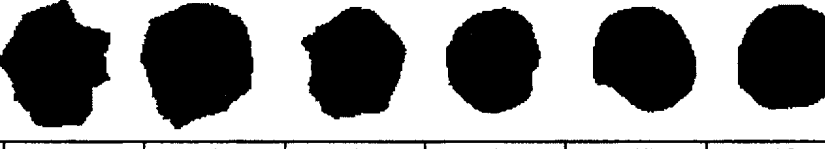
Many image analysis software packages are available both commercially and in the public domain. On one hand, the commercial packages, like Image Pro Plus, are usually expensive and are often designed for special applications. On the other hand, Image Java (IJ) and Image Tool (IT) that are available in the public domain provide nearly the same capabilities as most commercial packages and are widely used in the medical imaging community.

IJ is an image processing program developed by the U.S. National Institute of Health and can be run under any Microsoft Windows operating system. IJ was designed with an open architecture that provides extensibility via Java plugins. Custom acquisition, analysis and processing plugins can be developed using IJ's built in editor and Java compiler. User-written plugins make it possible to solve almost any image processing or analysis problem.

Because of the very limited functions of basic IJ, which identify particles from either a single image or stacks and only give information of area, gray level, centroid, and perimeter, a user-written plugin is needed in this research to obtain the sphericity value. Chinga (2002) has written a plugin which can calculate the roundness, compactness, form factor and aspect ratio (the definition of these shape values can be found in Russ 1999 and Hawkins 1993). By modification of Chinga's (2002) plugin, a shape description plugin (see Appendix) was developed which calculates the particle sphericity and diameter using Wadell (1932, 1933, and 1935). The particles from Rawle (1994) was

calculated using the IJ and the shape description plugin and the results are listed in Table (3-1).

Table 3-1 Shapes description of irregular particles of Rawle (1994)

							
	#1	#2	#4	#3	#6	#5	Low Sphericity
Elongation	1.4943	1.6919	1.5992	1.5257	1.3969	1.6257	
Roundness	0.5355	0.6406	0.5372	0.685	0.7625	0.7464	
Sphericity	0.8181	0.7688	0.7908	0.7992	0.8462	0.7843	
							
	#7	#12	#8	#9	#11	#10	Medium Sphericity
Elongation	1.5868	1.3837	1.4119	1.2439	1.3285	1.4396	
Roundness	0.6033	0.6574	0.6849	0.7393	0.811	0.7825	
Sphericity	0.773744	0.79925	0.805197	0.844327	0.835991	0.842129	
							
	#14	#13	#15	#16	#17	#18	High Sphericity
Elongation	1.1242	1.1335	1.1043	1.1582	1.1652	1.0543	
Roundness	0.6678	0.7457	0.7347	0.8621	0.861	0.8572	
Sphericity	0.866352	0.893946	0.913172	0.924166	0.931384	0.958333	
	Very Angular	Angular	Sub Angular	Sub Rounded	Rounded	Well Rounded	

The obtained centroids of particles in images can give the coordinate information of particles. With the known coordinates of one particle in an image stack (six images) and

the time between two images (1/60 seconds), the average settling velocity (five settling velocities) of the particle is calculated.

Several other functions are available in IJ to process some of the marginal quality images. These functions include contrast enhancement, which is done by balancing brightness and contrast, and edge enhancement, in which a high-pass filter is used to sharpen the images of individual particles. The results produced by IJ and It can be stored in text format for further analysis.

3.5 Experimental Methods

3.5.1 Procedure for Flocculation Test

After the initial sample with desired concentration was prepared in a 2 liter square beaker as mentioned in the previous section, the samples were loaded with the flocculator at high speed for 90 seconds. There are two reasons for this procedure. First, the high speed rotation can overcome the gravitational force of particles and make the particles within the suspension evenly distributed. Second, high speed rotation can de-flocculate the aggregated particles. The initial particle size distribution was measured using the digital imaging system at this time. The flocculator was then run at a constant rotational speed to produce a desired G value (25, 50, 100, and 200s^{-1}). After a certain time (5, 10, or 20, 40, 60, 80, 100, and 120 minutes), the flocculator was stopped, and the images were taken using the digital imaging system and the particle distribution was obtained.

Both the treated and untreated SBF cuttings were used in freshwater and seawater tests. The solids concentrations were 50, 100, 200, and 400mg/L and the fluid shears used were 25, 50, 100, and 200s⁻¹. Tests on a total of 64 combinations were performed.

3.5.2 Procedure for Floc Settling Test

Three different tests were conducted: (1) seawater produced flocs using untreated cuttings settling in seawater (2) seawater produced flocs using treated cuttings settling in seawater, and (3) seawater produced flocs using both untreated and treated cuttings settling in freshwater.

Unlike the traditional settling velocity tests which are intrusive, the present approach did not require taking samples from suspension except for the third test condition. For the first two test conditions, the settling velocities of the flocs were measured directly at the end of a 2 hour flocculation period. At this time, the steady state of flocculation is believed to be reached (the particle size distribution does not change any more). In order to better approximate the process, a lag time of 30 seconds from the time of stopping the flocculation to the beginning of settling was allowed. This is about the time required for the fast rotary motion to subside. For the third test condition, because the water that was used to produce flocs was different from that used to settle, samples must be transferred from the test Jar to a settling cylinder at the end of flocculation. A pipette (Burban et al. 1990, and Huang 1992) with inner diameter of 3mm was used to transfer the samples in this test condition. Because the flocs are very fragile, the transferring must be very

careful. The taking of samples was done very slowly so as not to introduce appreciable currents and shears. In order to prevent possible breakup of flocs and to minimize the initial downward speed of flocs as the fluid from the pipette was introduced into the settling cylinder, the method of Burban et al. (1990) was used. The pipette was first partially immersed into the water in the settling cylinder and then slowly drawn across the water surface. The flocs were found to slowly spread over a wide area in this way. The camera was mounted around 30cm below the water surface in the cylinder to simultaneously measure the floc sizes and settling velocities.

As one (usually several) floc arrived in the scope of the camera, the camera recorded its motion at the rate of 60 frames per second, the resulting positions of the floc from a series of continuous images and the time interval between these images could be used to determine the settling velocity. In the present study, five settling velocities for each floc were used to calculate the average settling velocity and ensure the repeatability and accuracy.

3.5.3 Test Procedure for Column Settling Test

All the valves of the settling column were closed. The column was filled with freshwater (or synthetic seawater depending on experiment) to the height of 240cm about 16 hours before the test to let the rheological properties of the fluid stabilize and to release entrapped air bubbles. The prepared dispersed particles (the dispersion of particles in fluids can prevent the entrapment of air bubbles, which will affect the accuracy of

measurement) were dropped in clusters into the column from the top. The motion of settling particles were recorded by a digital camera that was mounted near the bottom of the settling column to ensure all the particles reached their terminal settling velocity before their coming into the scope of the camera. The recording rate and the method to obtain settling velocity were the same as the previously discussed floc settling test.

3.6 Summary

Chapter 3 described the experimental methods and apparatus. In section 3.1, the procedure for the preparation of both treated and untreated cutting samples was introduced. The particle size distributions from sieve analysis were then presented. In section 3.2 to 3.4, the apparatus used for the experiments were described. The method for calculating the fluid shear generated by the flocculator was described. The image processing method was also discussed. Section 3.5 described the procedures for the flocculation and settling velocity experiments. The results will be presented and analyzed in Chapter 4.

Chapter 4

Experimental Results and Discussion

The experimental results are presented and analyzed in this Chapter. In section 4.1, three types of flocculation experiments are described. (1) untreated synthetic based drilling cuttings in seawater; (2) untreated synthetic based drilling cuttings in freshwater; and (3) treated synthetic based drilling cuttings in seawater. In section 4.2, the settling velocity experimental results for coarse particles are presented. These experiments are: (1) Seawater settling velocity of untreated cuttings from F3070-3090; (2) Seawater settling velocity of untreated cuttings from F3050-3069; (3) Freshwater settling velocity of untreated cuttings from F3070-3090; (4) Seawater settling velocity of treated cuttings from F3070-3090; (5) Seawater settling velocity of treated cuttings from F3050-3069; (6) Freshwater settling velocity of treated cuttings from F3070-3090. In section 4.3, the floc settling velocity results are described, these results include: (1) Seawater settling velocity data of flocs formed from untreated cuttings with concentrations of 25, 50, 100, and 200mg/L at 25, 50, 100, and 200G; (2) Seawater settling velocity data of flocs formed from treated cuttings with concentrations of 25, 50, 100, and 200mg/L at 25, 50, 100, and 200G; (3) Freshwater settling velocity of flocs formed in seawater at the concentration of

concentration of 100mg/L and shear rate of 100G; (4) Freshwater settling velocity of flocs formed in freshwater at the concentration of 100mg/L and shear rate of 100G.

4.1 Flocculation Experiments

In this research, three types of flocculation experiments were conducted: (1) untreated synthetic based drilling cuttings in seawater; (2) untreated synthetic based drilling cuttings in freshwater; and (3) treated synthetic based drilling cuttings in seawater. The seawater tests simulate offshore discharge processes and the freshwater test was performed to see the salinity effects. All three series of tests were conducted at concentrations of 25, 50, 100, and 200 mg/L and at the shear rates of 25, 50, 100 and 200 G (s⁻¹).

4.1.1 Untreated Cuttings in Seawater

Figure (4-1) is a processed picture of the untreated cutting/mud suspension before flocculation. The particle diameters were calculated by IJ software and the size distribution of the suspension is shown in Figure (4-2); this distribution follows a log normal distribution with a median diameter of 17.0µm. During a flocculation test, small particles collide with each other and adhere together. As a result, the main components of the suspension become flocs instead of individual particles. The floc particle size distribution changes with flocculation time and flocculation condition. In order to characterize the floc size distribution, the median particle size was used.

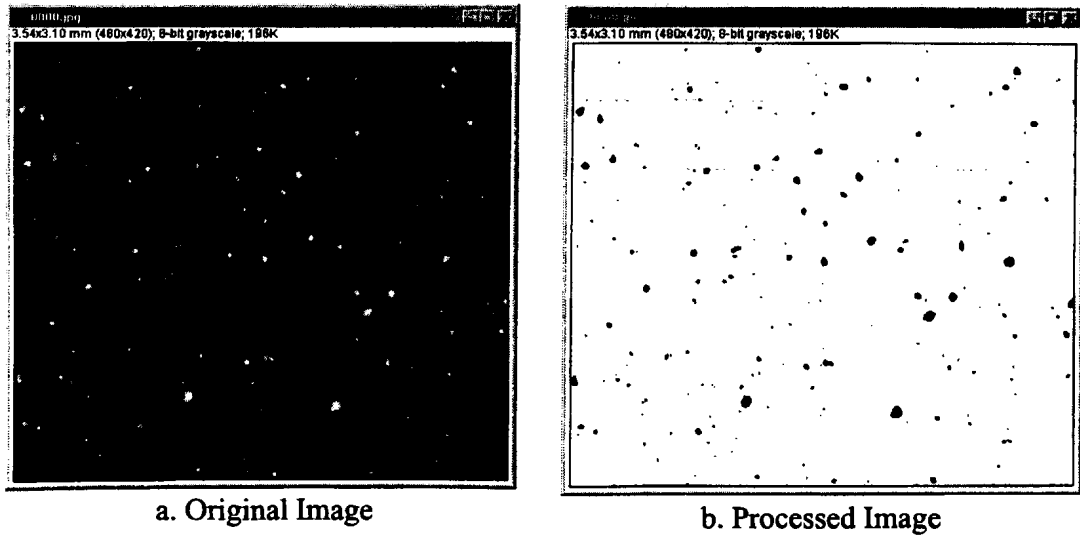


Figure 4-1 Suspension of untreated SBF drilling cuttings

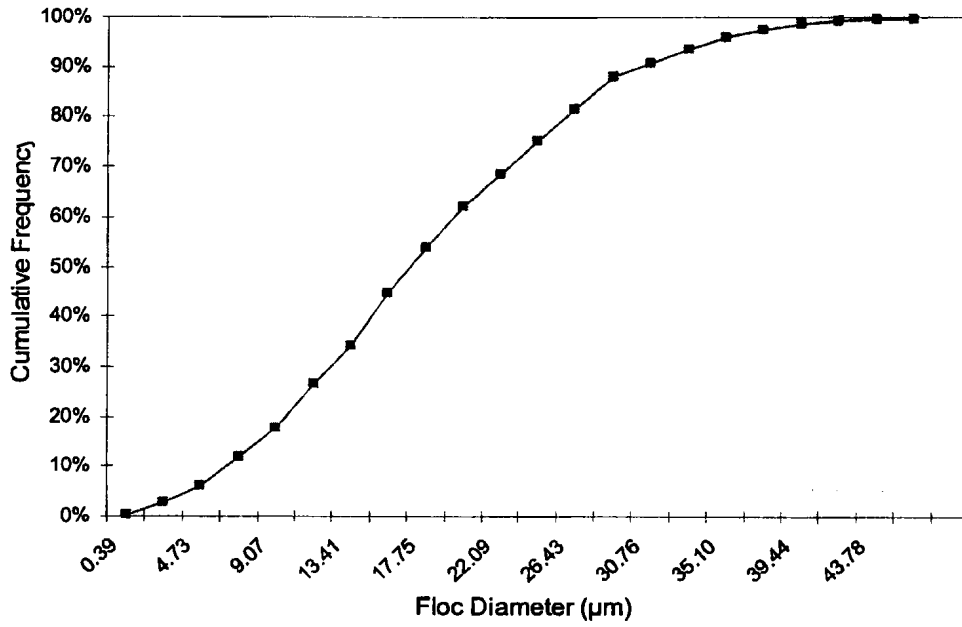


Figure 4-2 Particle size distribution of unflocculated untreated SBF drilling cuttings

The results of floc median diameter measurements as a function of flocculation time at the concentrations of 25, 50, 100, and 200 mg/L are plotted in Figure (4-3) to Figure (4-6). The times to reach steady state are estimated from Figure (4-3) to Figure (4-6) and listed in Table (4-1). Because the experiments were conducted in 20 minute time intervals after the first 20 minutes, only an approximate time to reach steady state can be estimated from Figures (4-3) to (4-6). The accurate time can be obtained by employing the flocculation model described in Chapter 2. Table (4-2) presents the average steady state median floc diameters for untreated drilling cuttings in seawater. These values are calculated from the measured data points, which are considered in steady state.

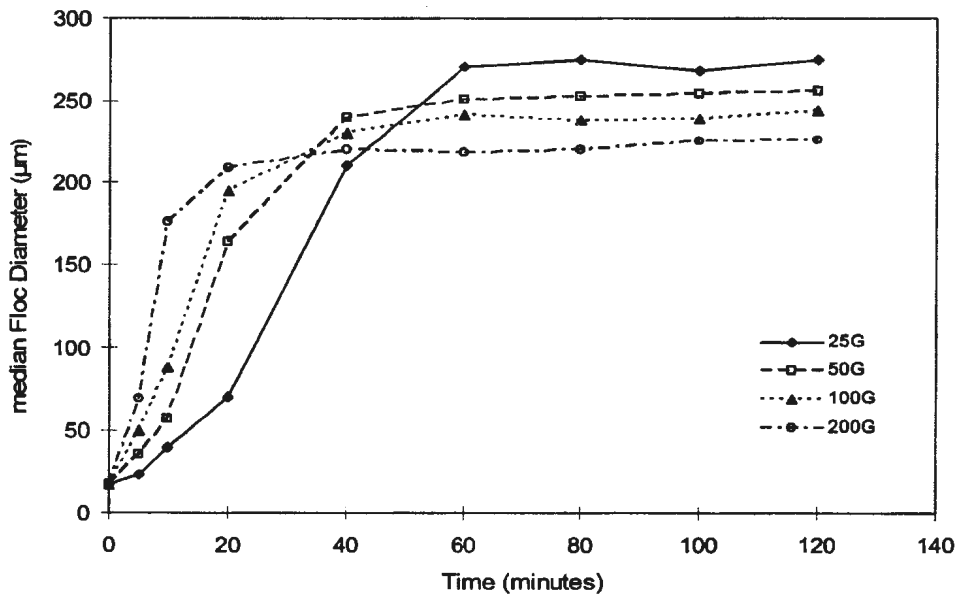


Figure 4-3 Time variation of median floc diameter for untreated cuttings at 25mg/L in seawater

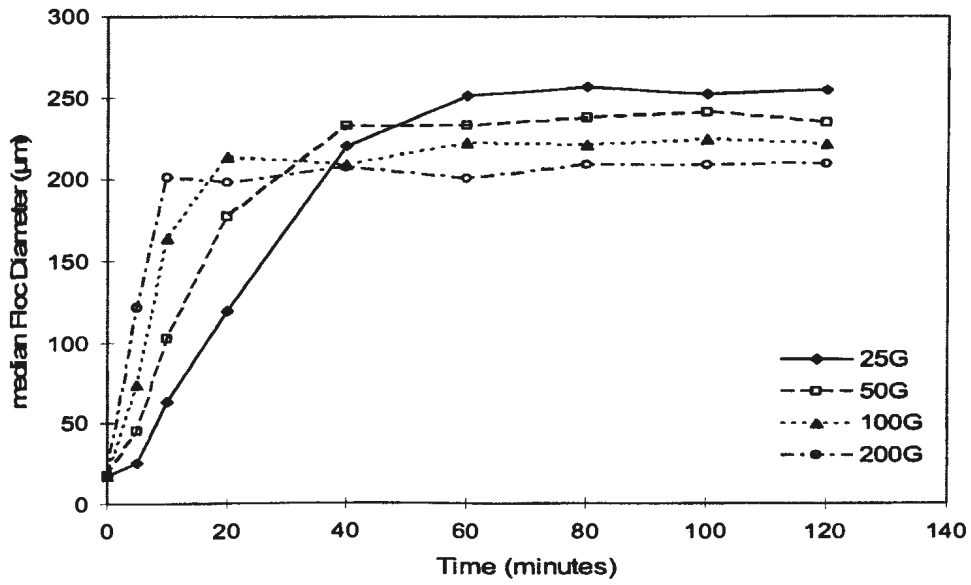


Figure 4-4 Time variation of median floc diameter for untreated cuttings at 50mg/L in seawater

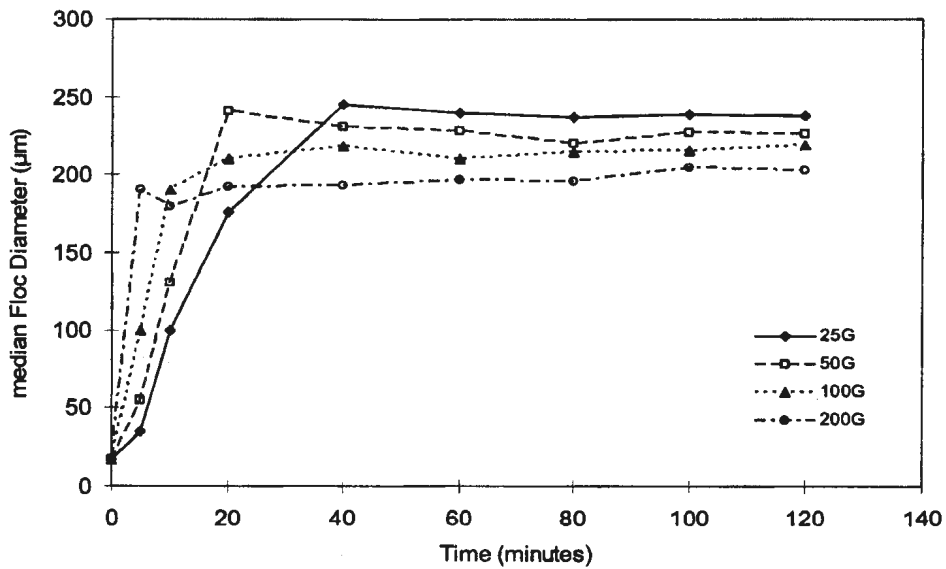


Figure 4-5 Time variation of median floc diameter for untreated cuttings at 100mg/L in seawater

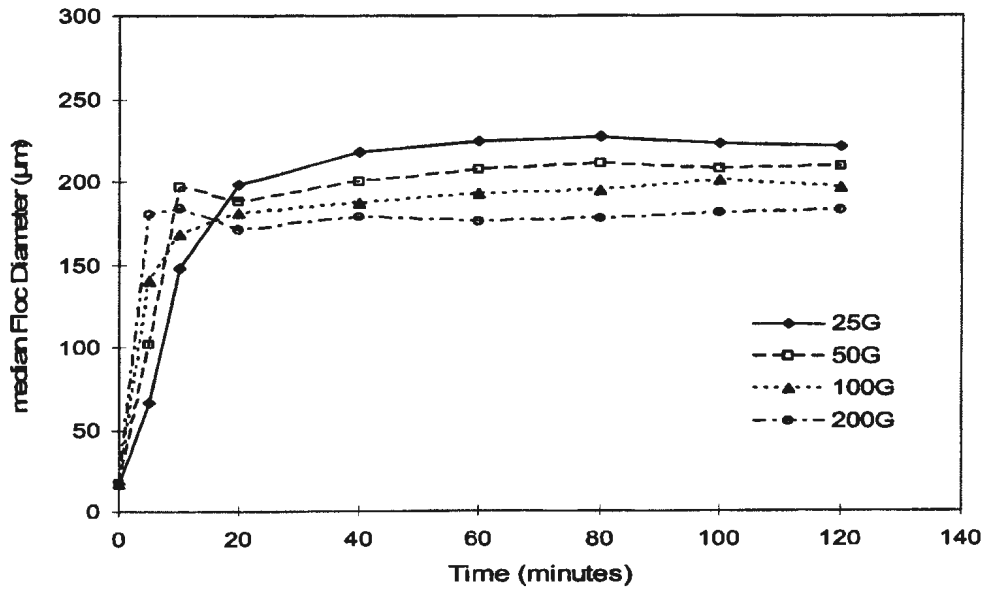


Figure 4-6 Time variation of median floc diameter for untreated cuttings at 200mg/L in seawater

Table 4-1 Time (minutes) to reach steady state of flocculation for untreated drilling cuttings in seawater

Concentration (mg/L)	Fluid Shear (s ⁻¹)			
	25	50	100	200
25	60	40	30	20
50	50	30	20	10
100	40	20	15	5
200	30	15	10	5

Table 4-2 Steady state floc median diameter (µm) for untreated drilling cuttings in seawater

Concentration (mg/L)	Fluid Shear (s ⁻¹)			
	25	50	100	200
25	273.1	253.4	242.2	219.8
50	254.3	238.7	224.4	209.2
100	238.6	223.5	213.8	197.4
200	223.1	208.3	199.6	178.8

It can be seen from Figures (4-3) to (4-6) and Tables (4-1) and (4-2) that the floc size increases with flocculation time until it reaches steady state (a state that the floc median size remains constant). Under the same concentration, the higher shear stresses resulted in lower steady state median diameters. Taking the concentration of 200mg/L for example, the floc diameter under 25G is 223.1 μ m while the diameter under 200G is 178.8 μ m. It was also demonstrated that under the same concentration, particles flocculate faster with higher shear rate. Taking the concentration of 200mg/L again, the time needed to reach steady state under 25G is 30 minutes while under 200G is 5 minutes.

Figures (4-7) and (4-8) and Tables (4-1) and (4-2) show that under the same shear stress, the particles flocculate faster in higher concentration than in lower concentration. For example, for the shear stress of 25G, the time needed to reach steady state under 25mg/L is 60 minutes while under 200mg/L it is 30 minutes. Another trend observed is that under the same shear stress, the steady state median floc diameters are smaller in higher concentration than in lower concentration. For example, for the shear stress of 25G, the diameter under 25mg/L is 273.1 μ m, while the diameter under 200mg/L is 223.1 μ m. Although this point has been demonstrated by a number of researchers (Huang 1992, Iacobellis 1984 and Tsai et al 1987, Xu 1988), but the reasons are still not well understood.

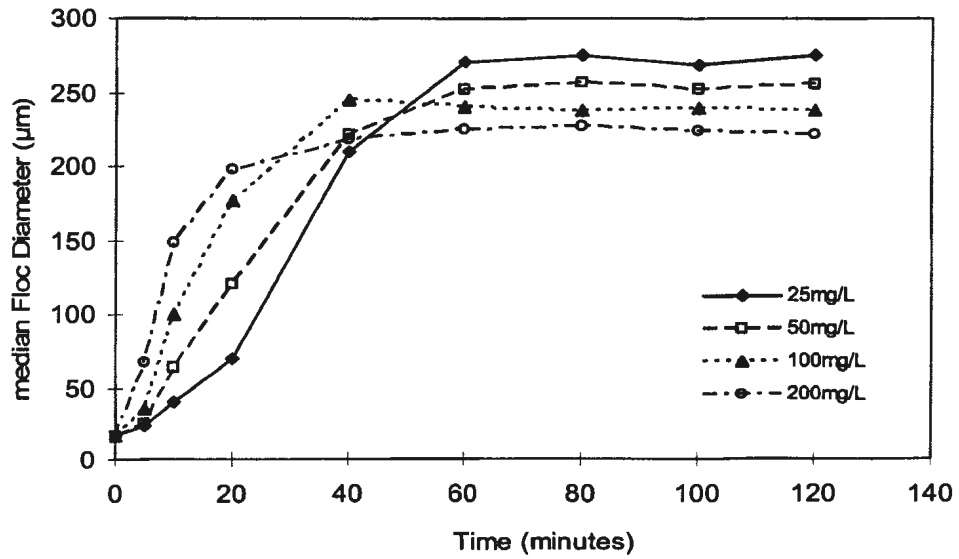


Figure 4-7 Time variation of median floc diameter for untreated cuttings at 25G in seawater

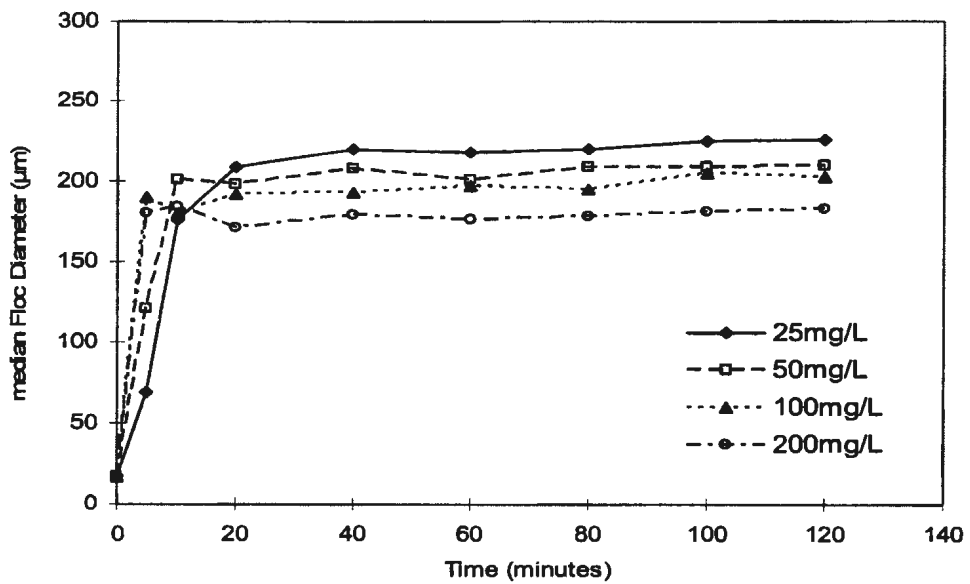


Figure 4-8 Time variation of median floc diameter for untreated cuttings at 200G in seawater

The data obtained for untreated SBF cuttings have similar characteristics as previous research (Huang 1992, Xu 1988) except the steady state median size are much larger. Taking the concentration of 100mg/L under 100G for example, the steady state median diameter reported by Xu (1988) is 47.3 μ m for Bentonite and 75.3 μ m for Barite, and by Huang (1992) is 105.5 μ m for WBFs, while in this research, it is 219.8 μ m for untreated SBF cuttings.

From the comparison above with previous studies, it was found that the steady state median floc diameters of untreated SBF cuttings in seawater are much larger than WBFs and mineral particles under the same conditions. A possible reason for this is that the organic/oil component in the untreated SBF cuttings functions as an adhering agent that helps to bond the particles together. Heat treated SBF cuttings in seawater tests were therefore performed to test this hypothesis.

4.1.2 Treated Cuttings in Seawater

The particle size distribution of treated cuttings before flocculation is shown in Figure (4-9). Same as untreated cuttings, the distribution of treated cuttings also follows a lognormal distribution, but with a median diameter of 14.7 μ m. Figures (4-10) to (4-13) show the results of floc median diameter as a function of flocculation time at concentrations of 25, 50, 100, and 200 mg/L under 25, 50, 100 and 200G for treated samples. Tables (4-3) and (4-4) present the time to reach steady state and the steady state median floc diameters.

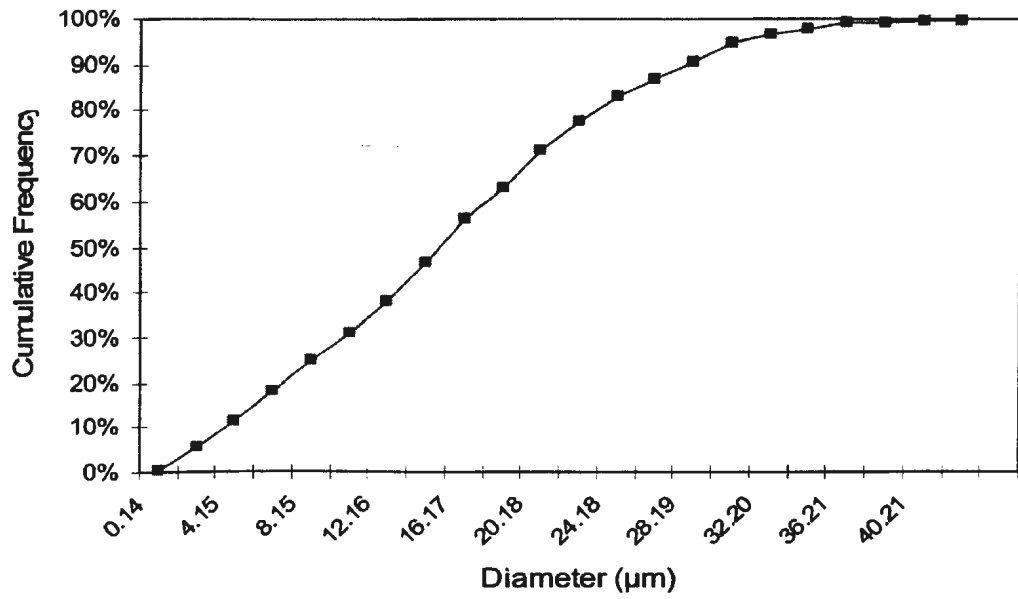


Figure 4-9 Particle size distribution of unflocculated treated SBF drilling cuttings

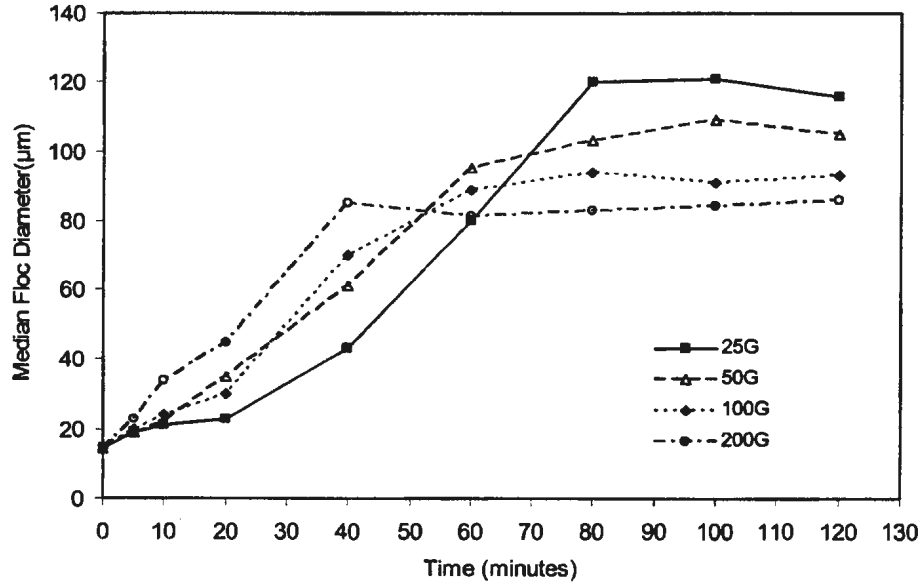


Figure 4-10 Time variation of median floc diameter for treated cuttings at 25mg/L in seawater

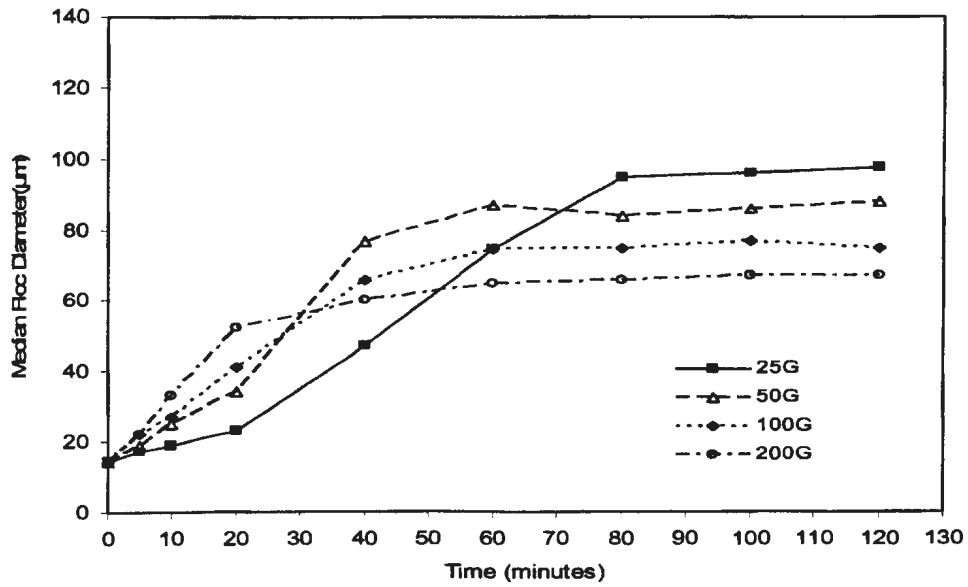


Figure 4-11 Time variation of median floc diameter for treated cuttings at 50mg/L in seawater

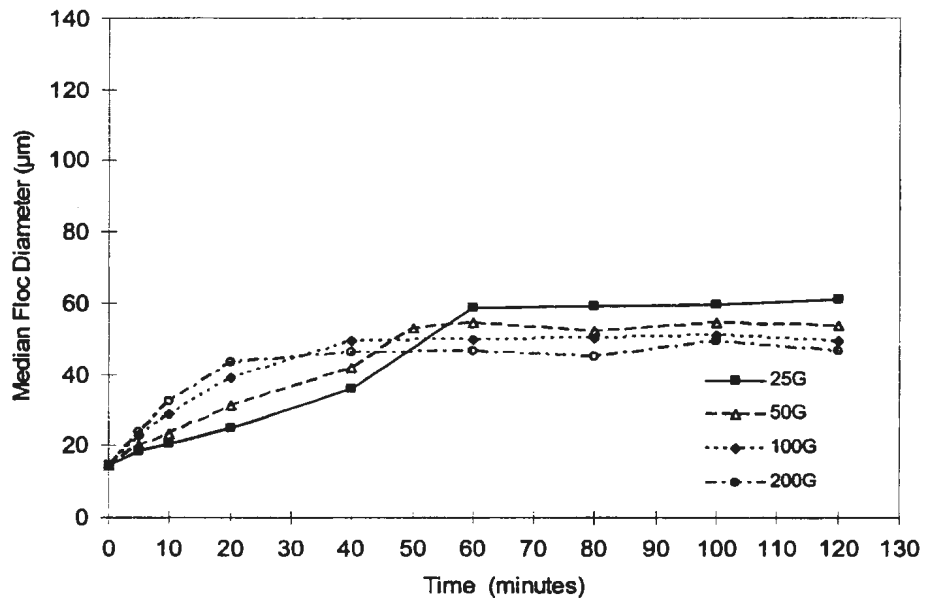


Figure 4-12 Time variation of median floc diameter for treated cuttings at 100mg/L in seawater

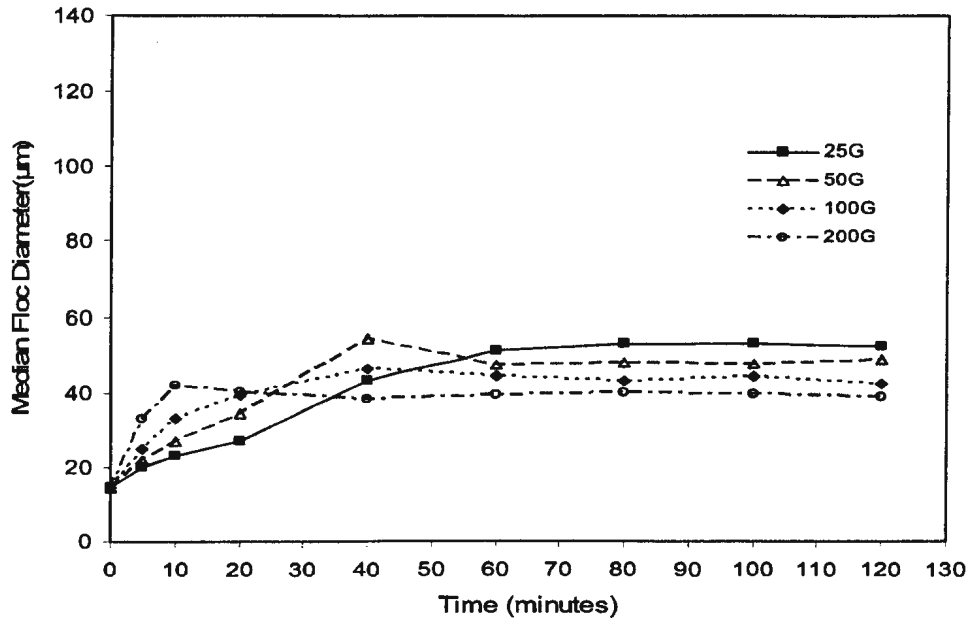


Figure 4-13 Time variation of median floc diameter for treated cuttings at 200mg/L in seawater

Table 4-3 Time (minutes) to reach steady state of flocculation for treated drilling cuttings in seawater

Concentration (mg/L)	Fluid Shear (s ⁻¹)			
	25	50	100	200
25	80	65	55	45
50	65	50	45	40
100	50	40	30	20
200	40	30	20	10

Table 4-4 Steady State Floc median diameter (µm) for treated drilling cuttings in seawater

Concentration (mg/L)	Fluid Shear (s ⁻¹)			
	25	50	100	200
25	129.3	110.5	93.1	83.2
50	96.3	80.4	76.8	65.6
100	61.8	54.9	50.7	44.2
200	52.5	47.1	42.3	38.4

It can be seen from Figures (4-10) to (4-13) and Table (4-3) and (4-4), that the floc size increases with flocculation time until it reaches steady state. Similar to the untreated cuttings, under the same concentration, the higher shear stresses resulted in lower steady state median diameters for treated cuttings. Taking the concentration of 200mg/L as an example, the floc diameter under 25G is 52.5 μ m while the diameter under 200G is 38.4 μ m. It was also demonstrated that under the same concentration, particles flocculate faster with higher shear rate. For example, at a concentration of 200mg/L, the time needed to reach steady state under 25G is 40 minutes while under 200G is 10 minutes.

Figures (4-14) and (4-15) and Tables (4-3) and (4-4) show that under the same shear stress, the particles flocculate faster in higher concentration than in lower concentration. Take the shear stress of 25G; the time needed to reach steady state under 25mg/L is 80 minutes while under 200mg/L it is 40 minutes. Under the same shear stress, the steady state median floc diameters are smaller in higher concentration than in lower concentration. At the shear stress of 25G for example, the diameter under 25mg/L is 129.3 μ m while the diameter under 200mg/L is 83.2 μ m.

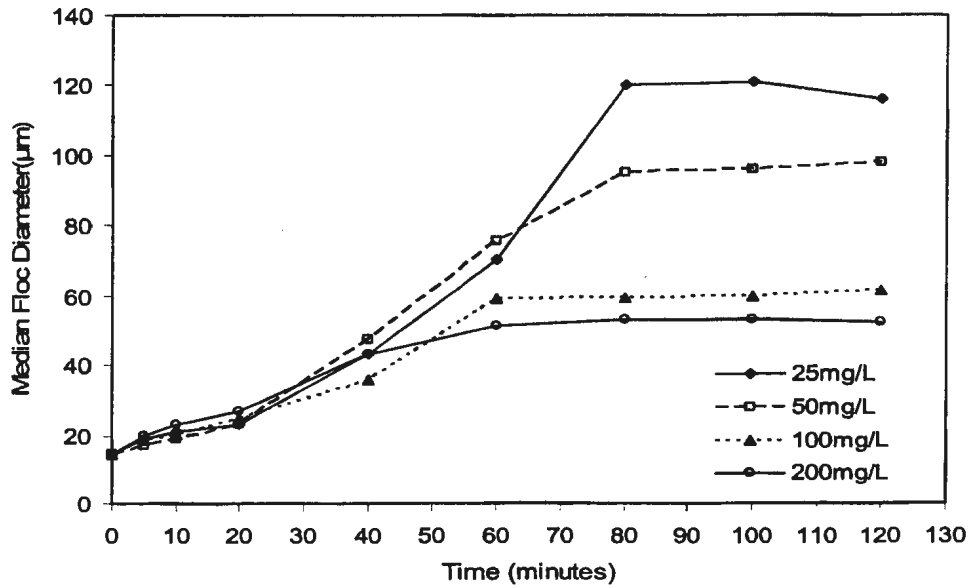


Figure 4-14 Time variation of median floc diameter for treated cuttings at 25G in seawater

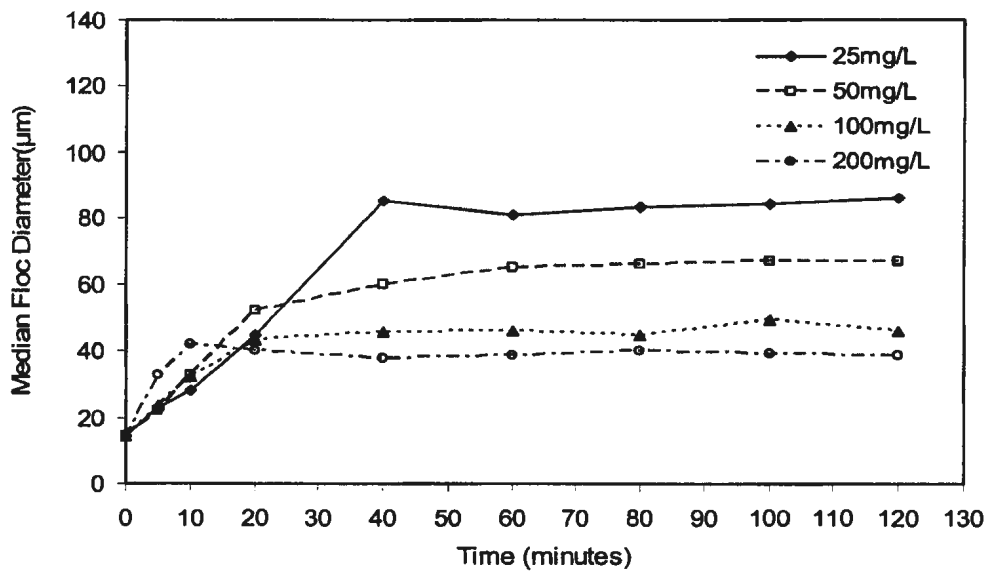


Figure 4-15 Time variation of median floc diameter for treated cuttings at 200G in seawater

Compared with untreated cuttings, it can be seen that treated cuttings show similar characteristics but have considerably smaller steady state median size. For example, at the concentration of 25mg/L and shear rate of 25G, the median size was reduced from 273.1 μ m to 129.3 μ m. At the same flocculation condition, Huang (1992) reported WBF flocs had a median diameter of 140.8 μ m. It is also indicated by the experimental results that treated cuttings flocculate slower than untreated cuttings. For example, for the case of 200G and 100mg/L, the time needed to reach steady state for untreated cuttings is 5 minutes while for treated cuttings it is 20 minutes. The time needed for Huang's (1992) WBFs is 10 minutes under this condition. One can see from the data above, that the treated cuttings behave more like WBFs.

4.1.3 Untreated Cuttings in Freshwater

Particles are usually charged due to an unequal distribution of ions over the particle and the surrounding solution. This charge is frequently responsible for the stability of colloids (Lyklema 1978). The dissolved salts in water can dissociate into constituent ions and therefore affect the floc stability through their effect on the extent of the diffuse layer around the particles and by their specific effect on the electric potential controlling colloid stability (Gregory 1978). To test SBF flocculation in water of different salinity is therefore important.

For the tests of untreated cuttings in freshwater, the same cuttings sample was used as in the seawater tests. The particle size distribution is given in Figure (4-2). Figures (4-16) to

(4-19) show the results of floc median diameter as a function of flocculation time at the same concentrations as before (25, 50, 100, and 200 mg/L) and Figures (4-20) to (4-21) present the results at same shear stress as before. Tables (4-5) and (4-6) present the time to reach steady state and the steady state median floc diameters.

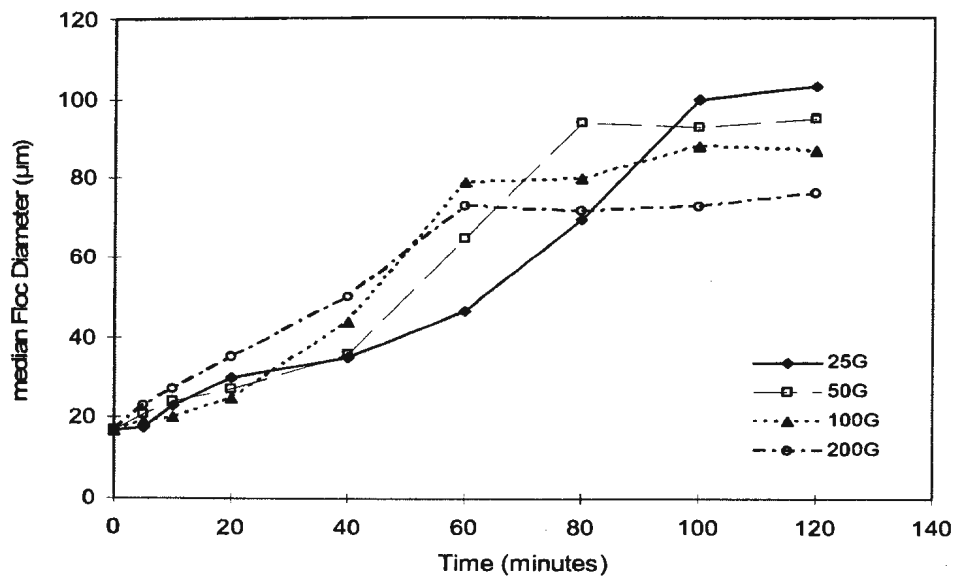


Figure 4-16 Time variation of median floc diameter for untreated cuttings at 25mg/L in freshwater

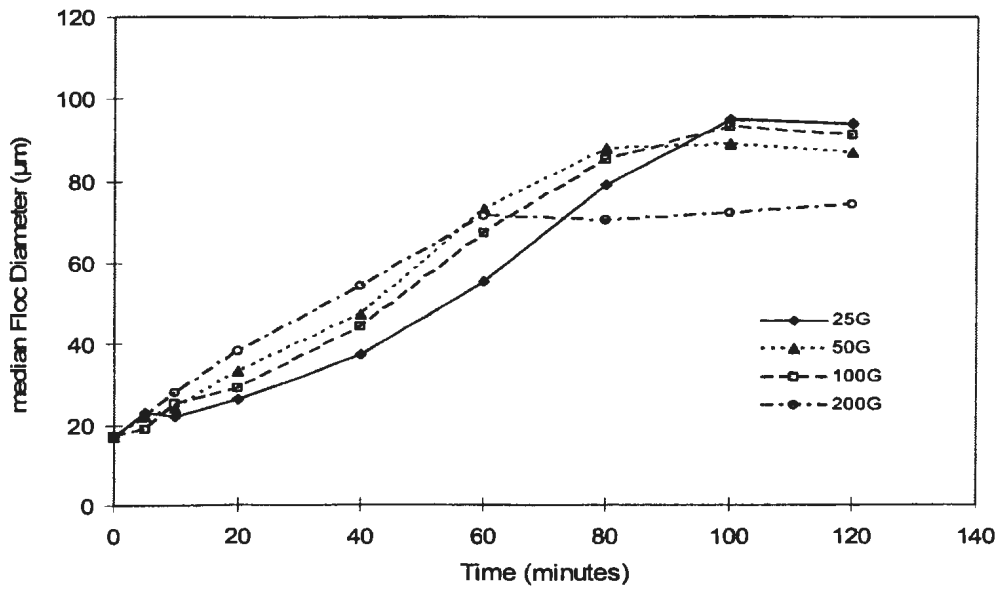


Figure 4-17 Time variation of median floc diameter for untreated cuttings at 50mg/L in freshwater

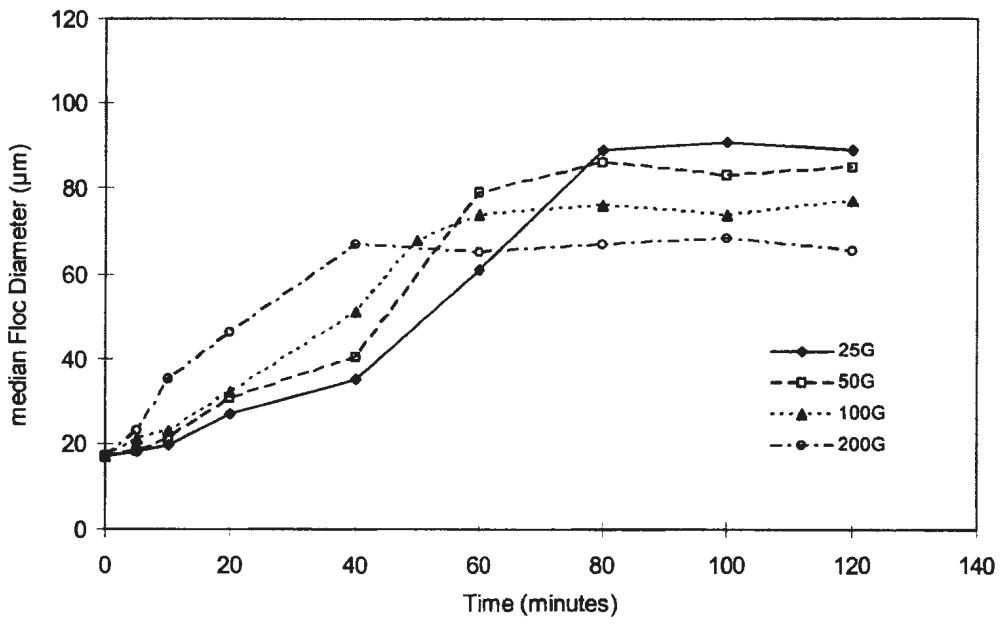


Figure 4-18 Time variation of median floc diameter for untreated cuttings at 100mg/L in freshwater

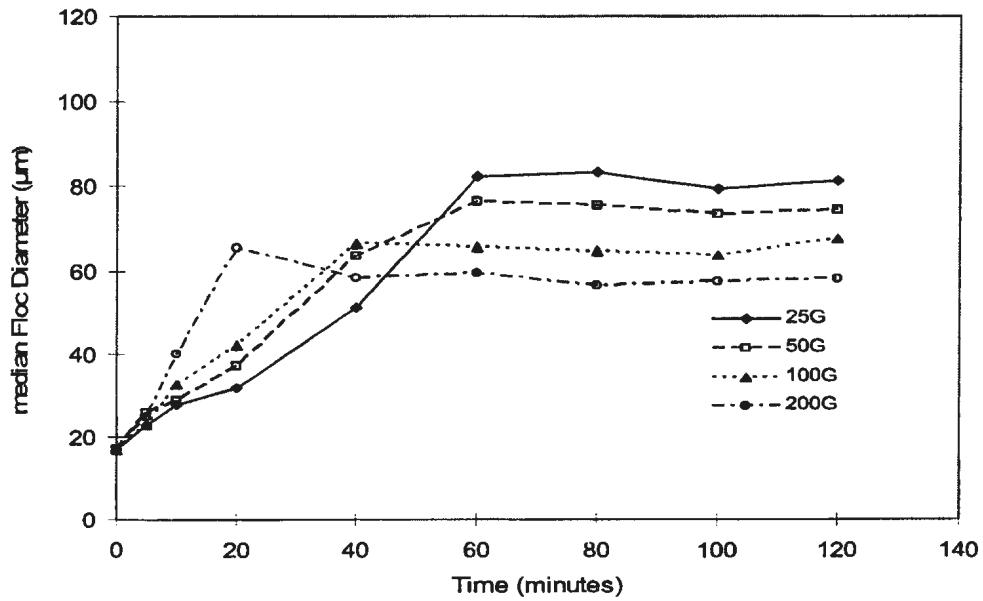


Figure 4-19 Time variation of median floc diameter for untreated cuttings at 200mg/L in freshwater

Table 4-5 Time (minutes) to reach steady state of flocculation for untreated drilling cuttings in freshwater

Concentration (mg/L)	Fluid Shear (s ⁻¹)			
	25	50	100	200
25	100	80	75	70
50	90	70	60	55
100	80	60	50	40
200	60	50	40	20

Table 4-6 Steady state floc median diameters (µm) for untreated drilling cuttings in freshwater

Concentration (mg/L)	Fluid Shear (s ⁻¹)			
	25	50	100	200
25	101.5	94.6	91.2	78.5
50	94.7	88.1	85.0	73.8
100	89.4	83.5	75.8	66.4
200	79.9	75.2	64.9	57.6

It can be seen from Figures (4-16) to (4-19) and Tables (4-5) and (4-6) that the floc size increases with flocculation time until it reaches steady state. Under the same concentration, the higher shear stresses resulted in lower steady state median diameters. Taking the concentration of 200mg/L as an example, the floc diameter under 25G is 79.9 μ m while the diameter under 200G is 57.6 μ m. It was also demonstrated that under the same concentration, particles flocculate faster with higher shear rate. For example, at the concentration of 200mg/L, the time needed to reach steady state under 25G is 60 minutes while under 200G it is 20 minutes.

Figures (4-20) and (4-21) and Tables (4-5) and (4-6) show that under the same shear stress, the particles flocculate faster in higher concentration than in lower concentration. For example, for the shear stress of 25G, the time needed to reach steady state under 25mg/L is 100 minutes while under 200mg/L it is 60 minutes. Under the same shear stress, the steady state median floc diameters are smaller in higher concentration than in lower concentration. For example, for the shear stress of 25G, the diameter under 25mg/L is 101.5 μ m while the diameter under 200mg/L it is 79.9 μ m.

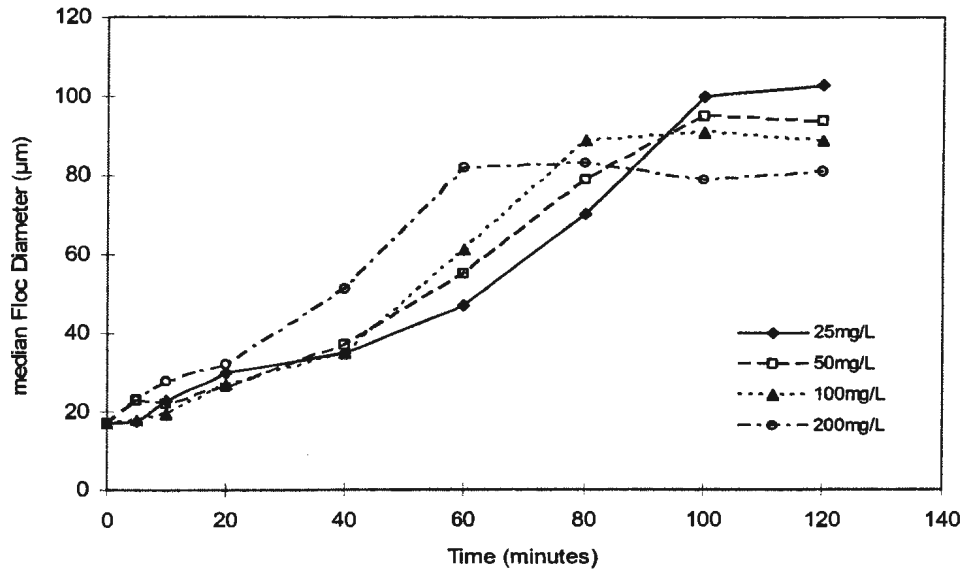


Figure 4-20 Time variation of median floc diameter for untreated cuttings at 25G in freshwater

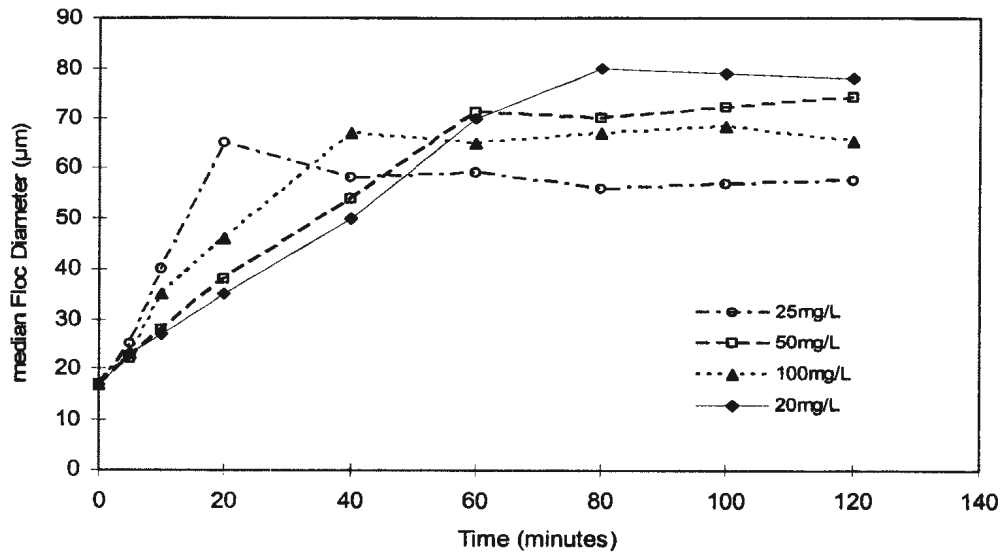


Figure 4-21 Time variation of median floc diameter for untreated cuttings at 200G in freshwater

It can be seen from Figure (4-16) to (4-21) that the untreated SBF cuttings have similar flocculation characteristics in seawater as in freshwater, but different flocculation rates. The time needed to reach steady state is much longer in freshwater than in seawater. The steady state median diameters are also smaller in freshwater than in seawater. For example, the time for particles at a concentration of 200mg/L under 200G to reach steady state is around 5 minutes in seawater but 20 minutes in freshwater. The steady state median size for this test condition is 178.8 μ m in seawater and 57.6 μ m in freshwater. A noticeable difference in the freshwater test compared to the seawater test is that the effect of concentration on median floc size is smaller for freshwater than for seawater. The reason is that in freshwater test conditions, because no salt is presents, the drilling cuttings/muds suspension remains in a dispersed state and under such a condition, the influence of the repulsive forces extends beyond that at which the attractive forces are significant. In this case, the double layer (the layer between the particle and surrounding water that has a particular distribution of ions) of counter-ions surrounding each particle is in a given state of equilibrium due to the particle surface attractive forces and the opposing tendency of the counter-ions to diffuse away from their high concentration near the particle surface (Gregory 1978). Therefore, although the relative motion by shear forces cause the collisions of small particles, the adhesion of particles is not significant and it needs a relatively long time to reach another equilibrium and hence it is hard to form very large flocs. However, when in the seawater environment, the increase in ambient medium of the concentration of ions with a charge of the same sign as that on the counter-ions results in a reduction in the diffusive tendency of the counter-ions (this

tendency decreases with decreasing magnitude of the counter-ionic concentration gradient). As a consequence, in seawater conditions, a new state of equilibrium is easily established with the double layer closer to the particle surface, which in the experiments, resulted in faster flocculation rate and larger steady state floc size.

4.2 Coarse Particle Settling Velocity Results

4.2.1 Settling Velocity Results for Untreated Cuttings

In this part, both the seawater and freshwater tests were performed using both treated and untreated cuttings to obtain a generalized correlation between settling velocity and particle size.

For the untreated drilling cuttings, the seawater settling velocity test results are reported in Figures (4-22) to (4-25). The Figures (4-22) and (4-24) show the settling velocity experimental data of various shaped particles from two different formations (F3050-3069 with a bulk density of 1900kg/m^3 and F3070-3090 with a bulk density of 1833kg/m^3). Figures (4-23) and (4-25) show the power law fitted curves. In order to find the effects of water density, samples from one of the formations were tested in freshwater and the results are presented in Figures (4-26) and (4-27).

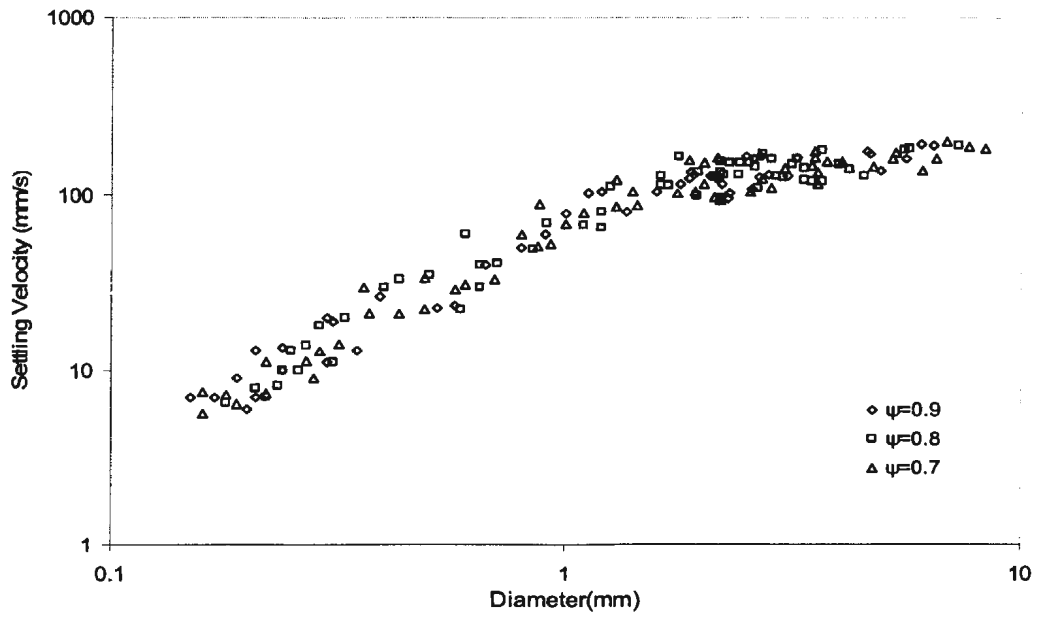


Figure 4-22 Seawater settling velocity data of untreated cuttings (F3070-3090) of various shapes

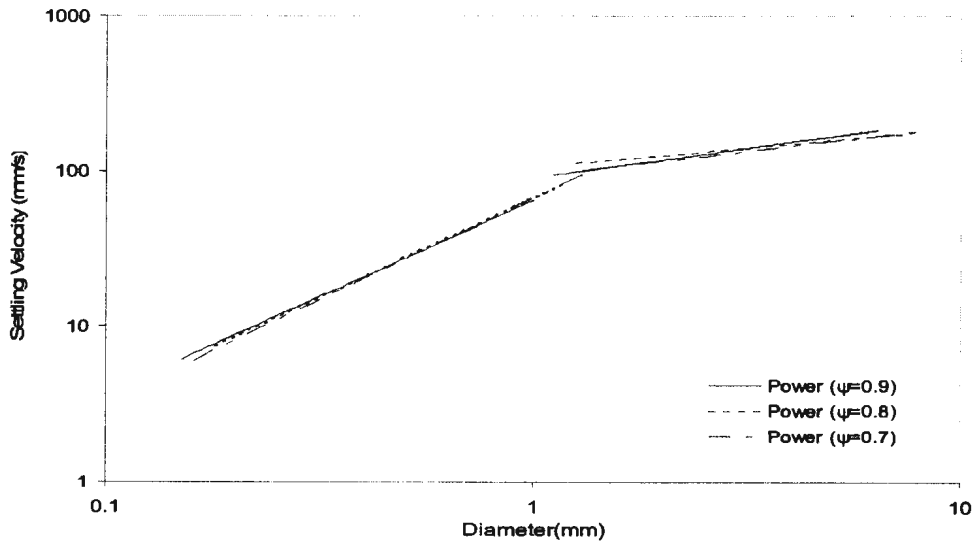


Figure 4-23 Power law fit of the seawater settling velocity data of untreated cuttings (F3070-3090) of various shapes

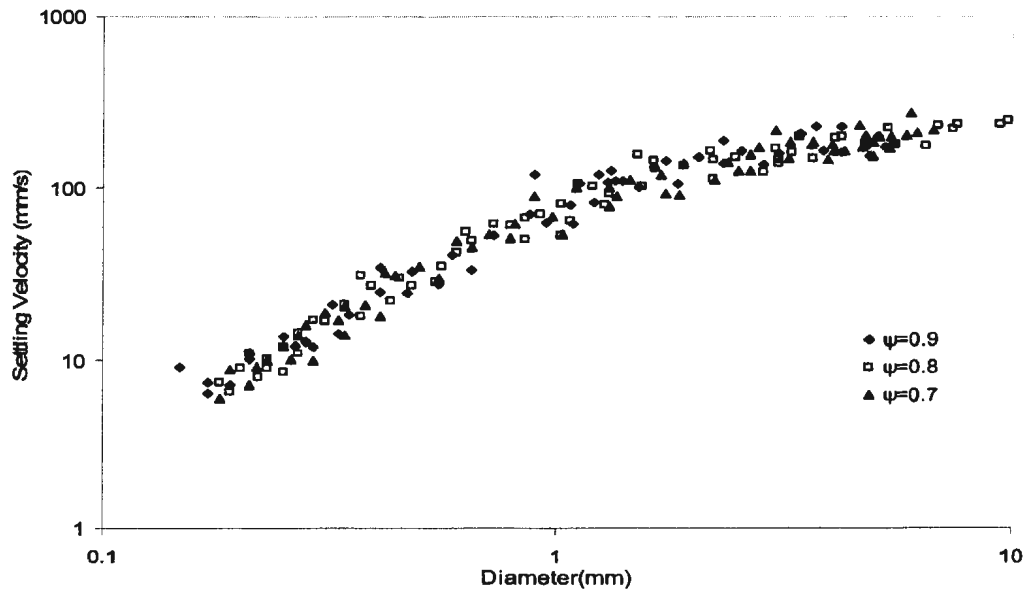


Figure 4-24 Seawater settling velocity data of untreated cuttings (F3050-3069) of various shapes

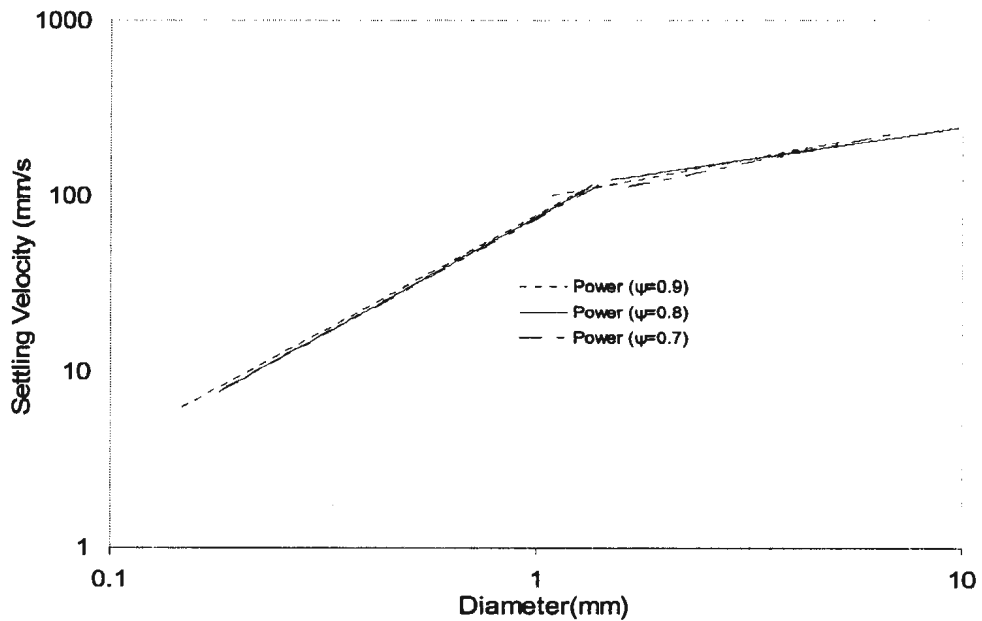


Figure 4-25 Power law fit of the seawater settling velocity data of untreated cuttings (F3050-3069) of various shapes

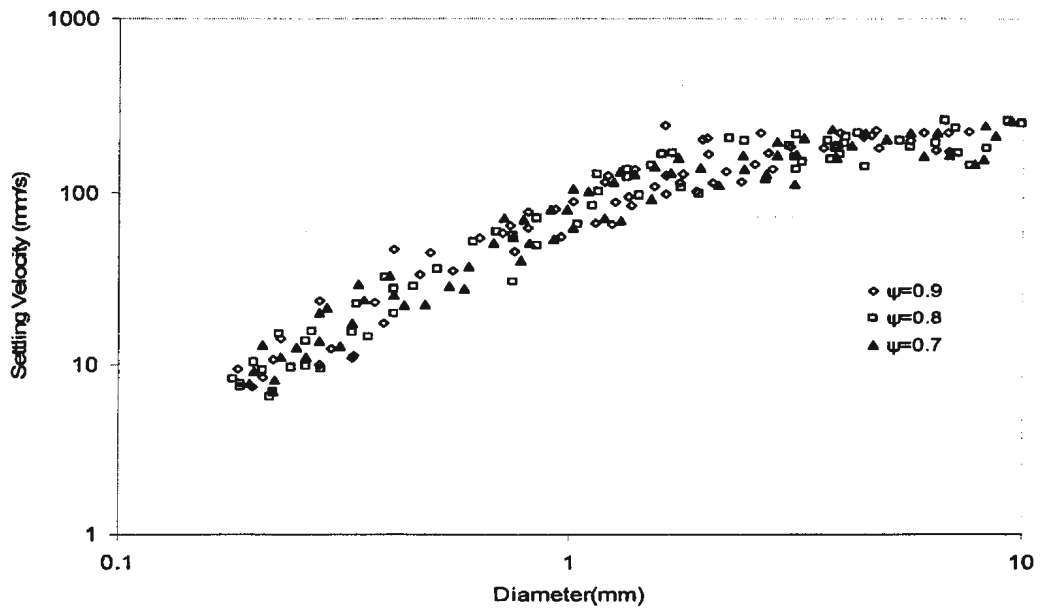


Figure 4-26 Freshwater settling velocity data of untreated cuttings (F3070-3090) of various shapes

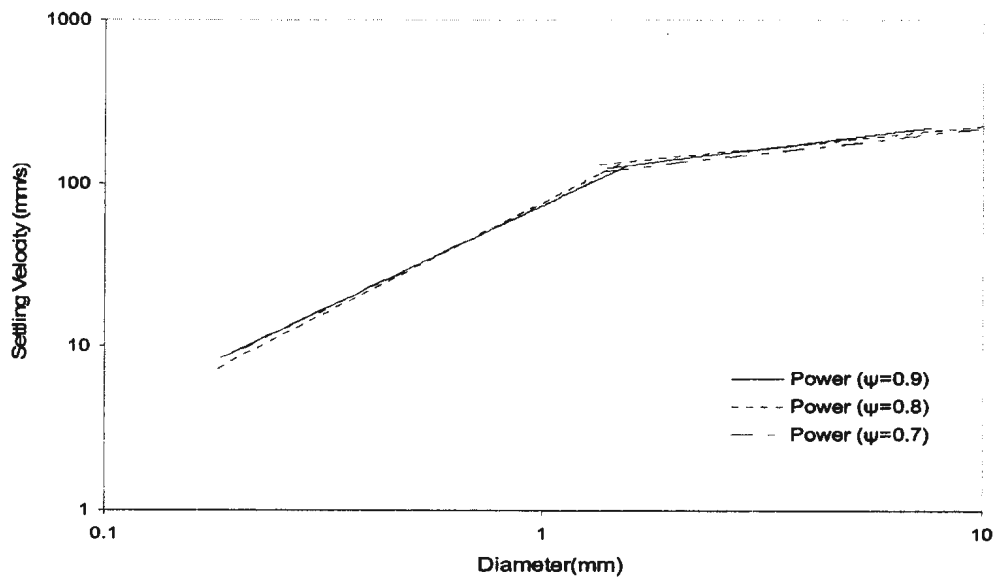


Figure 4-27 Power law fit of the freshwater settling velocity data of untreated cuttings (F3070-3090) of various shapes

From the power law fits presented in Figures (4-23), (4-25) and (4-27), it can be seen that the settling velocity of F3050-3069 is a little bit higher than F3070-3090 and the particles settle faster in freshwater than in seawater. It can also be seen that the shape effects on untreated drilling cuttings is not significant, the reason for this is that the density of untreated cuttings is not uniform because of the clump effects. Therefore the shape effect for untreated cuttings will not be considered in the present analysis.

As described in the previous chapters, the relationship between drag coefficient and Reynolds number is important in establishing of a settling velocity relationship. More than 550 data points from Figures (4-22), (4-24), and (4-26) were compiled using the definition of drag coefficient and Reynolds number, which are presented in Equations (4-1) and (4-2). The results are plotted in Figure (4-28).

$$C_D = \frac{4 (\rho_s - \rho_f) gD}{3 \rho_f u^2} \quad \text{Equation (4-1)}$$

$$Re = \frac{\rho_f Du}{\mu} \quad \text{Equation (4-2)}$$

where C_D is the drag coefficient,

ρ_s and ρ_f are the density of particle and fluid respectively.

D is the particle diameter,

μ is the dynamic viscosity (kg/m·s)

g is the gravitational acceleration (m/s²)

u is the particle settling speed (m/s)

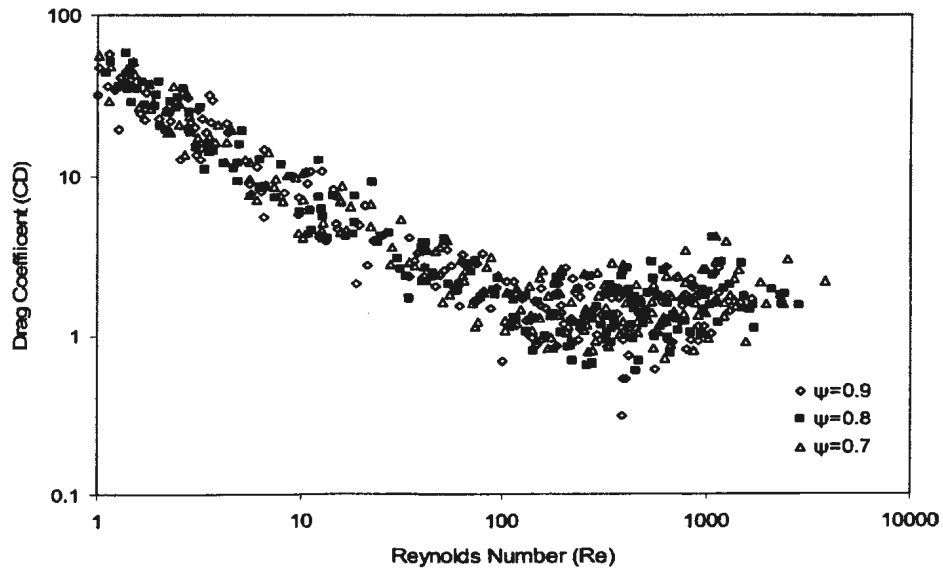


Figure 4-28 Drag coefficient vs Reynolds number for untreated drill cuttings (experimental data)

Through the regression analysis, a relation between drag coefficient and Reynolds number for Reynolds number between 1 and 1000 is found as

$$C_D = 1.69959 + \frac{56.26128}{Re} \quad \text{Equation (4-3)}$$

The correlation coefficient r is 0.955 and this relation is plotted in Figure (4-29). The relationships of Chien (1992) and Allen (1990) are plotted for reference. It can be seen from Figure (4-29), at the low Reynolds number range ($Re < 100$), the drag force on untreated SBFs cuttings is larger than on other types of cuttings reported by Chien (1992) and by Allen (1990). At the high Reynolds number range, the drag forces are very close to the drag force for other types of cuttings reported by Chien (1992) with sphericity of 0.7.

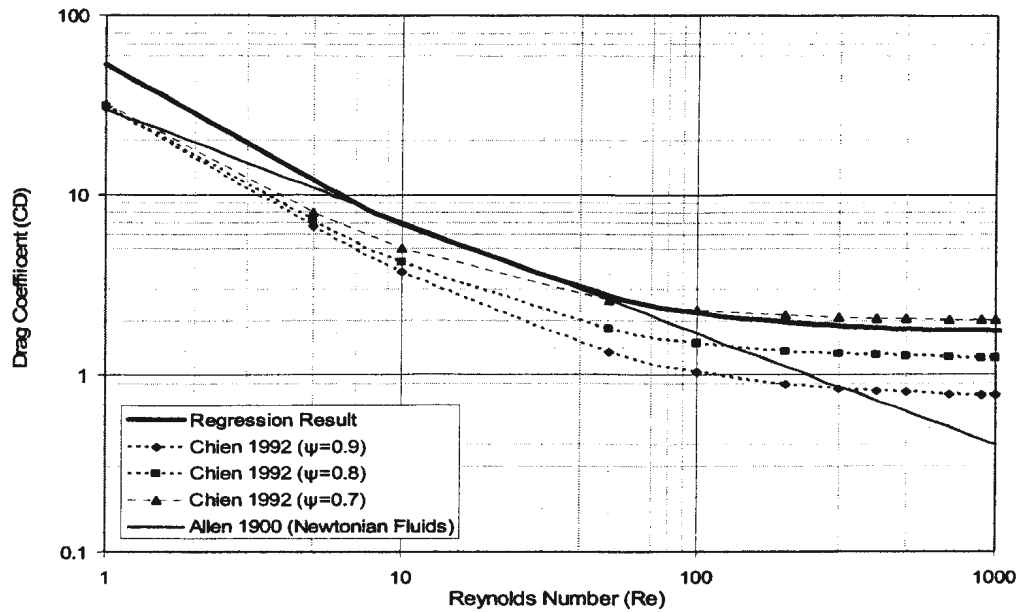


Figure 4-29 Drag coefficient versus Reynolds number for untreated drill cuttings (regression results)

A settling velocity correlation is then obtained by introducing the definition of drag coefficient, Equation (4-1) and particle Reynolds number, Equation (4-2) to Equation (4-3). By solving the correlation and taking the positive root of settling velocity, the settling velocity for untreated SBF cuttings is obtained as

$$u = \frac{-15.36 \mu + \sqrt{236.08 \mu^2 + 0.78(\rho_s - \rho_f)\rho_f D^3 g}}{\rho_f D} \quad \text{Equation (4-4)}$$

where u is the settling velocity (m/s),

ρ_s is the drilling cutting density (kg/m^3)

ρ_f is the fluid density (kg/m^3)

μ is the dynamic viscosity ($\text{kg/m}\cdot\text{s}$)

D is the particle diameter (m)

g is the gravitational acceleration (m/s^2)

The settling velocities of OBF cuttings with density of 1850kg/m^3 and quartz sands with density of 2650kg/m^3 have been reported by Gerard (1996) and Sleath (1984) respectively. Chien (1992) also reported the settling velocity of an other type of drilling cuttings. In order to compare the difference in settling velocity between SBFs cuttings and these materials, the densities of 1850kg/m^3 and 2650kg/m^3 were selected to use the equation (4-4) and results are plotted in Figure (4-30).

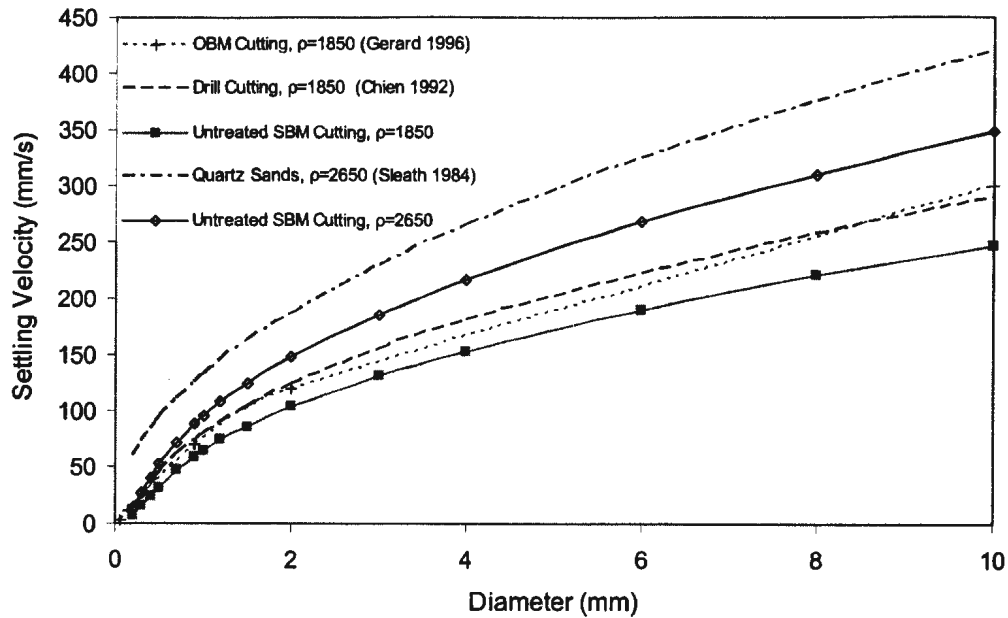


Figure 4-30 Settling velocity of untreated drill cuttings

It can be seen from Figure (4-30) that the drill cuttings settle much slower than quartz sands. The value calculated from Equation (4-4) is much smaller than the experimental

data of Gerard (1996). This may result from the experiment method employed. Gerard used a sediment balance to obtain the settling velocity and used sieves to obtain particle size, while this research used a digital imaging system to calculate projected particle diameter. The value of Chien (1992) is also larger than the value from Equation (4-4). This may be due to the type of cutting studied. There are a number of other factors that affect settling velocity beside particle density, such as particle sphericity.

4.2.2 Settling Velocity Results for Treated Cuttings

For the treated drilling cuttings, the sea water settling velocity test results are reported from Figures (4-31) to (4-34). The Figures (4-31) and (4-33) show the settling velocity experimental data of various shaped particles from two different formations while Figures (4-32) and (4-34) show the fitted curves. In order to find the effects of water density, samples from one of the formations were used to conduct freshwater tests and the results are presented in Figures (4-35) and (4-36).

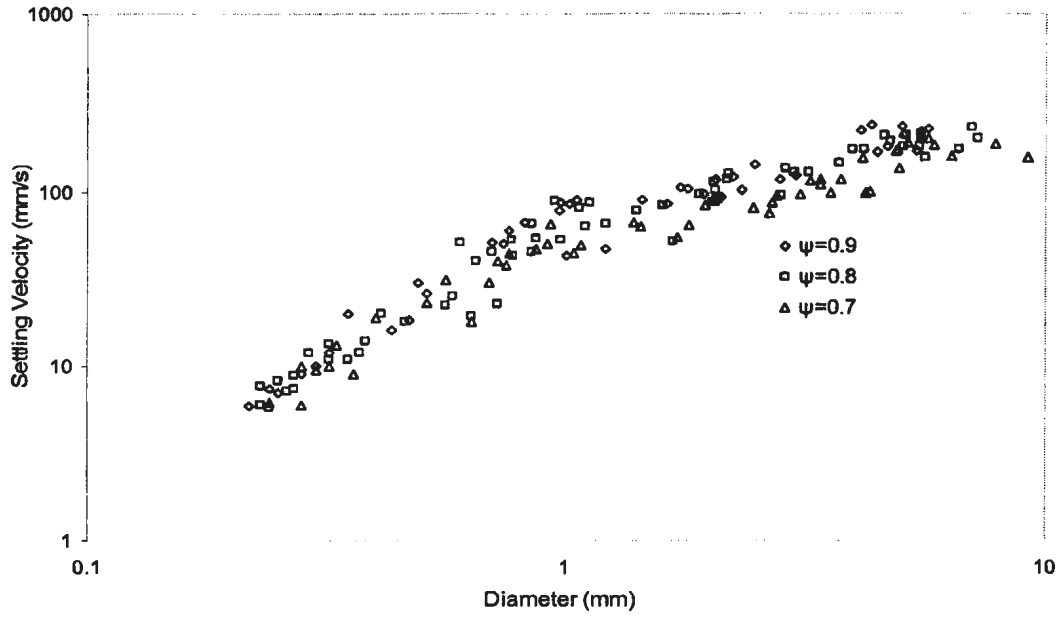


Figure 4-31 Seawater settling velocity data of treated cuttings (F3070-3090) of various shapes

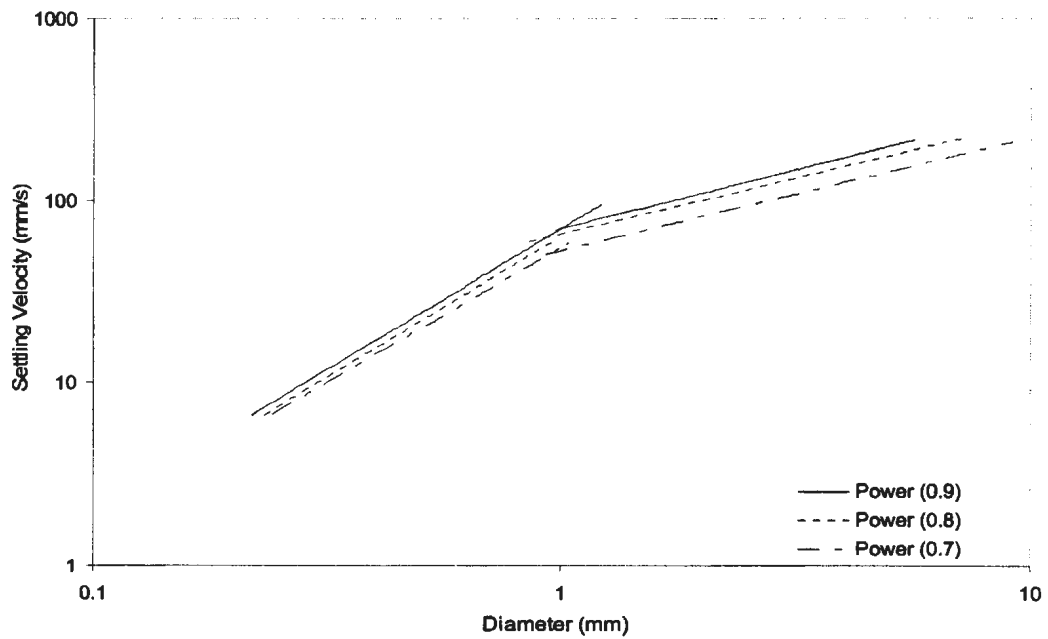


Figure 4-32 Power law fit of the seawater settling velocity data of treated cuttings (F3070-3090) of various shapes

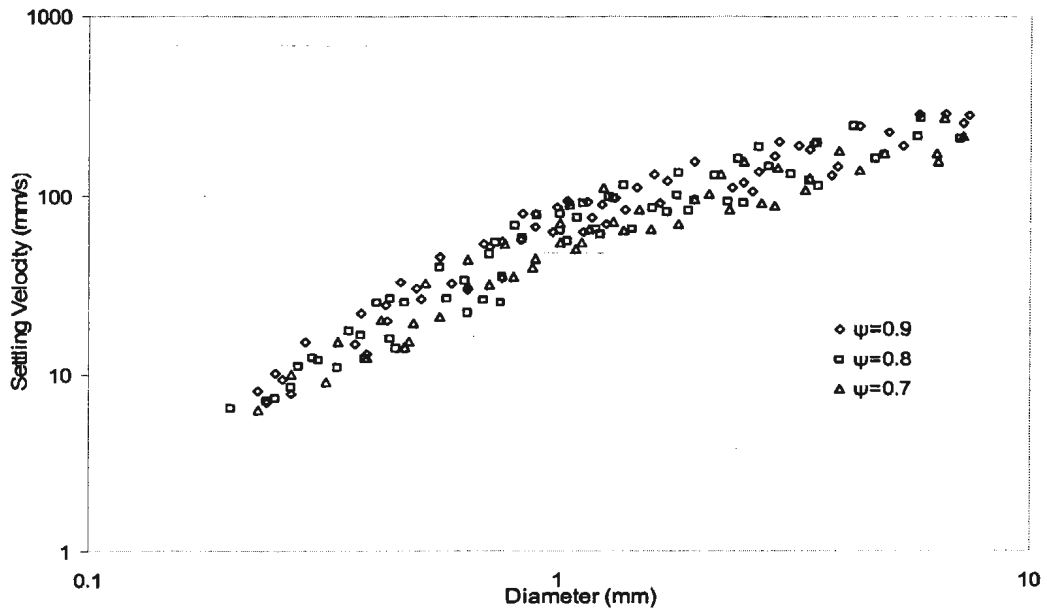


Figure 4-33 Seawater settling velocity data of treated cuttings (F3050-3069) of various shapes

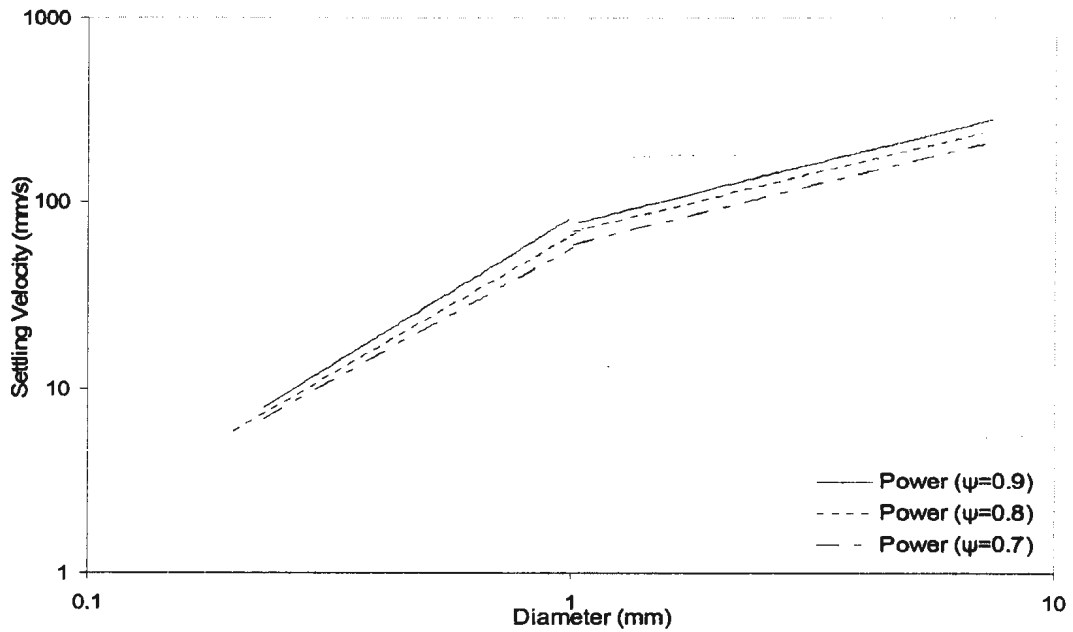


Figure 4-34 Power law fit of the seawater settling velocity data of treated cuttings (F3050-3069) of various shapes

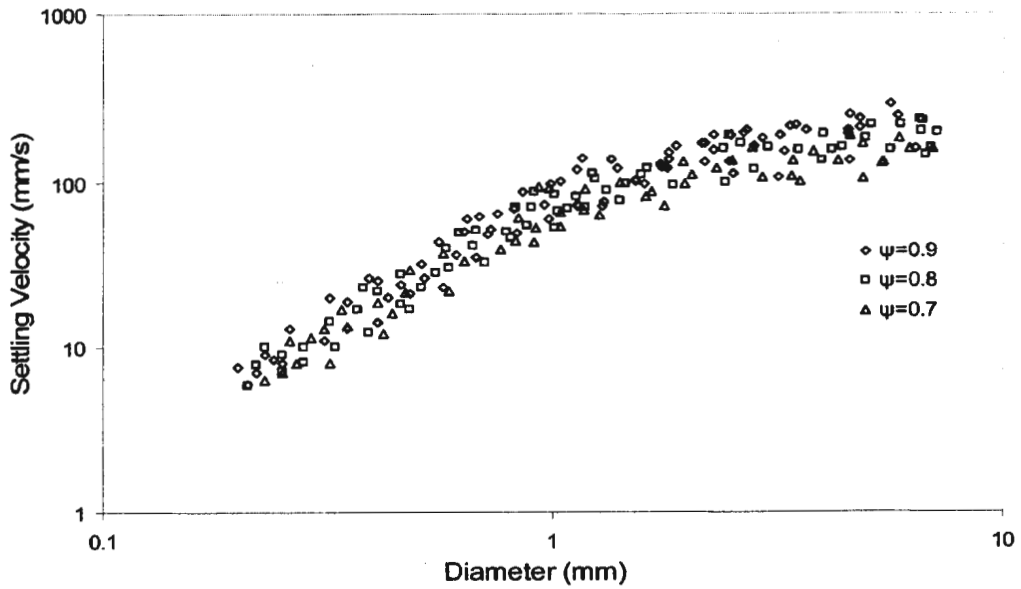


Figure 4-35 Freshwater settling velocity data of treated cuttings (F3070-3090) of various shapes

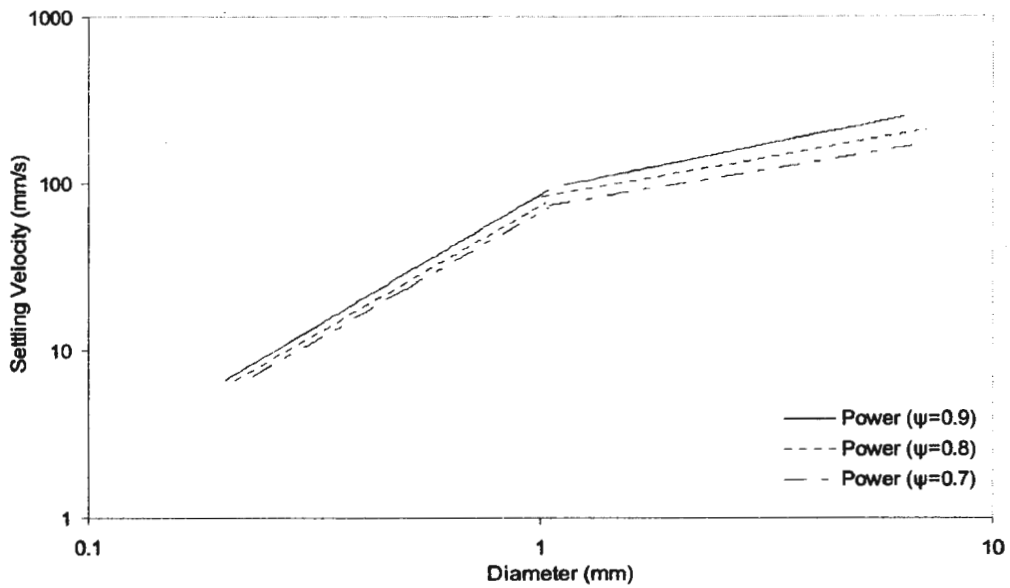


Figure 4-36 Power law fit of the freshwater settling velocity data of treated cuttings (F3070-3090) of various shapes

From the power law fit presented in Figures (4-32), (4-34) and (4-36), it can be seen that the settling velocity of F3050-3069 is a little bit higher than F3070-3090 and the particles settle faster in freshwater than in seawater. This is the same as the untreated cuttings. Unlike the untreated cuttings, it was shown that the sphericity of the particles has significant effects on the settling of treated drilling cuttings. The reason for this is that treated cuttings settle as individual particles instead of clumps. The density of treated cuttings is relatively uniform (unlike quartz sands, cuttings particles exist as an aggregate of rock particles and mud particles, therefore their densities are not as uniform as quartz sands).

Data points from Figures (4-31), (4-33), and (4-35) were compiled using Equations (4-1) and (4-2) and plotted in Figure (4-37).

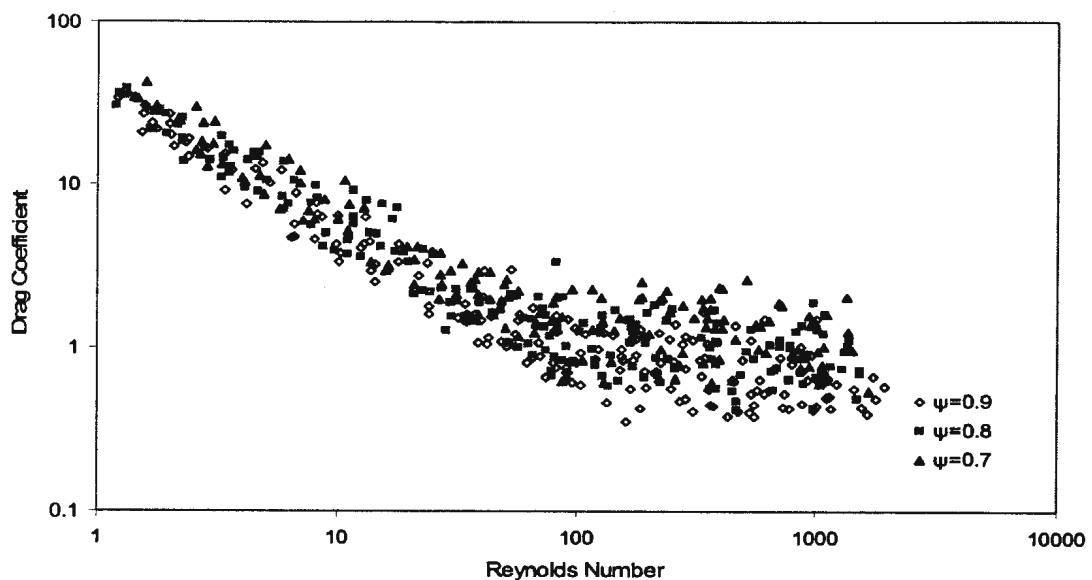


Figure 4-37 Drag coefficient versus Reynolds number for treated drill cuttings (experimental data)

Through the regression analysis, a similar relationship as Equation (4-3) between drag coefficient and Reynolds number for Reynolds numbers between 1 and 1000 is found as

$$C_D = a + \frac{b}{Re} \quad \text{Equation (4-5)}$$

This drag coefficient versus Reynolds number relation is plotted in Figure (4-38) and the relationships of Chien (1992) and Allen (1900) are plotted for reference. The values of a and b for particles with various sphericities are listed in Table (4-7) and plotted in Figure (4-39) and (4-40).

Table 4-7 Values of a , b for various shaped particles

Particle Sphericity	a	b	Correlation Coefficient, r
0.9	0.675	40.7016	.98
0.8	1.0424	43.3895	.98
0.7	1.20368	50.5447	.97

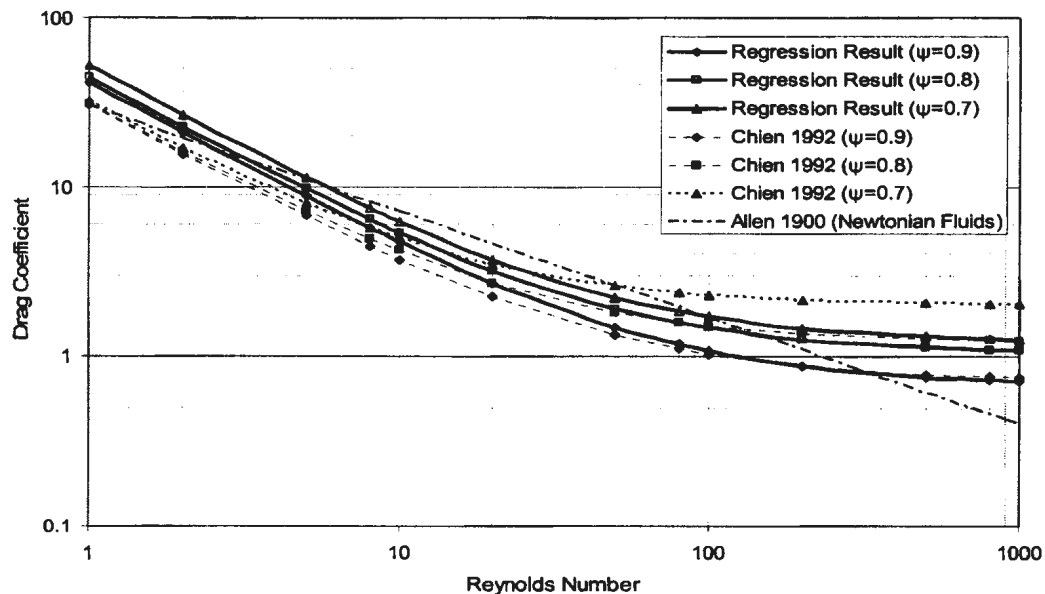


Figure 4-38 Drag coefficient vs Reynolds number for treated drill cuttings (regression results)

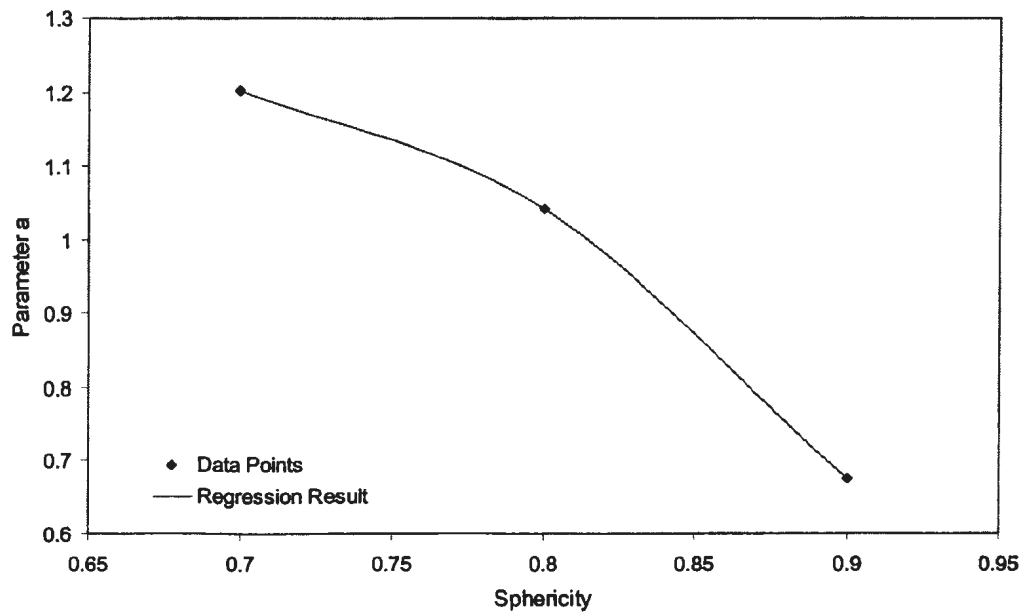


Figure 4-39 Relationship between parameter *a* and sphericity

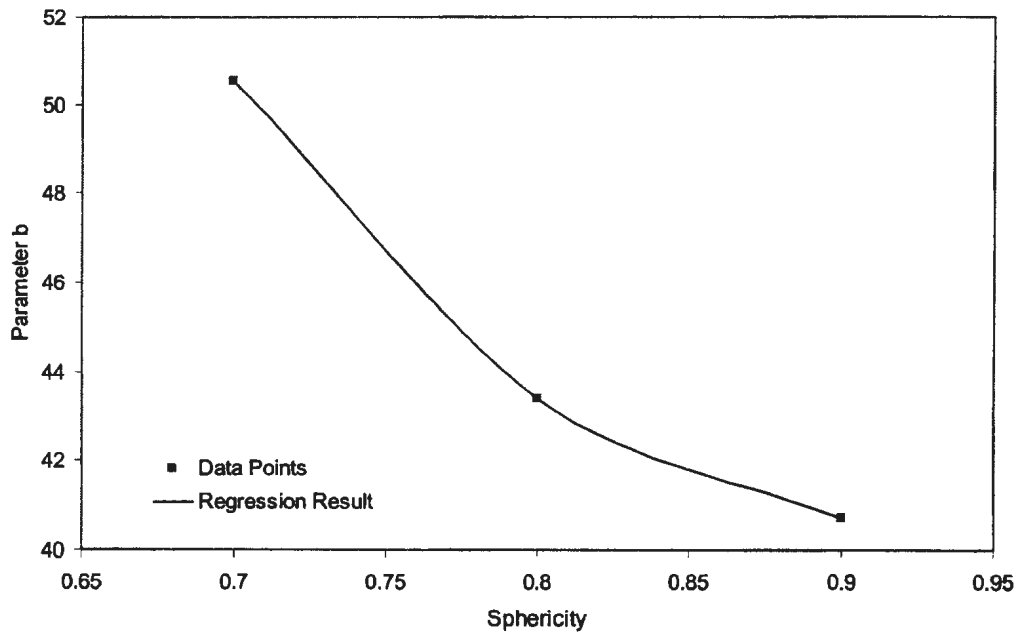


Figure 4-40 Relationship between parameter *b* and sphericity

Through regression analysis, the a and b are found as a function of sphericity

$$a = -3.4387 + 13.8462 \psi - 10.306 \psi^2 \quad \text{Equation (4-6)}$$

$$b = 225.7155 - 406.5995 \psi + 223.365 \psi^2 \quad \text{Equation (4-7)}$$

The correlation coefficients for a and b are 1.0. The sphericity ψ in Equations (4-6) and (4-7) ranges from 6.5 to 9.5.

A settling velocity correlation is then obtained using the same method described before; the settling velocity for treated SBF cuttings is obtained as

$$u = \frac{-3b\mu + \sqrt{9b^2\mu^2 + 48a(\rho_s - \rho_f)\rho_f g D^3}}{6a\rho_f D} \quad \text{Equation (4-8)}$$

Where u is the settling velocity (m/s),

ρ_s is the drilling cutting density (kg/m³)

ρ_f is the fluid density (kg/m³)

μ is the dynamic viscosity (kg/m·s)

D is the particle diameter (m)

g is the gravitational acceleration (m/s²)

a and b are the parameters given by Equation (4-6) and (4-7)

The calculated settling velocity curves of both treated and untreated SBFs produced cuttings with densities of 1850kg/m³ and 2650kg/m³ and with sphericity of 0.8 are plotted in Figure (4-41). The OBF cuttings of Gerard (1996) with density of 1850kg/m³, quartz

sands of Sleath (1984) with density of 2650kg/m^3 , and drill cuttings (unknown base fluid type) of Chien (1992) are plotted as reference.

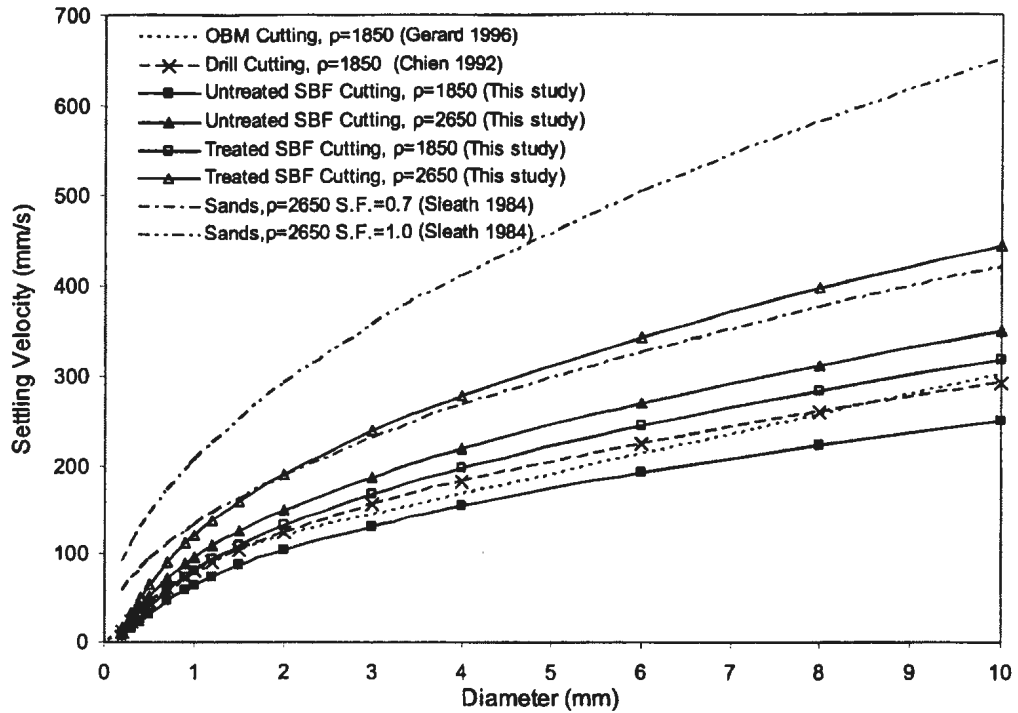


Figure 4-41 Settling velocity of various shaped treated SBF drilling cutting particles

From the Figure (4-41), it is shown that the treated cuttings of sphericity of 0.8 settle with a speed similar to quartz sand of *S.F.* of 0.7. It is also demonstrated that the treated cuttings settle faster than untreated cuttings. The treated cuttings also settle faster than OBF cuttings of Gerard (1996) and close to the cuttings of Chien (1992).

4.3 Floc Settling Velocity Results

Both the flocs formed using treated and untreated cuttings were used for floc settling tests. For seawater tests, flocs formed in all the combinations of concentration and shear rates were studied. For freshwater tests, only the flocs formed at the concentration of 100mg/L under 100G were tested.

4.3.1 Seawater Settling Velocity for Flocs formed from Untreated Cuttings

Figures (4-42) to (4-49) show the settling velocity data of flocs from untreated seawater tests. Figures (4-42), (4-44), (4-46), and (4-48) provide data points for all combinations of concentrations and shear rates. Figures (4-43), (4-45), (4-47) and (4-49) are the fitted curves of these data.

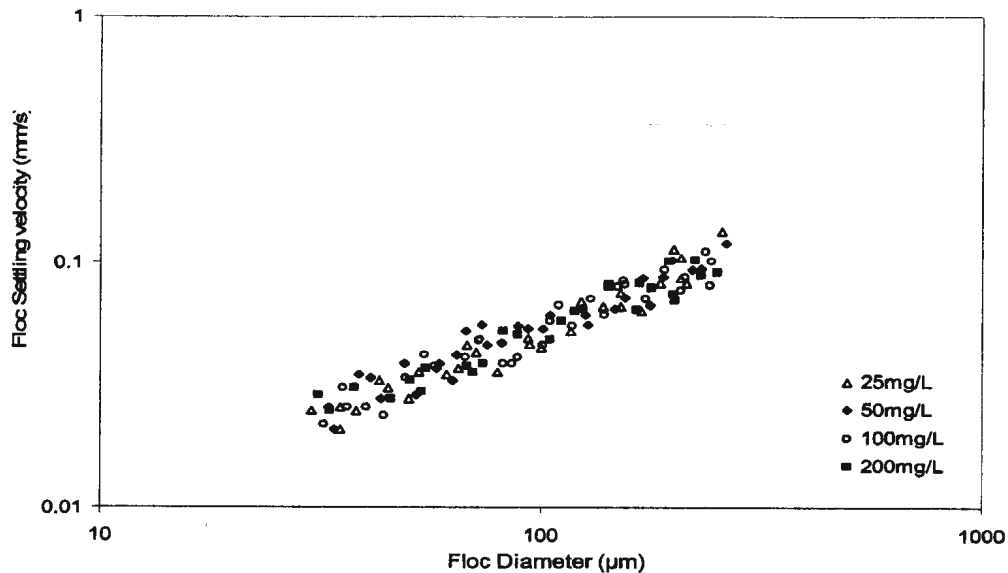


Figure 4-42 Seawater settling velocity data of flocs formed from untreated cuttings at 25G

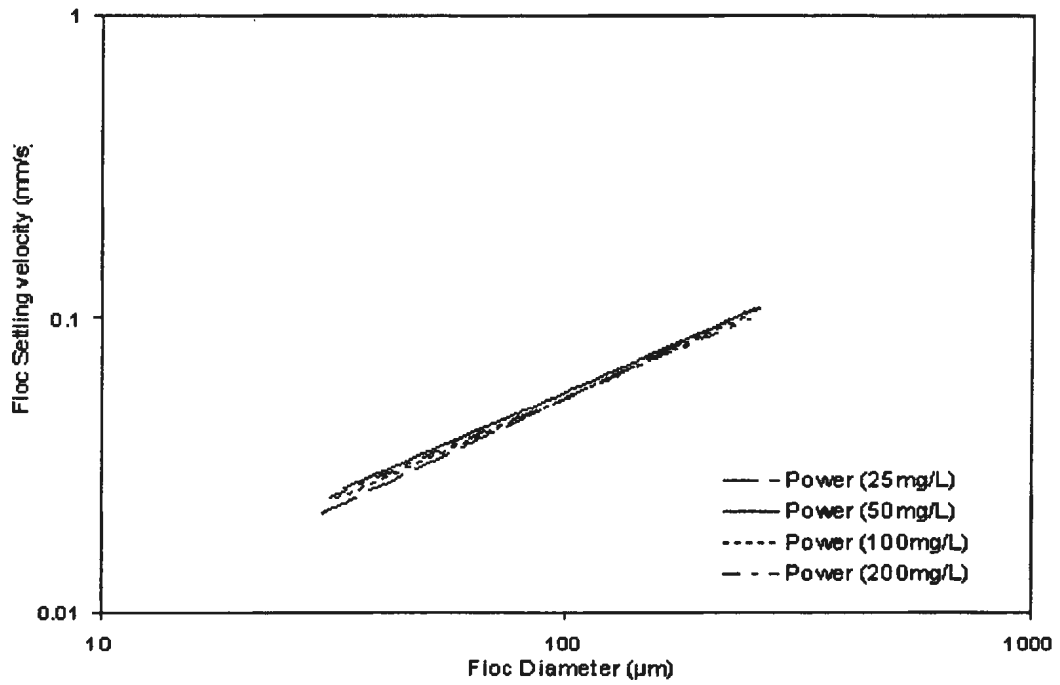


Figure 4-43 Power law fit of seawater settling velocity of flocs formed from untreated cuttings at 25G

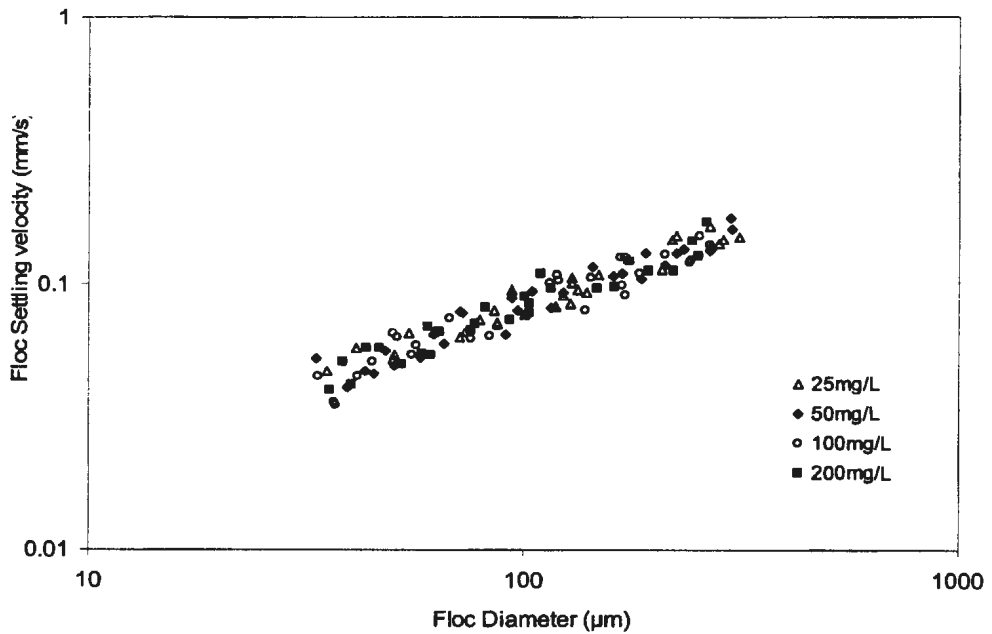


Figure 4-44 Seawater settling velocity data of flocs formed from untreated cuttings at 50G

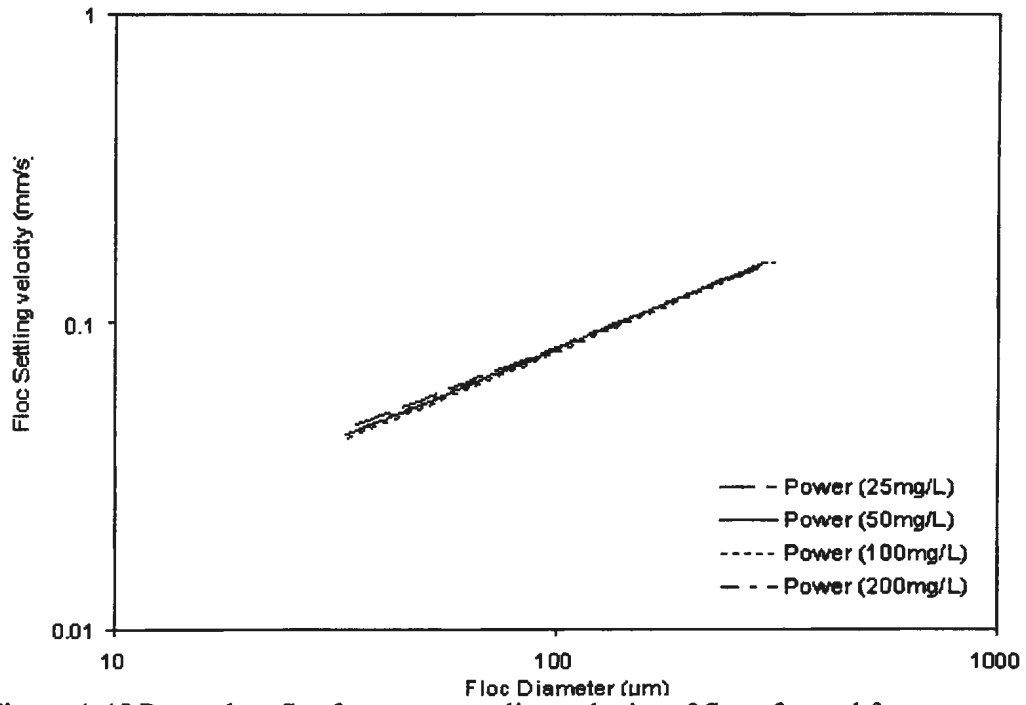


Figure 4-45 Power law fit of seawater settling velocity of flocs formed from untreated cuttings at 50G

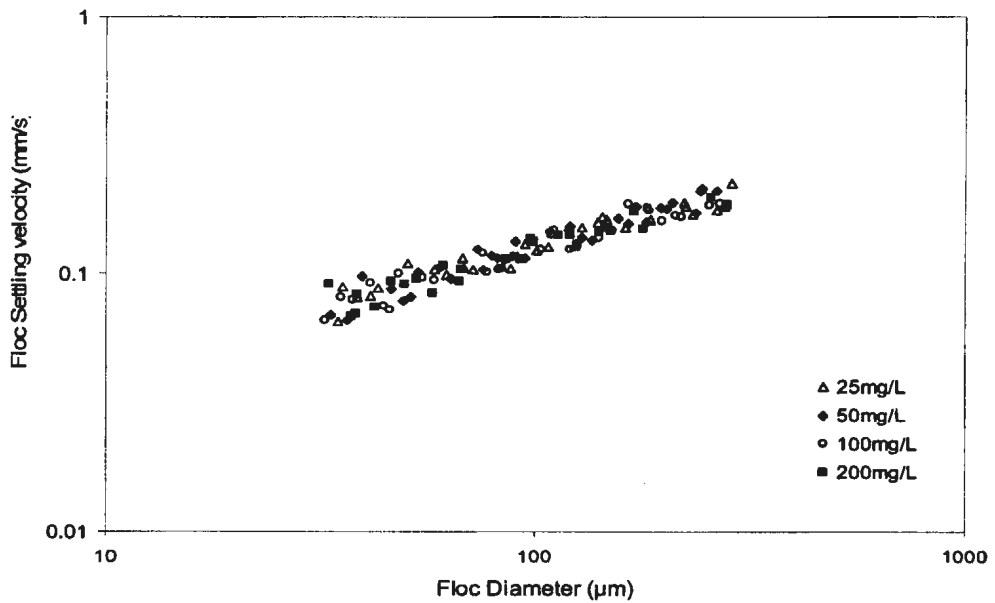


Figure 4-46 Seawater settling velocity data of flocs formed from untreated cuttings at 100G

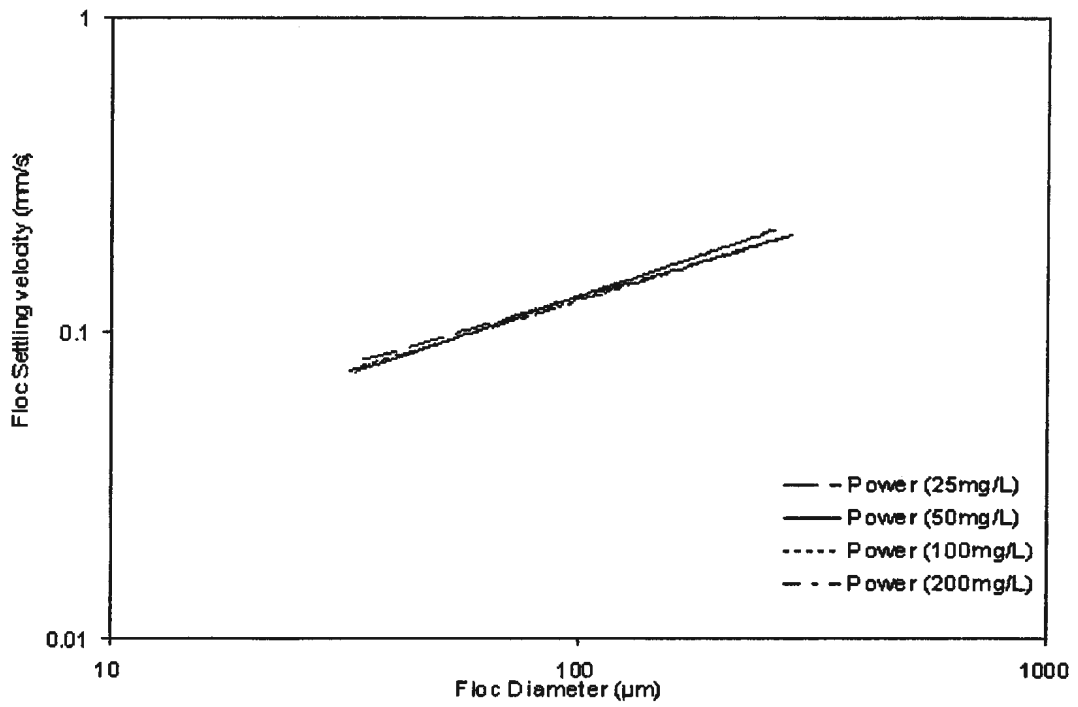


Figure 4-47 Power law fit of seawater settling velocity of flocs formed from untreated cuttings at 100G

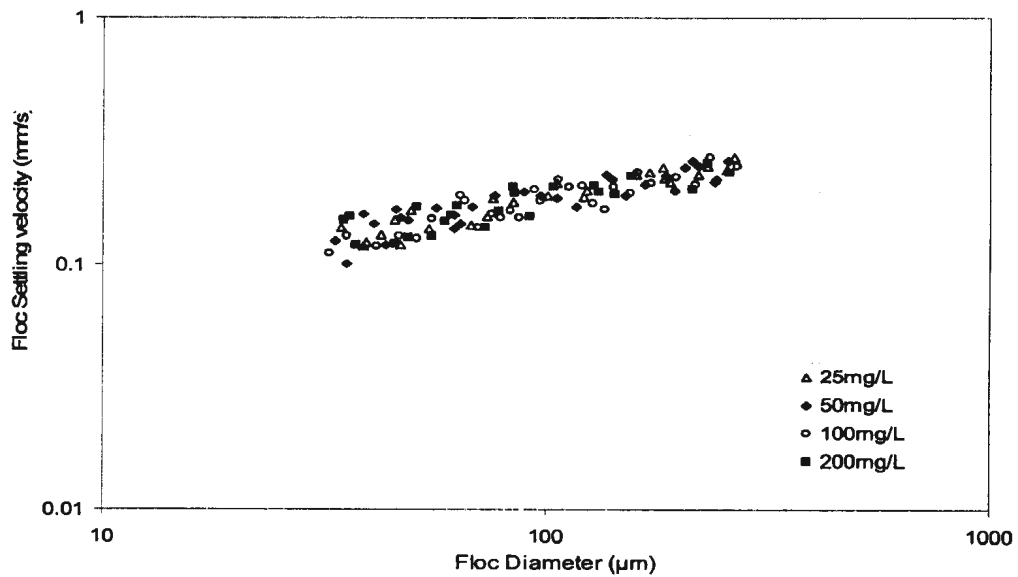


Figure 4-48 Seawater settling velocity data of flocs formed from untreated cuttings at 200G

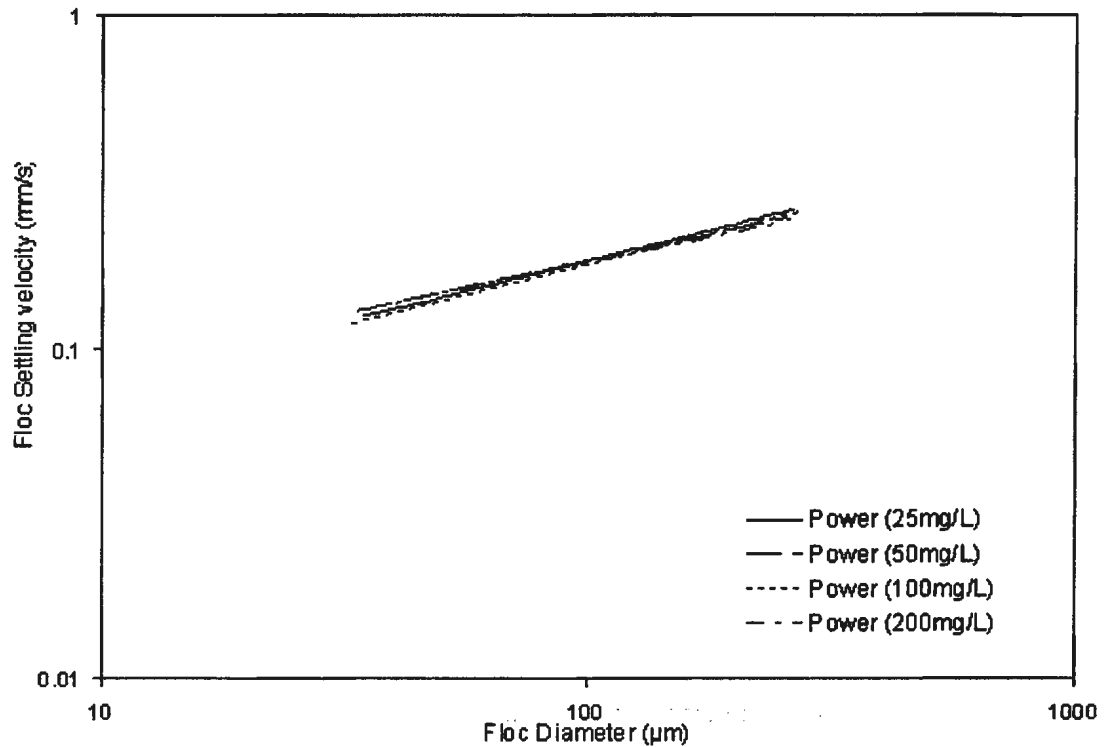


Figure 4-49 Power law fit of seawater settling velocity of flocs formed from untreated cuttings at 200G

It can be seen that all these data can be fitted by a power law.

$$u = AD^m \quad \text{Equation (4-9)}$$

where A and m are the constants determined experimentally.

It is shown by the power law fit in Figures (4-43), (4-45), (4-47) and (4-49) that, for the same diameter, flocs formed at higher shear rates have higher settling velocity. The data also show that the settling speed is almost the same for flocs formed at the same shear rate but different concentration. This may suggest that the flocs formed at different concentrations but same shear rates may have the same effective density. This finding is the same as Huang (1992)'s results for WBF flocs, but different from Burban et al.

(1990), which showed significant effects of concentration on floc settling velocity for natural particles.

Because of no effects of concentration on settling velocity were found, regression analysis was performed for the data at four different shear conditions. The A and m values for untreated seawater tests are listed in Table (4-8).

Table 4-8 A and m value for seawater tests of untreated cuttings

Shear Rate	A	m	Correlation coefficient, r
25G	0.00202	0.7124	0.94
50G	0.00579	0.5759	0.96
100G	0.01507	0.4614	0.96
200G	0.04034	0.3282	0.90

In order to get a generalized expression, the A and m values at different G are plotted in Figure (4-50). Through regression analysis, the A and m are found also follow a power law relationship. The values for the parameters are listed in Table (4-9).

Table 4-9 Values for the regression of A , m for seawater tests of untreated cuttings

	Parameter	Parameter e, k	Parameter f, j	Correlation coefficient, r
$A = eG^f$	A	$e=2.1568 \times 10^{-5}$	$f=1.4218$	0.99
$m = kG^j$	m	$k=2.2240$	$j=-0.3498$	0.99

By introducing the values from Table (4-9) into Equation (4-9), a generalized empirical equation is obtained for the settling of untreated drilling cutting flocs in sea water:

$$u = 2.16 \times 10^{-5} G^{1.42} D^{\frac{2.22}{G^{0.35}}} \quad \text{Equation (4-10)}$$

Where the u is floc settling velocity (mm/s)

G is the shear rate (s^{-1})

D is the floc diameter (μm)

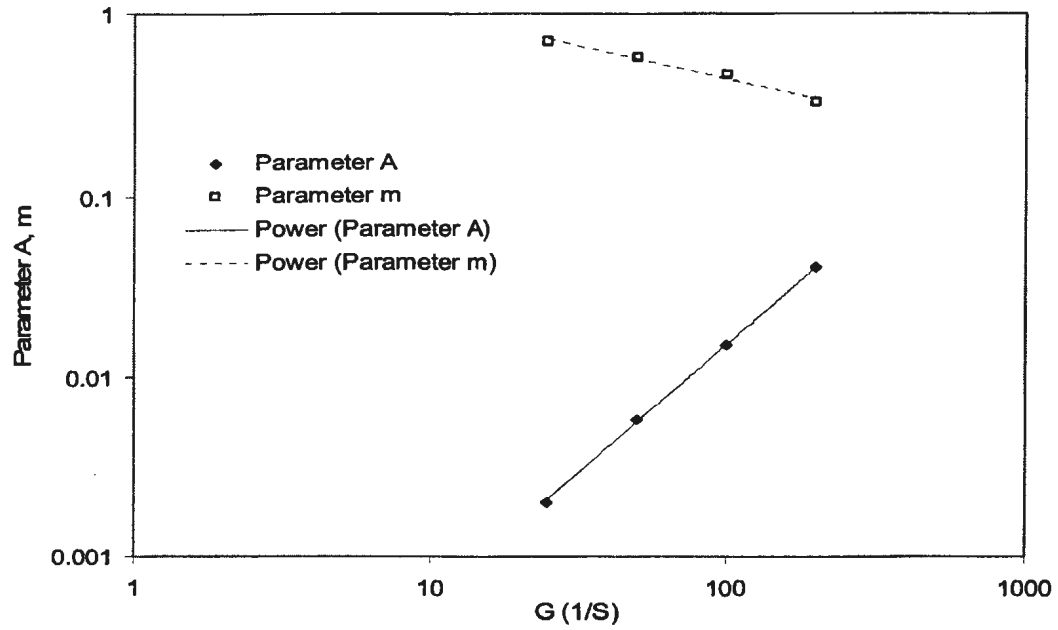


Figure 4-50 Parameters A and m for untreated cuttings as a function of shear rate G

The calculated settling velocity curves are plotted in Figures (4-51) and (4-52). The WBF flocs settling data by Huang (1992) and four groups of natural particle flocs settling data by Gibbs (1985) are plotted for reference.

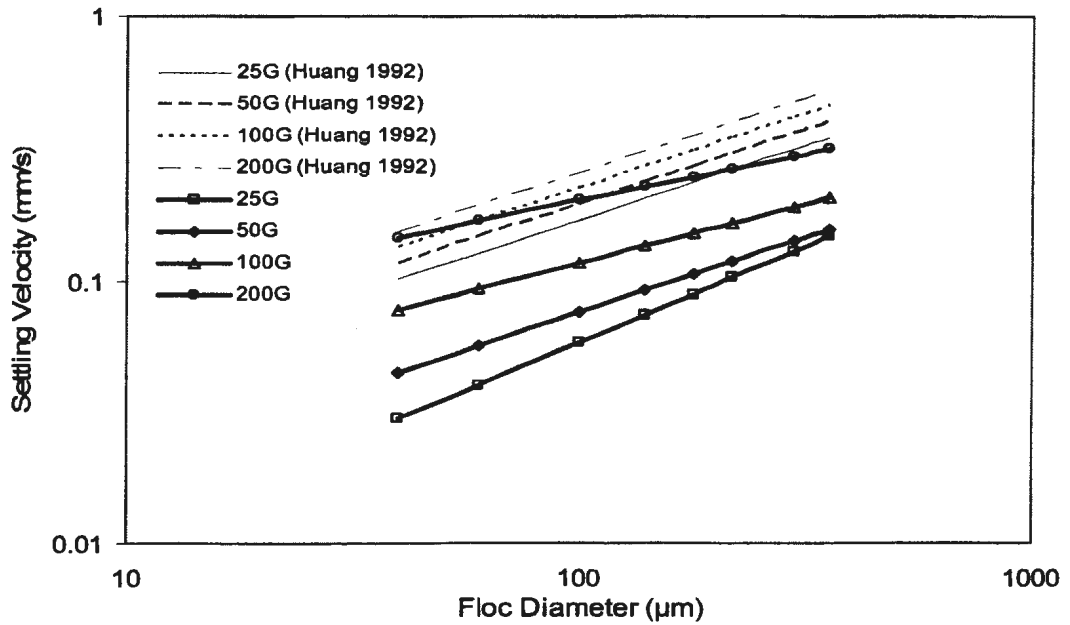


Figure 4-51 Relationship between seawater settling velocity and floc diameter of untreated SBF cuttings. The data for WBFs by Huang (1992) are presented for reference

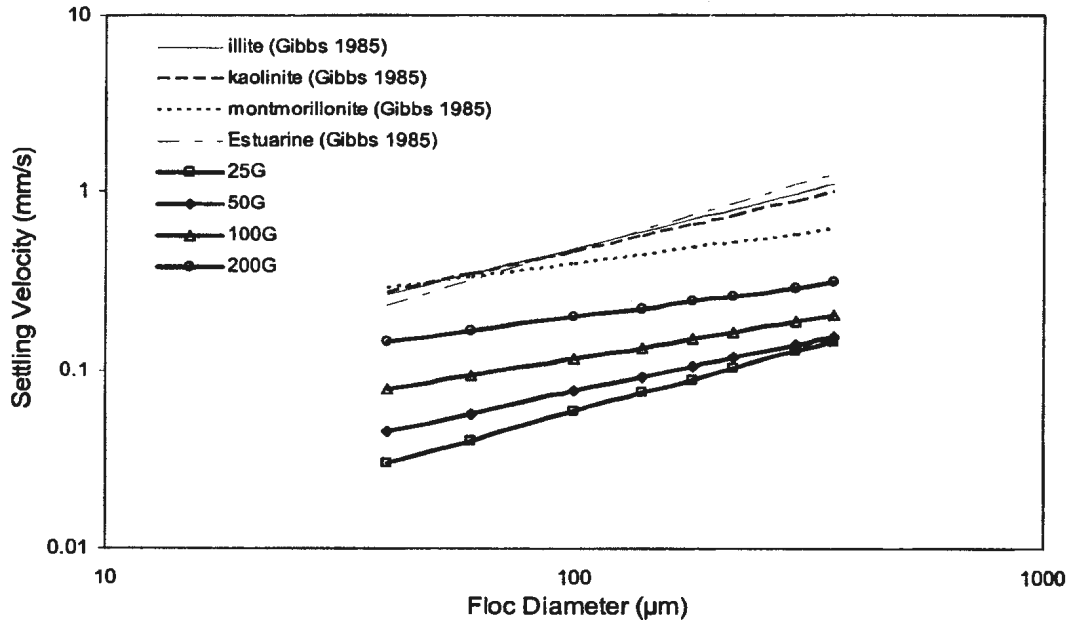


Figure 4-52 Relationship between seawater settling velocity and floc diameter of untreated SBF cuttings. The data for clay minerals by Gibbs (1985) are presented for reference

It can be seen from Figures (4-51) and (4-52), that the settling velocities of untreated SBF flocs are smaller than the settling velocities of WBF flocs. Both the seawater settling velocity of SBF and WBF flocs are smaller than freshwater natural particles. Together with the flocculation data, this may imply that the seawater flocs have larger particle size but smaller effective density. In other words, the flocs formed in freshwater may be more compact than the flocs formed sea water. The effect of salinity on the floc effective density will be discussed later.

4.3.2 Seawater Settling Velocity for Flocs formed from Treated Cuttings

Figures (4-53) to (4-60) show the settling velocity data of flocs from treated seawater tests. Figures (4-53), (4-55), (4-57), and (4-59) are data points for all combinations of concentration and shear rate. Figures (4-54), (4-56), (4-58) and (4-60) are the fitted curves of these data.

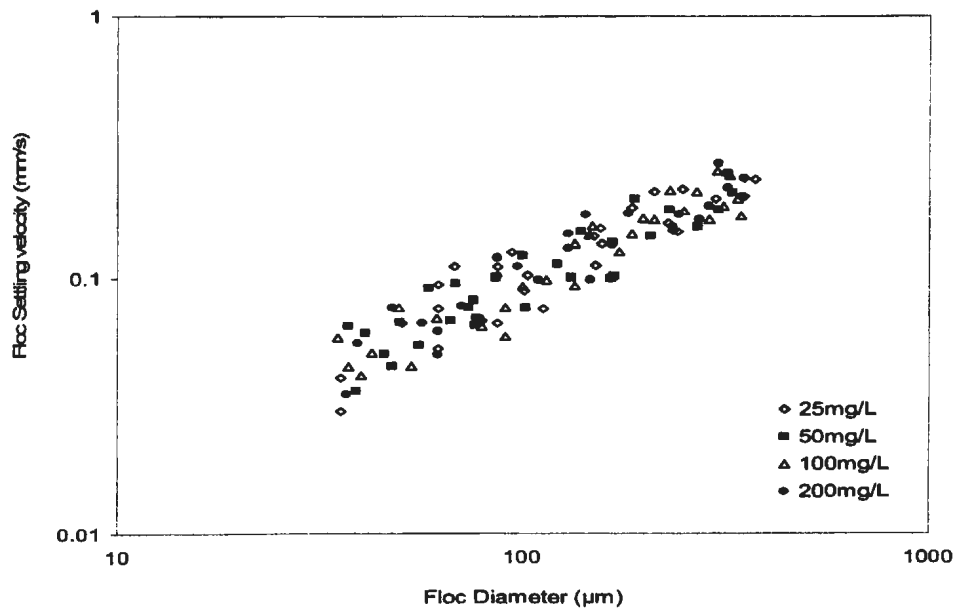


Figure 4-53 Seawater settling velocity data of flocs formed from treated cuttings at 25G

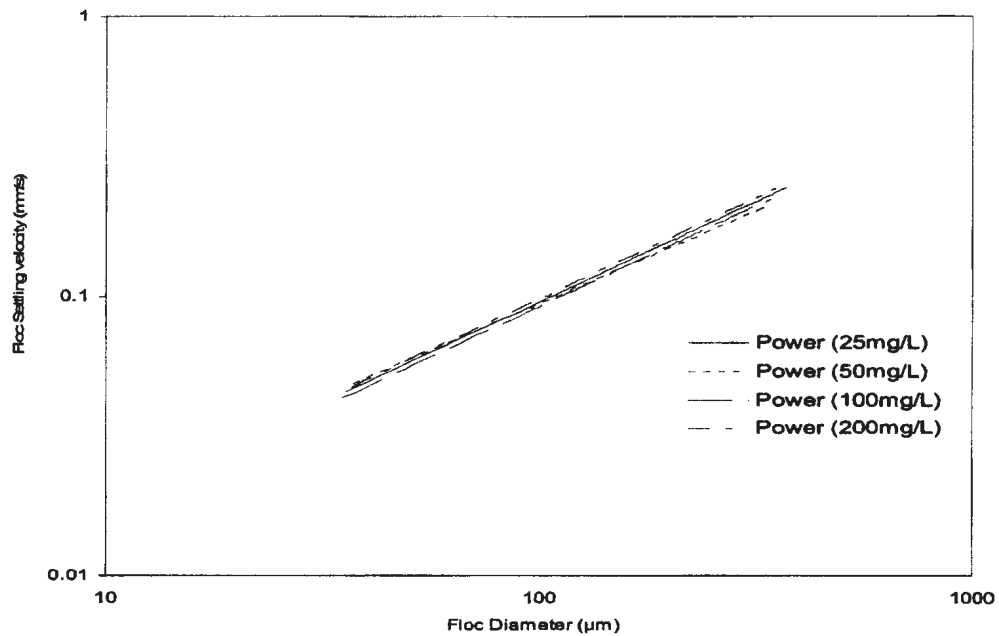


Figure 4-54 Power law fit of seawater settling velocity of flocs formed from treated cuttings at 25G

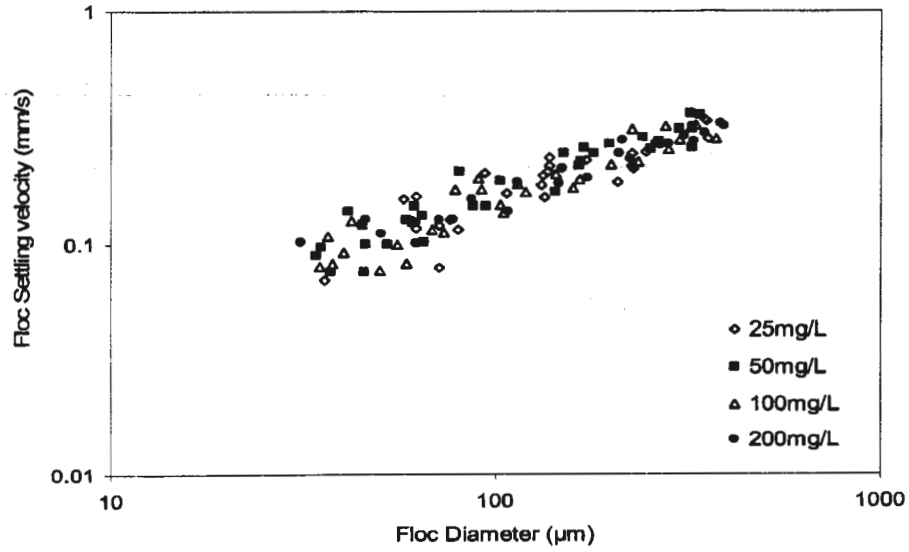


Figure 4-55 Seawater settling velocity data of flocs formed from treated cuttings at 50G

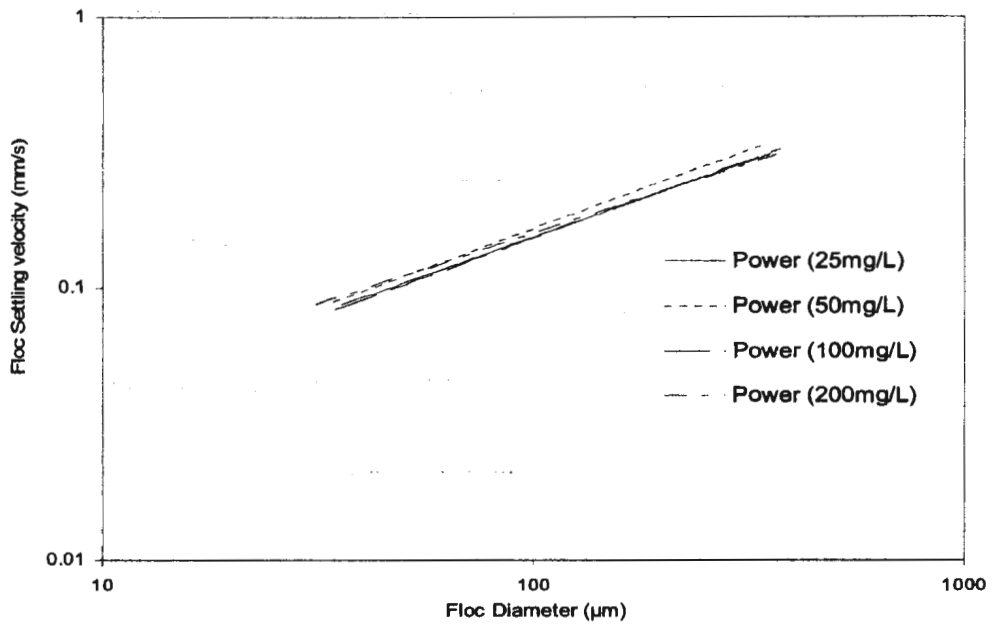


Figure 4-56 Power law fit of seawater settling velocity of flocs formed from treated cuttings at 50G

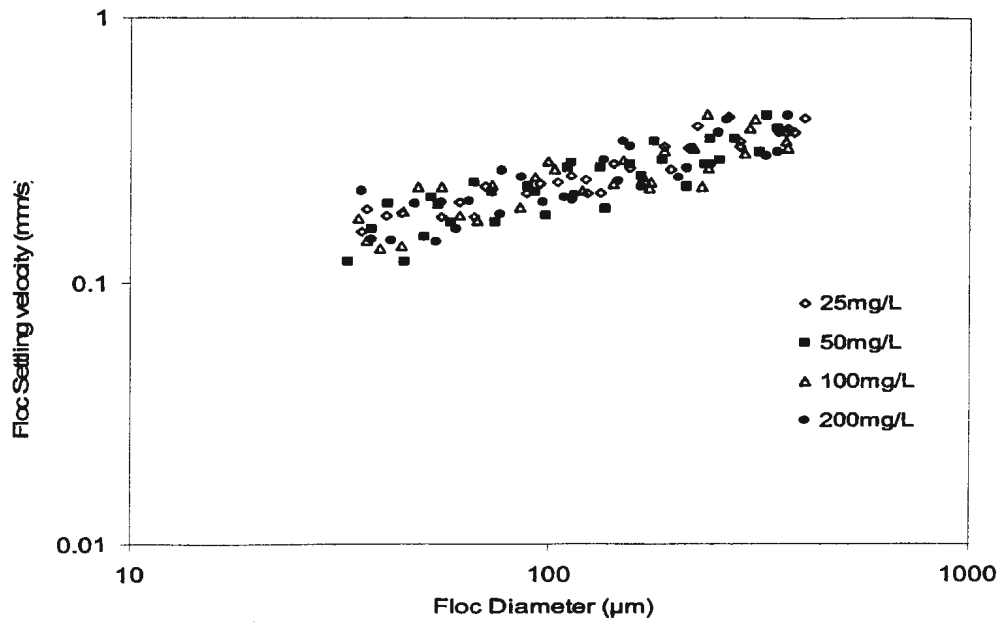


Figure 4-57 Seawater settling velocity data of flocs formed from treated cuttings at 100G

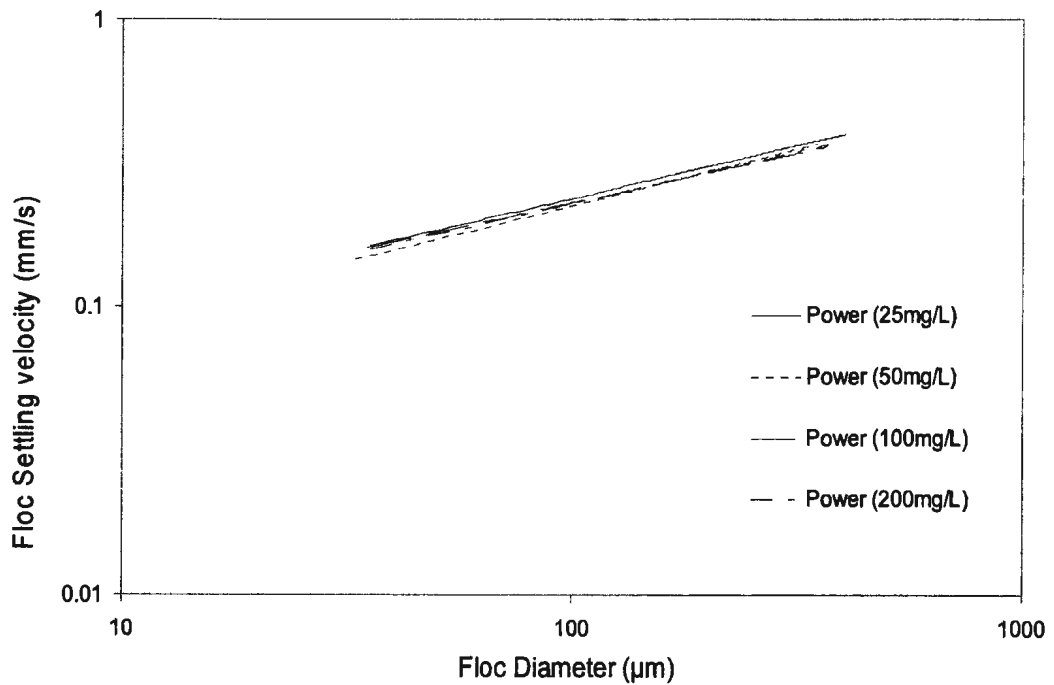


Figure 4-58 Power law fit of seawater settling velocity of flocs formed from treated cuttings at 100G

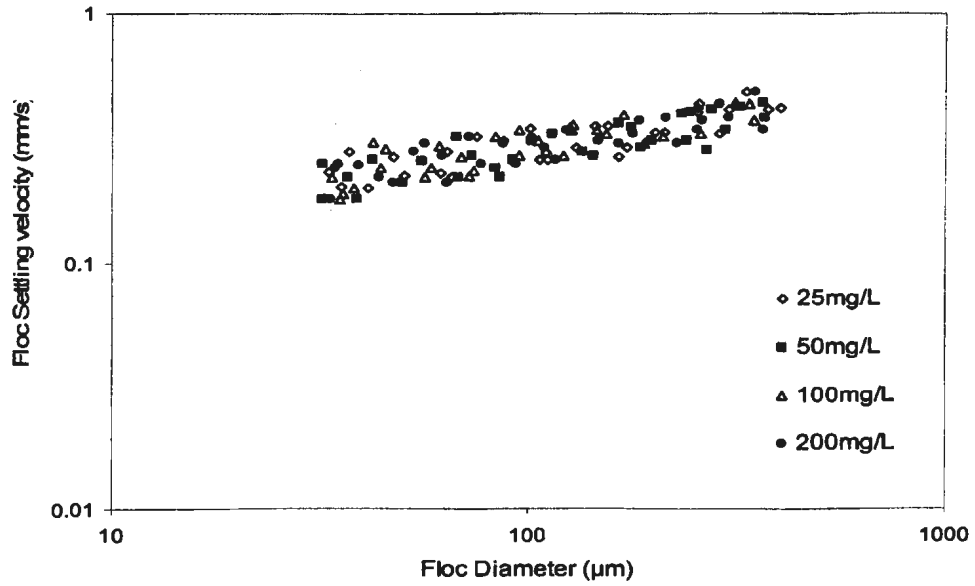


Figure 4-59 Seawater settling velocity data of flocs formed from treated cuttings at 200G

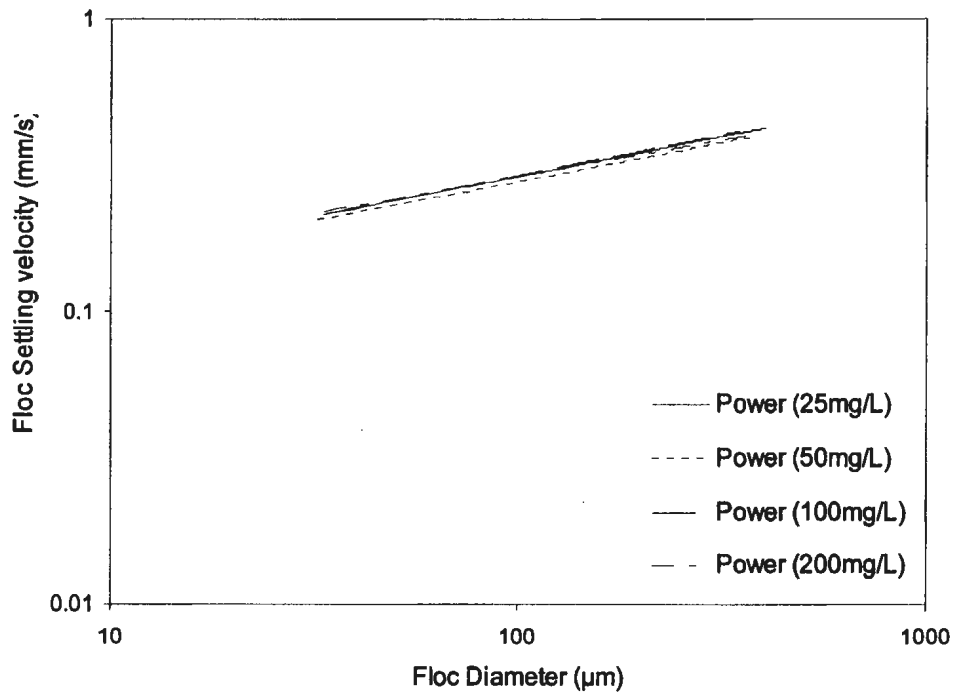


Figure 4-60 Power law fit of seawater settling velocity of flocs formed from treated cuttings at 200G

Like the data for untreated drilling cuttings, the data for treated cuttings can also be fitted by a power law model and the concentration effects on settling of treated cuttings are found to be insignificant.

The A and m values for untreated seawater tests are listed in Table (4-10) and the regression results of A and m for treated cuttings are listed in Table (4-11).

Table 4-10 A and m value for seawater tests of treated cuttings

Shear Rate	A	m	Correlation coefficient, r
25G	0.005	0.641	0.93
50G	0.013	0.531	0.90
100G	0.035	0.409	0.90
200G	0.065	0.326	0.91

Table 4-11 Values for the Regression of A , m for seawater tests of treated cuttings

	Parameter	Parameter e, k	Parameter f, j	Correlation coefficient, r
$A = eG^f$	A	$e=0.00022$	$f=1.072$	0.997
$m = kG^j$	m	$k=1.84$	$j=-0.324$	0.98

Figure (4-61) is a plot of parameter A and m as a function of shear rate for treated cuttings in sea water. By introducing the value from Table (4-9) into Equation (4-9), a generalized empirical equation was obtained for the settling of treated drilling cutting flocs in sea water

$$u = 2.22 \times 10^{-4} G^{1.07} D^{\frac{1.84}{G^{0.32}}} \quad \text{Equation (4-11)}$$

where the u is floc settling velocity (mm/s)

G is the shear rate (s^{-1})

D is the floc diameter (μm)

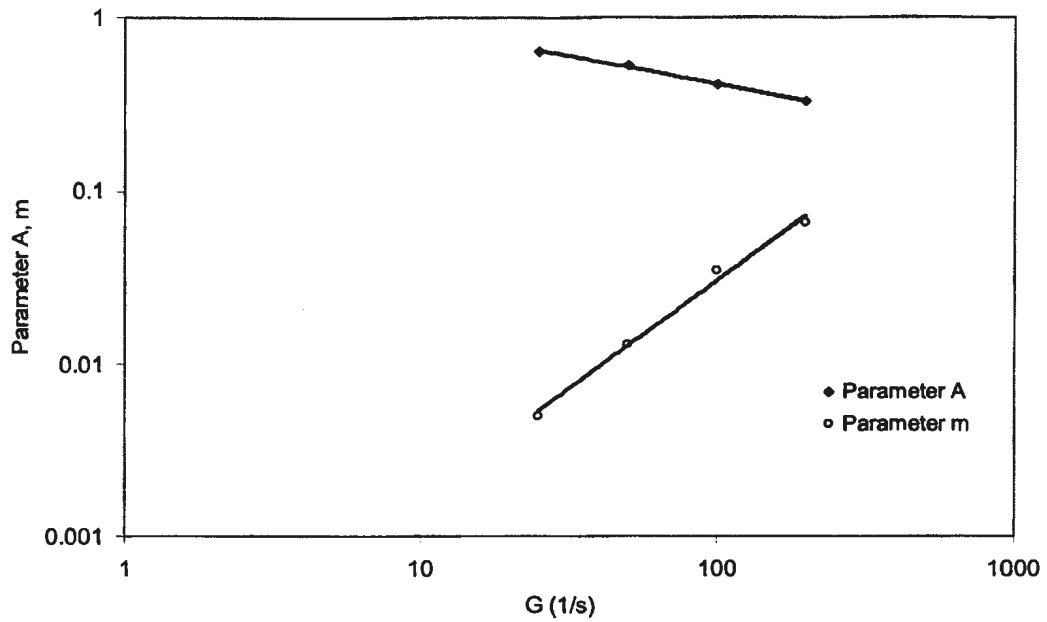


Figure 4-61 Parameters A and m for treated cuttings as a function of Shear rate G

The calculated settling velocity curves are plotted in Figures (4-62) and (4-63). The WBF flocs settling data by Huang (1992) and four groups of natural particle flocs settling data by Gibbs (1985) are plotted as reference.

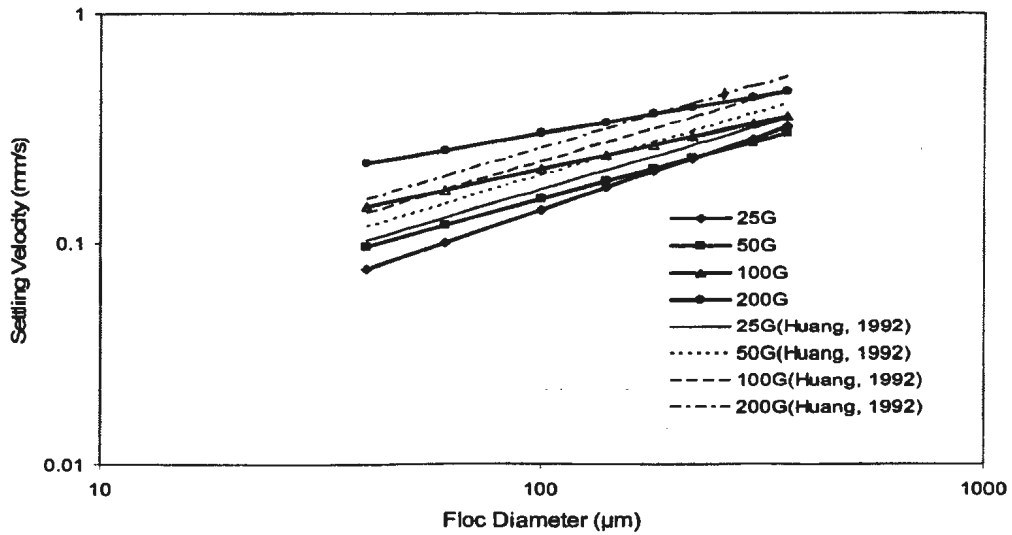


Figure 4-62 Relationship between seawater settling velocity and floc diameter of treated SBF cuttings. The data for WBFs by Huang (1992) are presented for reference

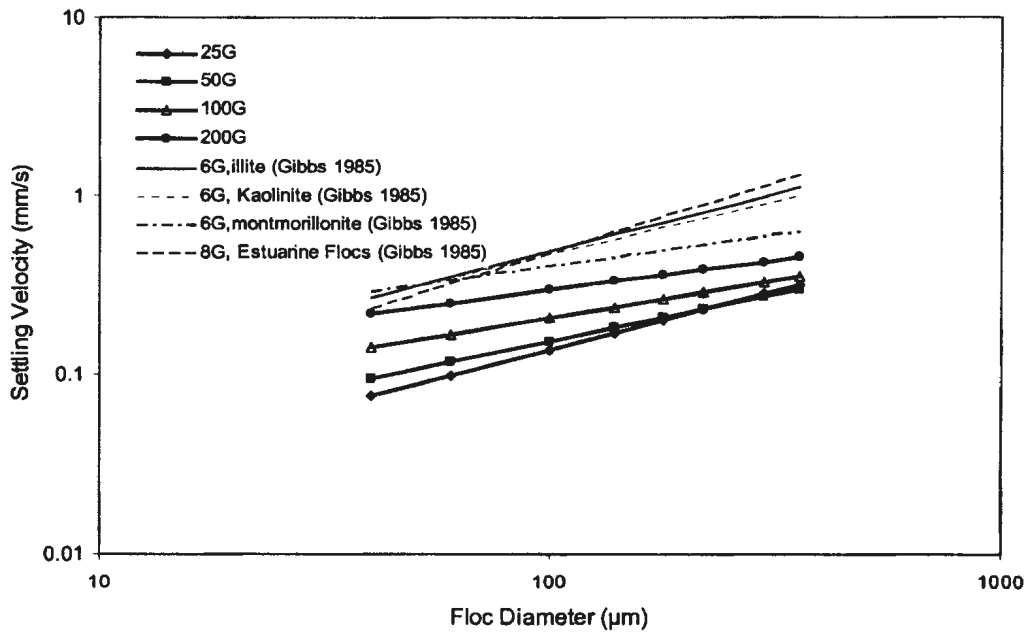


Figure 4-63 Relationship between seawater settling velocity and floc diameter of treated SBF cuttings. The data for clay minerals by Gibbs (1985) are presented for reference

It can be seen from Figures (4-62) and (4-63) that the settling velocity curves of treated SBF flocs are close to the settling velocity curves of WBF flocs and larger than the untreated cuttings. From Figures (4-52) and (4-63) it can be seen that the flocs formed from both the untreated and treated SBF cuttings seawater tests are smaller than natural particles in freshwater tests. This means that the salinity also has significant effects on the flocs settling, so freshwater settling tests need to be conducted to study the salinity effects

4.4.3 Freshwater Settling Velocity of Flocs

The flocs produced in seawater tests at the concentration of 100mg/L and shear rate of 100G were transferred into a settling column filled with freshwater for settling tests and the obtained data are plotted in Figure (4-64). The settling velocity data of freshwater produced flocs under the same concentration and shear rate are plotted in Figure (4-65).

Similar to the seawater tests, all data obtained in the freshwater tests follow the power law relationship. Figure (4-66) is the regression results of freshwater settling velocity data. The data from Gibbs (1985) and Burban et al (1990) are also plotted for reference.

The parameters are listed in Table (4-12)

Table 4-12 *A* and *m* value for the freshwater settling velocity of flocs formed at concentration of 100mg/L and shear rate of 100G

Floc Type	<i>A</i>	<i>m</i>	Correlation coefficient
Untreated formed in Seawater	0.0137	0.4887	0.95
Treated Formed in Seawater	0.0168	0.5528	0.96
Untreated formed in Freshwater	0.0263	0.4902	0.94
Treated formed in Freshwater	0.0464	0.4833	0.94

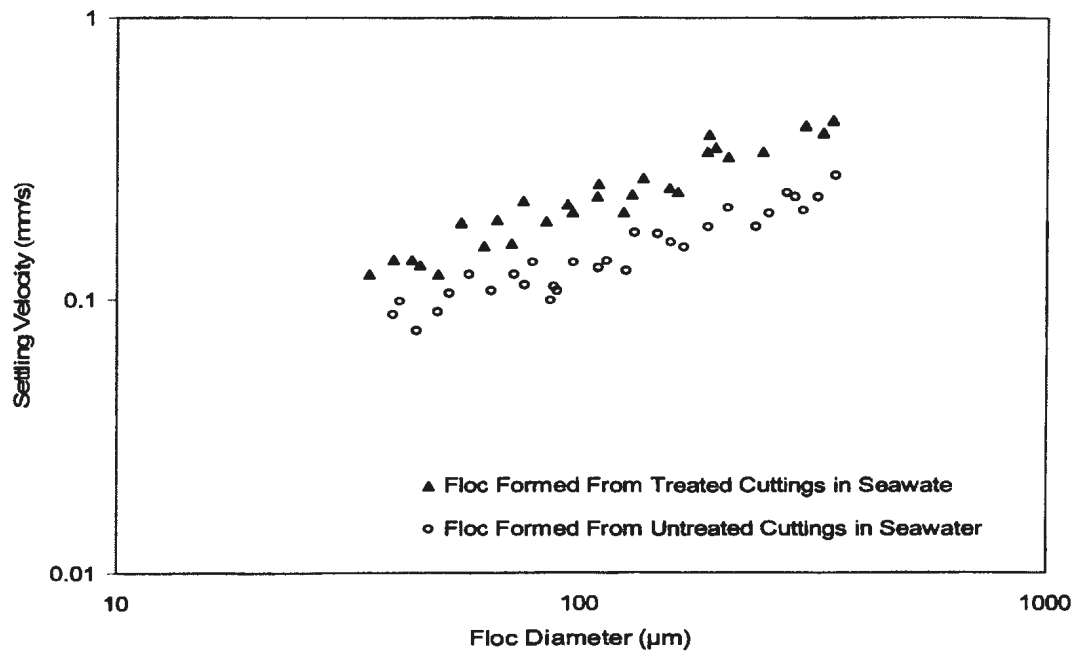


Figure 4-64 Freshwater settling velocity data of flocs formed in seawater at the concentration of 100mg/L and shear rate of 100G

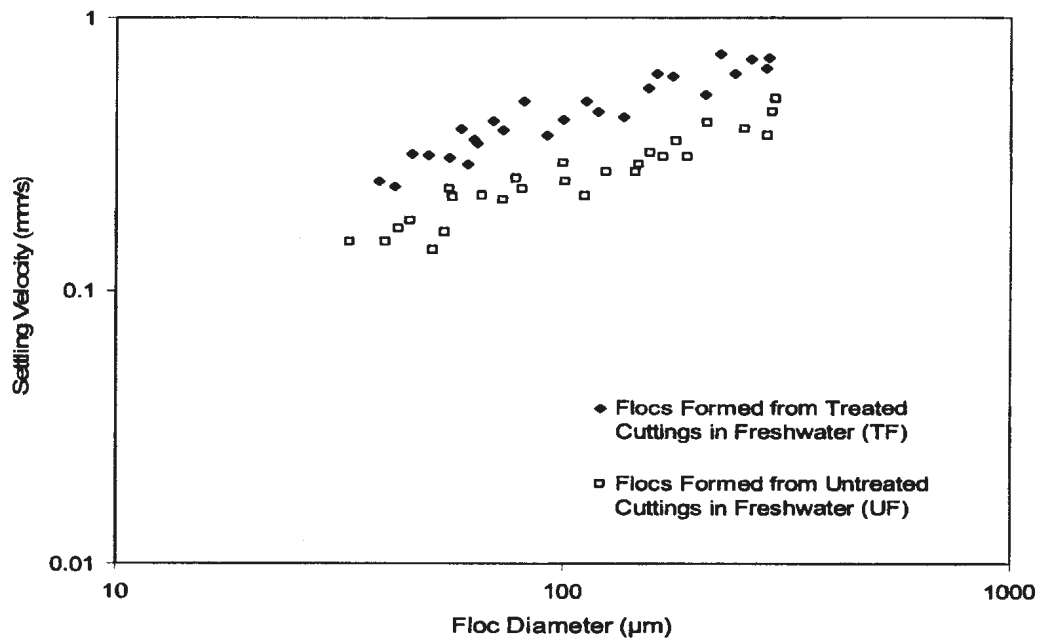


Figure 4-65 Freshwater settling velocity data of flocs formed in freshwater at the concentration of 100mg/L and shear rate of 100G

It can be seen from Figure (4-66), the TSS (Treated cuttings produced in Seawater and settle in Seawater) curve and TSF (Treated cuttings produced in Seawater and settle in Freshwater) curve are very close. The USS (Untreated cuttings produced in Seawater and settle in Seawater) curve and USF (Untreated cuttings produced in Seawater and settle in Freshwater) curve are also very close. This implies that for the flocs formed during seawater tests, the salinity of the water does not have significant effects on the settling velocities of the flocs, while it has great effect on the coarse cutting particles. It can also be seen from Figure (4-66) that the TSF curve lies far from TFF (Treated cuttings produced in Freshwater and settle in Freshwater) curve. Similarly, the USF curve also lies far from UFF (Untreated cuttings produced in Freshwater and settle in Freshwater) curve. This means, for the flocs produced at water with different salinities, the salinity does have effect on the settling velocity. It is illustrated by Figure (4-66) that in this case the freshwater formed flocs settle faster than seawater formed flocs. This implies that the freshwater produced flocs in this test conditions (100mg/L, 100G) have relatively larger effective density than seawater produced flocs. However, this conclusion can not be extended to all test conditions due to the limited test series in the present research. Figure (4-67) compares the settling velocity of seawater and freshwater produced natural sediments flocs, which shows that the seawater settling velocity is somewhat higher than freshwater settling velocity except for the case of 400G. It is shown by Figures (4-43), (4-45), (4-47), (4-49), (4-54), (4-56), (4-58), (4-60) and (4-66) that the treated cuttings have higher seawater settling velocity than untreated cuttings for all test cases.

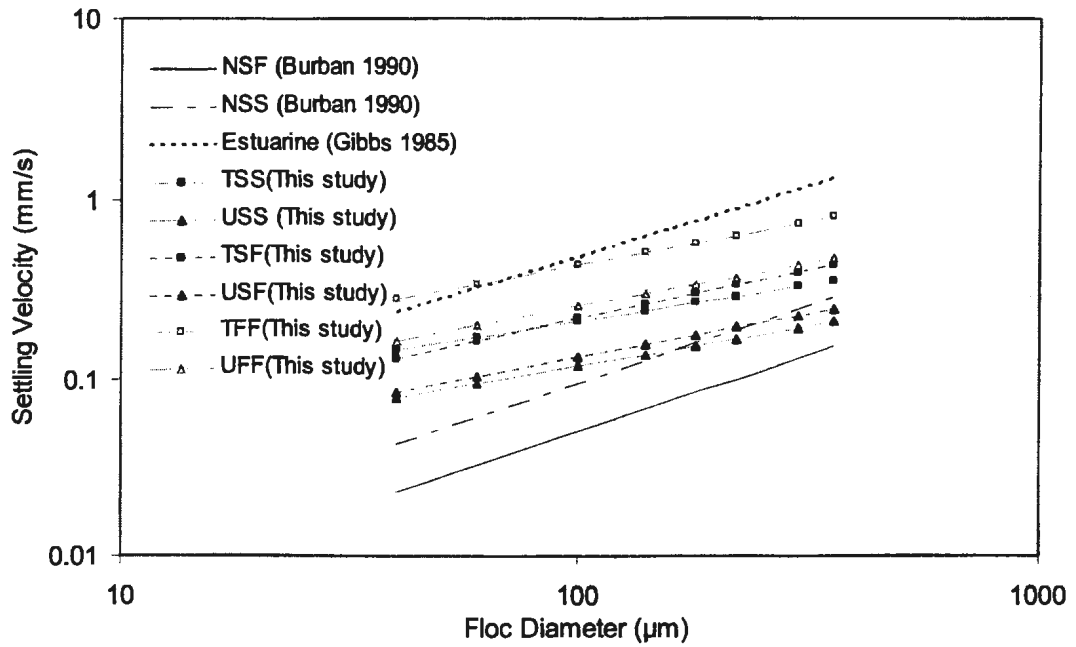


Figure 4-66 Settling velocity of flocs formed from SBF cuttings. The data of Gibbs (1985) and Burban et al. (1990) are plotted for reference.

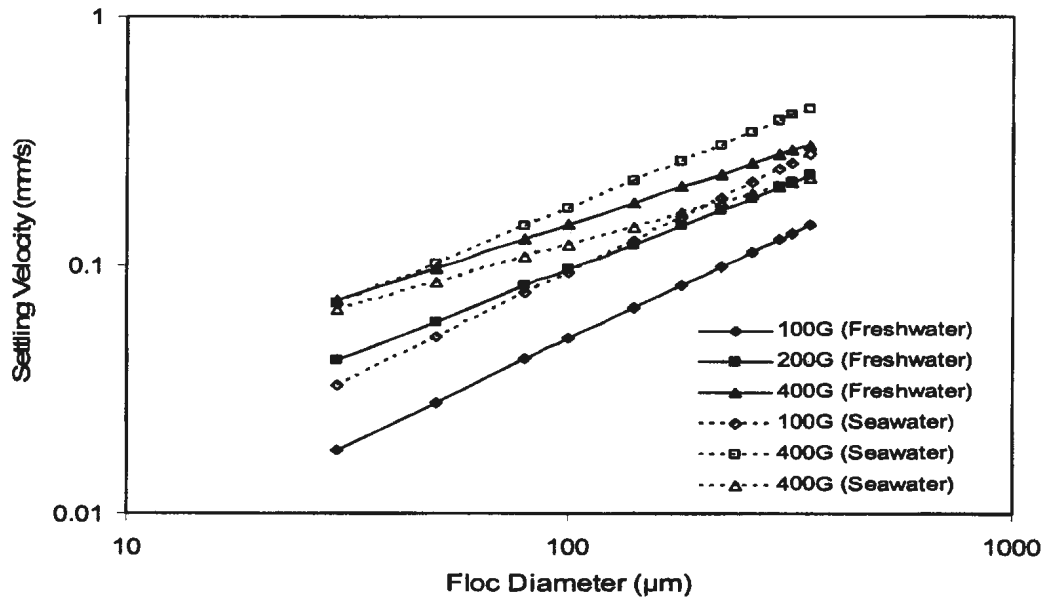


Figure 4-67 Settling velocity of natural sediment flocs produced at 100mg/L (data of Burban et al 1990)

4.4 Summary

The experimental results were presented and analyzed in Chapter 4. Time variations of floc median diameters were obtained for several different test conditions. It was found that the steady state particle size distribution depends on the conditions under which the steady state is approached. The median floc size decreases as the shear stress increases, particles flocculate faster in seawater than in freshwater, and flocs are smaller in freshwater than in seawater. Flocs produced from untreated cuttings flocculate faster than treated cuttings. Flocs produced from treated cuttings are smaller than untreated cuttings.

The drag coefficient correlations were derived for both treated and untreated coarse drilling cutting particles. The settling velocity equations were then developed based on the drag coefficient correlations. It was shown that the settling velocity of untreated drilling cutting particles is a function of particle size, bulk density and fluid properties. The settling velocity of treated cuttings is a function of particle sphericity as well as size, bulk density and fluid properties. It was also demonstrated that the treated cuttings settle faster than untreated cuttings with the same bulk density.

Empirical settling velocity equations were developed for flocs formed from both treated and untreated cuttings. It was shown by the floc settling experiments that the settling velocity of flocs is a function of both its size and fluid shear. The settling velocity increases as fluid shear increases.

As a summary, the equations developed from the present experiments are listed in Table (4-13).

Table 4-13 Summary of developed equations

No.	Equation
1	<p>Drag coefficient correlation for untreated coarse cutting particles</p> $C_D = 1.69959 + \frac{56.26128}{Re} \quad \text{Equation (4-3)}$
2	<p>Settling velocity for untreated coarse cutting particles</p> $u = \frac{-15.36\mu + \sqrt{236.08\mu^2 + 0.78(\rho_s - \rho_f)\rho_f D^3 g}}{\rho_f D} \quad \text{Equation (4-4)}$
3	<p>Drag coefficient correlation for treated coarse cutting particles</p> $C_D = a + \frac{b}{Re} \quad \text{Equation (4-5)}$ <p>where</p> $a = -3.4387 + 13.8462\psi - 10.306\psi^2 \quad \text{Equation (4-6)}$ $b = 225.7155 - 406.5995\psi + 223.365\psi^2 \quad \text{Equation (4-7)}$
4	<p>Settling velocity for treated coarse cutting particles</p> $u = \frac{-3b\mu + \sqrt{9b^2\mu^2 + 48a(\rho_s - \rho_f)\rho_f g D^3}}{6a\rho_f D} \quad \text{Equation (4-8)}$
5	<p>Seawater settling velocity for flocs formed from untreated cuttings</p> $u = 2.16 \times 10^{-5} G^{1.42} D^{\frac{2.22}{G^{0.33}}} \quad \text{Equation (4-10)}$
6	<p>Seawater settling velocity for flocs formed from treated cuttings</p> $u = 2.22 \times 10^{-4} G^{1.07} D^{\frac{1.84}{G^{0.32}}} \quad \text{Equation (4-11)}$

Chapter 5

Conclusions and Recommendations

5.1 Conclusions

A digital imaging system was developed to quantify the flocculation processes and settling behaviors of both treated and untreated SBF drilling cuttings. The system used a high speed CCD camera to record the particle motion and the images obtained were analyzed by Image Java (IJ) software using an edge-detection algorithm. An Image Java (IJ) plug-in was also programmed to obtain the shape information of the particles.

The flocculation tests for SBF attached drilling cuttings used a laboratory stirrer to generate fluid shear. The change of particle size with time was obtained as a function of both suspension concentration and fluid shear for three test conditions. It was demonstrated that:

1. The untreated cuttings can be easily flocculated by fluid shear especially in sea water conditions.
2. The removal of organic components from drilling cuttings using thermal treatment can reduce the flocculation tendency of drilling cuttings, which makes the treated cuttings more dispersible than untreated cuttings.

3. It was also shown by the freshwater tests that more time is needed in freshwater to reach flocculation steady state than in sea water.
4. The experiments showed that steady state median floc diameter in sea water tests is much larger than in fresh water tests.

For the settling of coarse ($D > 100\mu\text{m}$) cutting particles, settling velocity correlations have been derived for both treated and untreated particles at Reynolds numbers between 1 and 1000 from the settling column tests. As the shapes of irregular particles have significant effects on settling, a simplified equation was introduced in this research to calculate the sphericities of drilling cuttings particles. From the experiments, following conclusions can be drawn:

1. The untreated drilling cuttings particles were observed to settle as clumps instead of individual particles. The shape effects on settling can not be distinguished for this type of particle as the effective density of these clumps is not uniform.
2. The settling velocity equation for untreated SBF cuttings was found as a function of clump density, diameter, fluid density and rheology.
3. The settling velocity for treated cuttings is a function of sphericity as well as the particle density, diameter, fluid density and rheology.
4. The removal of oily components from SBF attached cuttings significantly changed the particle size distribution and made the cuttings more dispersible.

5. For cuttings of the same density, the experimental results showed that the treated cuttings settle faster than untreated cuttings. This is because the fluid will impose more friction force on porous clumps than on solidified particles.

As flocs have a porous structure and their density can not be measured directly, the methods used before for coarse cutting particles cannot be employed to obtain the settling velocity of this kind of material. Through the experiments and regression analysis, it was found that:

1. For the flocs formed at the same concentration, increasing fluid shear caused decreasing settling velocity.
2. For the same test condition, the treated cuttings were found to have a higher settling velocity than untreated cuttings.
3. The seawater settling velocity for flocs was found to be a function of both floc diameter and shear rate and follow a power law relationship.
4. For the seawater produced flocs settling in freshwater, experimental results showed that the salinity has almost no significant effect on settling velocity.
5. Concentration of drilling cutting suspension had no distinguishable effects on settling of flocs in the present research.

5.2 Research Contributions

Each drilling procedure (rate of penetration, number of turns per minutes, drilling muds, bits and teeth used, etc.) produces different types of cuttings. A change in any of these variables will result in the changes of size, shape and density of cuttings. These, in turn, influence the flocculation and settling velocities of particles, which are significant parameters affecting their dispersion in the marine environment. Because the transport models are very sensitive to the cuttings characteristics, such as cutting type, size distribution, shape, and settling velocity (Carles 1998, 1999, Gordon et al. 1995) and there is a gap in the research in modeling of flocculation and settling for SBF attached cuttings, this research gives a first attempt to obtain quantitative information for the flocculation and settling of SBF attached drilling cuttings. The flocculation results from this work provide important information for modeling the initial dilution of SBF drilling cuttings, while the settling velocity results are useful for the modeling of deposition and resuspension processes.

One of the potential applications of the digital imaging system developed in this work is that it can be used to perform in-situ direct measurements of particulate materials. However, the image quality is very sensitive to the lighting strategies, so more work needs to be done for the further application of this system.

5.3 Recommendations

For the present work, the floc particle size distribution was obtained using a digital imaging system; the results are different from those volume size distributions obtained by laser diffraction methods. In order to accurately characterize the floc size distribution, future experiments using different measurement methods, but the same cutting type, are suggested in order to obtain data for comparison.

As for the flocculation experiment, the ultimate accuracy of the current experimental method has not been verified due to the critical lighting technology. A suggestion is that different lighting methods be used in future work to find the effect of lighting methods on experimental results.

For the shape of irregular particles, a simplified equation using the equivalent diameters was introduced to approximate the sphericity value. Because of the limitation of the present experimental methods, the equivalent diameters were obtained in a vertical plane from two dimensional images. These vertical equivalent diameters may have great bias from the horizontal equivalent diameters which are more important in settling and can be derived from images obtained from horizontal plane. This bias will affect the diameter and sphericity values, especially for the flat type particles. The diameter and sphericity of this type of particles are greatly affected by their settling directions. The sphericity equation used in this study is not accurate for flat particles and some drilling cutting particles, especially treated cuttings particles, are of this type. Thus the method for calculating sphericity needs to be improved. A possible method is by using the stereology

technology which can make quantitative estimation of the three dimensional characteristics, e.g. surface area and volume, and give an accurate estimate of sphericity value. A detailed description of the sterology methods is given by Howard and Reed (1998).

Although the present work studied the flocculation process of untreated SBF drilling cuttings, there is still an important process that has not been fully understood. This is the process of how the fine small particles separate from the clumps. Current work focused on the flocculation of already diluted cutting suspensions but not the dilution process. For treated cuttings and WBF type cuttings, the cuttings particles can flocculate immediately once discharged because no more separation will occur for individual particles, but for oily type cuttings, the particles behave as clumps after discharge and the fine particles will separate from the clumps under the effects of turbulence and this process has not been studied. More work on the dilution of oily type drilling cuttings under different fluid shear needs to be done. Moreover, although the shape effects on settling of drilling cuttings has been established in the present work, the characteristics of cuttings produced under different drilling procedures (rate of penetration, number of turns per minutes, drilling mud type, bits and teeth used, etc.) are still needed to be studied for the application of present finding. A database of the drilling cutting characteristics under different drilling procedures is needed to be developed. Some preliminary work in this field has been done by Carles (2000).

It was shown by a number of researchers (Ho 1964, Murray 1970, Nelsen 1984, Nelsen 1993) that turbulence has effects on the settling of suspended particles and this is especially significant for very fine particles. This work only studied the still water settling mechanism, more work needs to be done to obtain the effective settling velocity under a turbulent environment.

REFERENCES

- Adler, P.M. 1981. Heterocoagulation in shear flow. *Journal of Colloid and Interface Science*, 83(1):106-115.
- Allen, H. S. 1900. The motion of a sphere in a viscous fluid. *Philoso. Mag.* 50(5):323-338, 519-534.
- Allen, T. 1990. *Particle Size Measurement*, Fourth Edition, Chapman and Hall, p.125.
- Arcilla., A.S., A. Rodriguez, and M. Mestres. 1998. A three dimensional simulation of pollutant dispersion for the near and far field in coastal waters. *Journal of Marine Environmental Engineering*, 4:217-243.
- Argamann, Y., and Kaulfman, W.J. 1970. Turbulence and flocculation. *Journal of Sanitary Engineering Division*, 96:223-241
- Ayers, R.C., Jr. 1981. Fate and effects of drilling discharges in the marine environment. Proposed North Atlantic OCS oil and gas lease sale 52. Statement delivered at public hearing, Boston, Mass., November 19, 1981. Bureau of land management, U.S. Department of the Interior.
- Batchlor, G.K., and J.T.Green. 1972. The Hydrodynamic Interaction of Two Small Freely-Moving Spheres in a Linear Flow Field. *Journal of Fluid Mechanics*, 56(2):375-400.
- Berkelmann, K.G., and U.Renz. 1988. Simultaneous Lase-Doppler-Velocimetry and Particle Sizing in the Freeboard of a Fluidized Bed Combustor. In: *Applications of Laser Anemometry to Fluid Mechanics*. Edited by R.J.Adrian, T.Asanuma, D.F.G.Dura, F.Durst, and J.H.Wgitelae. New York:Springer-Verlag.
- Biddle, P. and Miles, J.H. 1972. The nature of contemporary silts in British estuarines, *Sedim. Geol.* 7:23-33.
- Boadway, J.D. 1978. Dynamics of growth and break up of alum floc in presence of fluid shear. *Journal of Environmental Engineering Division*. 104:901-915.
- Bhole, A.G., Hydrodynamics of flocculation in water treatment, Ph.D. Thesis, University of London 1970.
- Brandsma, M.G. and R.C. Sauer, 1983, The OOC model: prediction of short term fate of drilling fluids in the Ocean. *Proceedings of Minerals Management Service Workshop on Discharges Modeling*, Santa Barbara, CA, February 7-10, 1983.

- Bryden, I.G. and Carles, L.J. 1998. Predicting the behaviour of drilled cuttings released into sea water. *Proceedings of the 8th International Offshore and Polar Engineering Conference*, Montreal, Canada. May 24-29, 1998. Vol 2. pp301-306.
- Burban, P.-Y., W.Lick, and J. Lick. 1989. The flocculation of fine-grained sediments in estuarine waters, *Journal of Geophysical Research*. 94(C6):8323-8330.
- Burban, P.-Y., Y-J. Xu, J. McNeil, and W. Lick. 1990. Settling speeds of flocs in fresh water and seawater. *Journal of Geophysical Research*. 95(C10):18213-18220.
- Camp, T.R. 1968. Floc volume concentration, *Journal of American Water Works Association*, 60:656-673.
- Camp, T.R. 1969. Hydraulics of mixing tanks. *Journal of the Boston Society of Civil Engineers*, 56(1):1-28, Jan 1969.
- Camp, T.R., and P.C. Stein. 1943. Velocity gradients and internal work in fluid motion, *Journal of Boston Society of Civil Engineers*, 30: 219-237, 1943.
- Casson, L.W. and D.F. Lawler. 1990. Flocculation in turbulent flow: Measurement and modeling of particle size distribution. *Journal of American Water Works Association*, 82(8):54-68.
- Carles, L.J., and I. G., Bryden. 1998. Characterisation of offshore drill-cuttings for simulation purposes. *Proceedings of the Eighth International Offshore and polar Engineering Conference*, Montreal, Canada, May 24-29, 1998. Vol. II pp308 .
- Carles, L.J., and I. G., Bryden. 1999. The sensitivity of a dispersion model to cuttings settling speeds. *Society of Underwater Technology Journal*, 24(1):19-24.
- Carles, L. 2000. Physical characteristics and aquatic settlement properties of offshore drill-cuttings. Ph.D. Thesis. Robert Gordon University, Aberdeen, Scotland, UK.
- Chen, R.C., and L.S.Fan. 1992. Particle image velocimetry for characterizing the flow structure in three-dimensional gas-liquid fluidized beds. *Chemical Engineering Science*, 47(13/14):3615-3622.
- Chien, S-F. 1992. Settling velocity of irregular shaped particles. SPE paper: No.26121.
- Chinga, G. 2002. Shape Description plugin. Personal contact.
- Clark, M.N. 1982. Discussion of forces acting on floc and strength of floc, American Society of civil Engineers, *Journal of Environmental Engineering Division*, 108(E3):592-594.
- Clift, R., J.R. Grace, and M.E. Weber. 1978. *Bubbles, Drops, and Particles*. Academic Oress, New York
- Coats, D., 1991. Deposition of drilling particulates off point concentration, California. California OCS Phase II Monitoring Program, Final Report. OCS Study 91-033.

- Minerals Management Service, U.S. Department of the interior, Pacific OCS region. November 1991.
- Cornwell, D.A. and M.M. Bishop. 1983. Determining velocity gradient in laboratory and full scale systems. *Journal of American Water Works Association*, 75(9):470-475.
- Curran, K., J. P. S. Hill, and T. G. Milligan. 2002. The role of particle aggregation in size-dependent deposition of drill mud. *Continental Shelf Research*, 22:405-416.
- Darley, H.C.H., and G.G. Gray, 1988, *Composition and properties of drilling and completion fluid.*, fifth edition, Gulf Publish Co., Houston, TX, 643pp.
- Delichatsios, M.A., and Probst, R.F. 1975. Coagulation in turbulent flow: Theory and experiment, *Journal of Colloid and Interface Science*. 51(3):394-405.
- deMargerie, S. 1988. Modeling of drill cuttings discharges. *Proceedings of the 1988 International Conference on Drilling Waste*. Calgary, Alberta, Canada, April 5-8, 1988.
- Eisma, D. 1986. Flocculation and de-flocculation of suspended matter in estuaries. *Netherlands Journal of Sea Research*, 20(2/3):183-199.
- Eisma, D.T. Schuhmacher, H.Boekel, J.Van Heerwaarden, H.Franken, M.Laan, A.Vaars, F.Eijgenraam, and J.Kalf. 1990. A camera and image-analysis system for in situ observation of flocs in natural waters. *Netherland Journal of Sea Research*, 27(1):43-56.
- Elimelech, M., and L. Song. 1992. Theoretical investigation of colloid separation from dilute aqueous suspension by oppositely charged granular media. *Separation Technology*. 61:44-51.
- Filella, M., and J.Buffle. 1993. Factors controlling the stability of submicron colloids in natural waters. *Colloids and Surfaces A: Ohysicochemical and Engineering Aspects*, 73:255-273.
- Gerard, A.L.D. 1996. Laboratory investigations on the Fate and Physicochemical Properties of Drilling Cuttings after Discharged into the Sea, In: *Physical and Biological Effects of Processed Oily Drill Cuttings*, E&P Forum Report, Paper 3. 16-24.
- Gibbs, R. J. 1985a. Settling velocity, diameter, and density for flocs of illite, kaolinite, and montmorillonite, *Journal of sedimentary petrology*. 55(1):65-68.
- Gibbs, R. J. 1985b. Estuarine flocs: their size, settling velocity and density. *Journal of Geophysical Research*, 90(C2): 3249-3251.
- Gibbs, R. J., Matthews, M.D., and Link, D.A. 1971. The relationship between sphere size and settling velocity. *Journal of Sedimentary Petrology*, 41(1):7-18.
- Gordon, D.C., Loder, J. and Hannah C. 1995. Fate and effects of operational drilling wastes. Summary of the Internal Review of PERD Projects, 23 January 1995.

- Graf, W.H. 1971. *Hydraulics of sediment transport*. McGraw-Hill, New York.
- Gregory J. 1978. Flocculation by inorganic salts, In: *The scientific basis of flocculation*, edited by K.J. Ives, Sijthoff & Noordhoff International Publishers, The Netherlands.
- Gripenberg, Stina. 1934. A study of the sediments of the north baltic and adjoining seas. *Fennia*, 60(3):1-231.
- Han, M., and D.F. Lawler, 1991. The (relative) insignificance of G in flocculation, *Journal of American Water Works Association*, 84(10):70-79.
- Hannah, C.G., Shen, Y., Loder, J.W., Muschenheim, D.K. 1995. bblt: Formation and exploratory applications of a benthic boundary layer transport model. Technical Report 166, Canadian Technical Report of Hydrography and Ocean Sciences.
- Hannah, C.G., Shen, Y., Loder, J.W. 1996. Shear dispersion in the benthic boundary layer. In: *Estuarine and Coastal Modeling, Proceedings of the 4th International Conference*, ASCE, New York, pp454-465.
- Hawley, N. 1982. Settling velocity distributions of natural aggregates. *Journal of Geophysical Research*. 87:9489-9498.
- Hawkins, A. E. 1993. *The shape of power-particle outlines*. John Wiley & Sons Inc.
- Hiscock John. 2000. Quantitative flow visualization system for gas-liquid two phase flows. M.Eng Thesis. Memorial University of Newfoundland, St.John's, Canada.
- Ho, H.W. 1964. Fall velocity of a sphere in an oscillating fluid. PhD thesis, University of Iowa, Iowa City, Iowa.
- Hodgin, D.O. and S.L.M. Hodgins. 2000. Modelled predictions of well cuttings deposition and produced water dispersion for the proposed White Rose development. Technical Report, Seaconsult Marine Research Ltd. Canada.
- Hoerner, S.F. 1958. *Fluid Dynamic Drag*, Midland Park, New Jersey.
- Howard C.V. and M.G. Reed 1998. *Unbiased stereology: three-dimensional measurement in microscopy*. Springer-Verlag New York Inc. New York, USA.
- Howard N.E. 2000. OPSCI application notes: Lens selection. OAN-003. <http://www.opsci.com>.
- Hunt, J.R. 1982. Particle dynamics in seawater: Implications for predicting the fate of discharged particles. *Environmental Science Technology*, 16(6):303-309.
- Hunt, J.R. and J.D. Pandya.1984. Sewage sludge coagulation and settling in seawater. *Environmental Science Technology*, 18(2):119-121.
- Huang, H. 1992. Transport properties of drilling muds and Detroit river sediments. PhD Dissertation. University of California, Santa Barbara. May 1992.

- Iacobellis, S. The flocculation of fine-grained lake sediments subjected to a uniform shear stress. M.S. Thesis, University of California, Santa Barbara.
- Ives, K.J. 1978a. Rate theories. In: *The scientific basis of flocculation*. Sijthoff & Noordhoff International Publishers B.V., Alphen aan den Rijn, The Netherland
- Ives, K.J. 1978b. Experimental methods (2). In: *The scientific basis of flocculation*. Sijthoff & Noordhoff International Publishers B.V., Alphen aan den Rijn, The Netherland.
- Kajihara, M. 1971. Settling velocity and porosity of large suspended particle, *Journal of Oceanogr. Soc. Jpn.*, 27:158-162.
- Kawana, K., and T. Tanimoto. 1976. Temporal variation of suspended matter near the sea bottom in Hiro bay, *Mer.*, 14:47-52.
- Kawana, K., and T. Tanimoto. 1979. Suspended particle near the bottom in Osaka Bay, *Journal of Oceanogr. Soc. Jpn.*, 35:75-81.
- Khondaker, A.N. 2000. Modeling the fate of drilling waste in marine environment -- an overview. *Computers & Geosciences*, 26:531-540.
- Kranck, K. 1975. Sediment deposition from flocculated suspensions. *Sedimentology*, 22:111-123.
- Lai, R.L., H.E. Hudson, and J.E. Singley. 1975. Velocity gradient calibration of jar test equipment. *Journal of American Water Works Association*, 67: 553.
- Lick, W., J. Lick, and C.K. Ziegler 1992. Flocculation and its effect on the vertical transport of fine-grained sediment. *Hydrobiologia*, 235/236:1-16.
- Lick, W., J. Lick. 1988. Aggregation and disaggregation of fine-grained lake sediment. *Journal of Great Lake Research*, 14(4):514-523.
- Lick, W., H. Huang, and R. Jepsen. 1993. Flocculation of fine-grained sediments due to differential settling. *Journal of Geophysical Research*, 98(C6):10279-10288.
- Luo, D-S. 1998. *Pattern recognition and image processing*. Horwood Publishing Limited, England.
- Lyklema, J. 1978. Surface chemistry of colloids in connection with stability. In: *The scientific basis of flocculation*. Sijthoff & Noordhoff International Publishers B.V., Alphen aan den Rijn, The Netherland.
- Matsuo, T., and Unno, H. 1981. Forces acting on floc and strength of floc. *Journal of Environmental Engineering Division, ASCE*. 107(E3):527-545.
- McCabe, W. L., J. C. Smith. 1967. *Unit operations of chemical engineering*, 2nd ed., McGraw-Hill.
- McCave, I.N. 1975. Vertical flux of particles in the ocean. *Deep Sea Research*, 22:491-502.

- McCave, I. N., and J. P. M. Syvitski. 1991. Principles and methods of geological particle size analysis. In: Principles, methods, and application of particle size analysis. Edited by J. P. M. Syvitski. Cambridge University Press, New York, NY, USA.
- Michell, S.J. 1970. *Fluid and Particle Mechanics*. Pergamon Press Ltd., London.
- Migniot, C. 1989. Bedding-down and rheology of muds. Part I, *La Houille Blanche*, No.1, 11-29 (in French).
- Murray, S. P. 1970. Settling velocities and diffusion of particles in turbulent water. *Journal of Geophysical Research*, 75(9): 1647-1654.
- Muschenheim, D.K., Milligan, T.G. 1996. Flocculation and accumulation of the fine drilling waste particulates on the Scotian shelf (Canada), *Marine Pollution Bulletin*, 32(10):740-745.
- Muschenheim, D.K., Milligan, T.G., Gordon, D.C. 1995. New technology and suggested methodologies for monitoring particulates wastes discharged from offshore oil and gas platforms and their effects on the benthic boundary layer environment, Technical report 2049, Canadian technical report of Fisheries and Aquatic Sciences.
- NRC (National Research Council), 1983, *Drilling discharges in the marine environment*, National Academy Press, Washington D.C. 1983.
- NEB, CNOPB, CNSOPB (National Energy Board, Canada-Newfoundland Offshore Petroleum Board, and Canada-Nova Scotia Offshore Petroleum Board). 2002. Offshore waste treatment guidelines.
- Neff, J.M., 1987. Biological effects of drilling fluids, drilling cuttings and produced waters, Pages 469-538, In: *Long-term Effects of Offshore Oil and Gas Development*, D.F. Boesch and N.N. Rabalais, Eds, Elsevier Applied Science Publishers, London.
- Neff, J.M., Bothner, M.H., Maciolek, N.J., Grassle, J.F. 1989. Impacts of exploratory drilling for oil and gas on the benthic environment of Georges Bank. *Marine Environmental Research*, 27:77-114.
- Nielsen, P. 1993. Turbulence effects on the settling of suspended particles. *Journal of Sedimentary Petrology*, 63(5):835-838.
- Nielsen, P. 1984. On the motion of suspended particles. *Journal of Geophysical Research*, 89(C1):616-626.
- Oberdier, L. M. 1984. An instrumentation system to automate the analysis of fuel-spray imaging using computer vision. In: *Liquid Particle Size Measurement Techniques*, ASTM STP 848. Edited by J.M. Tishkoff, R.D. Ingebo, and J.B. Kennedy.
- O'Reilly, J.E., T.C. Sauer, R.C. Ayers, Jr., M.G. Brandsma, R. Meek, 1988, Field validation of the OOC mud discharge model, *Proceedings of the 1988 International Conference On Drilling Waste*, Calgary, Alberta, Canada, April 5-8, 1988.

- Ozretich, R.J., D.J. Baumgartner 1990. The utility of buoyant plume models in predicting the initial dilution of drilling fluids. *Oceanic Processes in Marine Pollution*, Volume 6. Baumgartner, I.W. Wuedall (eds). Robert E. Krieger Publishing, Malaban, FL. pp151-168.
- Paker, D.S. 1982. Discussion of forces acting on floc and strength of floc. *Journal of Environmental Engineering Division, ASCE*. 108(EE3):594-598.
- Paker, D.S., Kaufman, W.J., and Jenkins, D. 1972. Floc breakup in turbulence flocculation processes. *Journal of Sanitary Engineering Division*. 98:79-99.
- Raudkivi, A.J. 1976. *Loose boundary hydraulics*, Pergamon, New York.
- Rawle, A. 1994. The basic principals of particle size analysis. A section of the Malvern user guide.
- Rushton, J.H., E.W. Costich, and H.J. Everett, 1950. *Chemical Engineering Progress*, 46:395-467.
- Russ, J.C. 1999. *The image processing handbook*. CRC Press.
- Sheldon, R.W. 1968. Sedimentation in estuary of the river crouch, England. *Limnol. Oceanogr.* 13:72-83.
- Silver, M.W., and A.L. Alldredge, 1981. Bathypelagic marine snow: deep sea algal and detrital community, *Journal of Marine Research*, 39:501-530.
- Sleath, J.F.A. 1984. *Sea Bed Mechanics*. John Willey & Sons.
- Smoluchowski, M., 1917. Versuch einer mathematischen theories der koagulationskinetic kolloider losungen, *Zeitschr. Phys. Chem.*, 92, 129, 1917.
- Spielman, L.A. 1978. Hydrodynamic Aspects of Flocculation. In: *The scientific basis of flocculation*. Sijthoff & Noordhoff International Publishers B.V., Alphen aan den Rijn, The Netherland.
- Tambo, N., and Hozumi, H. 1979. Physical characteristics of flocs –II. Strength of flocs. *Water Research*. 13:421-427.
- Tambo, N., and Watanabe, Y. 1979. Physical characteristics of flocs –I. The floc density function and aluminum floc. *Water Research*. 13:409-419.
- Torbin, L.B., and Gauvin, W.H., 1960. *Canadian Journal of Chemical Engineering*, 38:142-153.
- Tsai, C.H., S.Iacobellis, and W.Lick. 1987. Flocculation of fine grained sediments due to a uniform shear stress. *Journal of great Lake Research*, 13(2):135-146.
- U.S. EPA, 1999. Development document for proposed effluent limitations guidelines and standards for synthetic-based drilling fluids and other non-aqueous drilling fluids in the oil and gas extraction point source category. EPA-821-B-98-021, United States Environmental protection Agency, Washington, D.C.

- U.S. MMS, 2000. Environmental impacts of synthetic based drilling wastes. OCS Study, MMS 2000-064, U.S. Department of the Interior, Minerals Management Service, Houston, TX.
- Valioulis, I.A., and E.J. List. 1984a. Numerical simulation of a sediment basin. 1. Model development. *Environmental Science and Technology*, 18(4):242-247.
- Valioulis, I.A., and E.J. List. 1984b. Collision efficient of diffusing spherical particles: hydrodynamics, Van der waals and electrostatic forces. *Advances in Colloid and Interface Science*, 20:1-20.
- Van de Ven, T.G.M., and S.G. Mason. 1977. The microrheology of colloid Dispersions: VII. Orthokinetic doublet formation of Spheres. *Colloid and Polymer Science*, 255:468-479.
- Van Duuren, F.A., Defined velocity gradient model flocculator, *Journal of Sanitary Engineering Division, ASCE*, 94(SA4):671-682, 1968.
- Van Leussen, W. 1994. Estuarine macroflocs and their role in fine-grained sediments transport. PhD Thesis. University of Utrecht, The Netherland, 488pp.
- Wadell, H. 1932. Volume, shape, and roundness of rock particles, *Journal of Geology*, 40:443-451.
- Wadell, H. 1933. Sphericity and roundness of rock particles, *Journal of Geology*, 41:310-331.
- Wadell, H. 1934. The coefficient of resistance as a function of Reynolds number for solids with various shapes. *Journal of Franklin Institute*, April, 1934, 459-490.
- Wadell, H. 1935. Volume, shape, and roundness of quartz particles, *Journal of Geology*, 43:250-280.
- Wagner, E.G. 1993. Jar test instructions, conduct of jar tests and the important information obtained", booklet from Phipps and Bird, 8741 Landmark Rd., Richmond, VA 23228, July 1993.
- Walker, H.A., J.F. Paul, V.J. Bieman, Jr., 1990. A convective-dispersive transport model for wastes disposed of at the 106-mile ocean disposal site. . *Oceanic Processes in Marine Pollution*, Volume 6. Baumgatner , I.W. Wuedall (eds). Robert E. Krieger Publishing, Malaban, FL. pp 53-62.
- Whitehouse, V.G., Jeffrey, L.M. and Debrecht, J.D. 1960. Differential settling tendencies of clay minerals in saline waters. In: *Clay and Clay Minerals, Proc. 7th Natn Conf. Clays and Clay Minerals*. National Academy of Science-national Research Council.
- Winterwerp, J.C. 1998. A simple model for turbulence induced flocculation of cohesive sediments, *Journal of Hydraulic Research*, 36(3):309-326.
- Xu, Y-J. 1988. The Flocculation of bentonite and barite in sea water. MS Thesis. University of California, Santa Barbara. March 1988.

Zhang, Y., and D.G. Talley. 1990. An imaging-processing technique for determining focus and statistical information about nonspherical particles in sprays. In: *Liquid Particle Size Measurement Techniques*, Volume II, ASTM STP 1083. Edited by E.D. Hirleman W.D. Bachalo, and P.G. Felton.

Appendix 1

Java Code for Particle Shape Calculation

```
import ij.*;
import ij.plugin.filter.*;
import ij.process.*;
import ij.gui.*;
import ij.measure.*;
import ij.text.*;
import java.util.*;
```

```
/**
```

Besides area, perimeter and angle, this plugin calculates shape descriptors. The measurement can be conducted either in MEAN or in SINGLE mode. The mean and standard deviation of shape values are given for every image in a stack in MEAN mode while shape values of every particle in an image are calculated in SINGLE mode. The definitions are given according to Russ, 1999 (The image processing Handbook) and Hawkins 1993 (The Shape of Power-Particle Outlines). The following descriptors are used:

Form factor: $4\pi \cdot \text{area} / \text{sqr}(\text{perimeter})$
Roundness: $4 \cdot \text{area} / \pi \cdot \text{sqr}(\text{major axis})$
Sphericity: $\text{sqr}((4/\pi) \cdot \text{area}) / \text{major axis}$
Elongation: $\text{major axis} / \text{minor axis}$

The Analyze/Set Measurements... "Limit to Threshold" option must be checked (only thresholded pixels are included in measurement calculations). Use Image/Adjust/Threshold to set the threshold limits. Edge particles must also be excluded during measurement.

Notes:

The ImageJava Shape_Description plugin was originally written by Gary Chinga, the first version only calculates the mean particle shape factors. By adoption of Haibo Niu's Suggestion, Gary Chinga released his second version with the added option to calculate single particle shape descriptors. The code presented here is a modified version of Gary Chinga's second release.

Haibo Niu 2002

```
*/
```

```
public class Shape_Descriptors implements PlugInFilter, Measurements {
```

```

ImagePlus imp;
ResultsTable rt;
int counter,slice,i,c;
TextWindow mtw;
String title,headings,aLine ;
float[] areas,Dia,per,mAxis,miAxis,angle,FF,Sphe,Round,Elong;
float mArea, mDia, mPer, mMajor, mMinor, mAngle, mSphe, mRound, mFF,
      mElong, ps;
float sArea,sDia, sPer,sAngle,sSphe,sRound, sFF,sElong;

boolean canceled=false;
private static String[] items = {"Single particle details","Mean particle details"};
protected static final int SINGLE=0,MEAN=1;
protected static int Choice;

public int setup(String arg, ImagePlus imp) {
    if (IJ.versionLessThan("1.28"))
        return DONE;
    this.imp = imp;
    return DOES_8G;
}

public void run(ImageProcessor ip) {
    Calibration cal = imp.getCalibration();
    ps = (float) cal.pixelWidth;
    getDetails();
    if (canceled) return;
    int measurements = Analyzer.getMeasurements();
    // defined in Set Measurements dialog
    Analyzer.setMeasurements(0);
    measurements |= AREA+PERIMETER+ELLIPSE;
    //make sure area and perimeter are measured
    Analyzer.setMeasurements(measurements);
    Analyzer a = new Analyzer();
    ParticleAnalyzer pa = new ParticleAnalyzer();
    pa.showDialog();

    int nSlices = imp.getStackSize();
    for (i=1; i<=nSlices; i++) {
        IJ.run("Clear Results");
        imp.setSlice(i);
        mArea = 0; mDia=0; mPer=0; mAngle=0; mSphe=0; mRound=0;
        mFF=0;mElong=0;
    }
}

```

```
sArea = 0; sDia=0; sPer=0; sAngle=0; sSphe=0; sRound=0;
sFF=0;sElong=0;
```

```
if (!pa.analyze(imp))
    return;
rt =Analyzer.getResultsTable(); //get the system results table
counter = rt.getCounter();
// IJ.setColumnHeadings(rt.getColumnHeadings());
if (counter>0) {
    areas = rt.getColumn(ResultsTable.AREA);
        // get area measurements
    per = rt.getColumn(ResultsTable.PERIMETER);
        // get perimeter measurements
    angle= rt.getColumn(ResultsTable.ANGLE);
        // get angle measurements
    mAxis= rt.getColumn(ResultsTable.MAJOR);
        // get area measurments
    miAxis= rt.getColumn(ResultsTable.MINOR);
        // get area measurments
    calculateShape();

    if (Choice==SINGLE) {
        for (int ii=0; ii<counter; ii++){
            c=ii+1;
            mArea=areas[ii];
            mDia=Dia[ii];
            mPer=per[ii];
            mAngle=angle[ii];
            mElong=Elong[ii];
            mSphe=Sphe[ii];
            mRound=Round[ii];
            mFF=FF[ii];
            writeResults();
        }
    }
    if (Choice==MEAN) {
        c=counter;
        mArea=calculateMean(areas);
        mDia=calculateMean(Dia);
        mPer=calculateMean(per);
        mAngle=calculateMean(angle);
        mFF=calculateMean(FF);
        mSphe = calculateMean(Sphe);
    }
}
```

```

        mRound=calculateMean(Round);
        mElong=calculateMean(Elong);

        sArea=calculateStd(mArea,areas);
        sDia=calculateStd(mDia,Dia);
        sPer=calculateStd(mPer,per);
        sAngle=calculateStd(mAngle,angle);
        sFF=calculateStd(mFF,FF);
        sSphe = calculateStd(mSphe,Sphe);
        sRound=calculateStd(mRound,Round);
        sElong=calculateStd(mElong,Elong);
        writeResults();
    }
}
else {c=0; writeResults();}
}
}

void calculateShape(){
    Dia = new float[areas.length];
    FF = new float[areas.length];
    Round = new float[areas.length];
    Sphe = new float[areas.length];
    Elong = new float[areas.length];
    for (int ii=0; ii<counter; ii++){
        Dia[ii] = (float) (Math.sqrt((4/Math.PI)*areas[ii])/(mAxis[ii]/mAxis[ii]));
        FF[ii] =(float) ((4*Math.PI*areas[ii])/(sqr(per[ii])));
        Round[ii] = (float) ((4*areas[ii])/(Math.PI*sqr(mAxis[ii])));
        Sphe[ii] = (float) (Math.sqrt((4/Math.PI)*areas[ii])/mAxis[ii]);
        Elong[ii] = (float) (mAxis[ii]/miAxis[ii]);
    }
}

float calculateMean(float[] dataset){
    double mValue=0;
    for (int j=0; j<counter; j++){mValue += dataset[j];}
    return (float) (mValue/counter);
}

float calculateStd(float mValue,float[] dataset){
    float sValue=0;
    if (counter==1) {return (float) (sValue);}
    else{

```

```

        for (int j=0; j<counter; j++){sValue += sqrt(mValue-dataset[j]);}
        return (float) (Math.sqrt(sValue/(counter-1)));
    }
}

void writeResults(){
    if (Choice==MEAN)
        aLine = I + "\t" + c + "\t" + IJ.d2s(mArea,2) + "\t" + IJ.d2s(sArea,2)
            + "\t" + IJ.d2s(mDia,2) + "\t" + IJ.d2s(sDia,2) + "\t"
            + IJ.d2s(mPer,2) + "\t" + IJ.d2s(sPer,2) + "\t" + IJ.d2s(mAngle,2)
            + "\t" + IJ.d2s(sAngle,2) + "\t" + IJ.d2s(mElong,2) + "\t"
            + IJ.d2s(sElong,2)+"\t"+IJ.d2s(mSphe,2)+"\t"+ IJ.d2s(sSphe,2)
            + "\t" + IJ.d2s(mRound,2) + "\t" + IJ.d2s(sRound,2) + "\t"
            + IJ.d2s(mFF,2) + "\t" + IJ.d2s(sFF,2);

    else

        aLine = i+"\t"+c+"\t"+IJ.d2s(mArea,2)+"\t"+IJ.d2s(mDia,2)+"\t"
            +IJ.d2s(mPer,2)+"\t"+IJ.d2s(mAngle,2)+"\t"
            +IJ.d2s(mElong,2)+"\t"+IJ.d2s(mSphe,2)+"\t"
            +IJ.d2s(mRound,2)+"\t"+IJ.d2s(mFF,2);

    if (mtw==null) {
        if (Choice==MEAN){
            title = "Mean values of "+imp.getShortTitle();
            headings = "Slice\tCount\tArea\tstd\tDiameter\tstd \tPerimeter\tstd
                \tAngle\tstd\tElong\tstd\tSphe\tstd\tRound\tstd\tFormFactor\tstd";
            mtw = new TextWindow(title, headings, aLine, 850, 180);
        }
        else {
            title = "Single particle values of "+imp.getShortTitle();
            headings = "Slice\tCount\tArea\tDiameter\tPerimeter\tAngle
                \tElong\tSphe\tRound\tForm Factor";
            mtw = new TextWindow(title, headings, aLine, 550, 180);
        }
    } else
        mtw.append(aLine);
}

double sqr(double x) {return x*x;}
void getDetails() {
    GenericDialog gd = new GenericDialog("Particle details...");
    String units = imp.getCalibration().getUnits();
    gd.addChoice("Display", items, items[Choice]);
}

```

```
if (!units.startsWith("pixel"))
gd.addMessage("    (Pixel size = "+IJ.d2s(ps,2)+" "+units+"");
gd.showDialog();
if (gd.wasCanceled()){
    canceled = true;
    return;
}
Choice = gd.getNextChoiceIndex();
}
}
```